

DESIGN AND DEVELOPMENT OF FREQUENCY SELECTIVE SURFACE FOR VARIOUS PRACTICAL APPLICATIONS

a thesis submitted in fulfillment of the requirements for the
degree of

Doctor of Philosophy

By

KANISHKA KATOCH



DEPARTMENT OF ELECTRONICS AND COMMUNICATION ENGINEERING

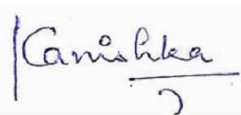
JAYPEE UNIVERSITY OF INFORMATION TECHNOLOGY

WAKNAGHAT, SOLAN, H.P., INDIA

OCTOBER, 2021

CANDIDATE'S DECLARATION

I hereby declare that the work which is being presented in this thesis entitled “**Design and Development of Frequency Selective Surface for Various Practical Applications**” in fulfillment of the requirement for the degree of Doctor of Philosophy in electronics and communication engineering in the department of electronics and communication engineering of Jaypee University of Information Technology, Wanknaghat, Solan, Himachal Pradesh, India is an authentic record of my work carried out under the supervision of **Prof. Samir Dev Gupta and Dr. Naveen Jaglan**. I have not submitted this work elsewhere for any other degree or any other Institute/University.



Kanishka Katoch

(Enrolment No. 186002)

Department of Electronics and Communication Engineering, Jaypee University of Information Technology, Solan, India

Date.....

TABLE OF CONTENT

TABLE OF CONTENT	ii
CANDIDATE’S DECLARATION	ii
SUPERVISORS’ CERTIFICATE	ix
ACKNOWLEDGEMENT	x
ABSTRACT	xii
LIST OF SYMBOLS	xv
LIST OF ACRONYMS	xvii
LIST OF FIGURES	xix
LIST OF TABLES	xxiii
CHAPTER 1	
Introduction	1-26
1.1 UWB Technology	1
1.2 Frequency Selective Surface: An Overview	2
1.2.1 Periodic Structure	3
1.2.2 Principle of operational theory in FSS	4
1.3 Factors affecting the frequency response of FSS	5
1.3.1 Shape and size of element	5
1.3.2 Angle and polarization of the incident plane wave	7
1.3.2.1 Effect of angle of incidence	7
1.3.2.2 Effect of incident wave polarization	7
1.3.3 Dielectric substrate	8
1.3.3.1 Thin layer dielectric substrate	8

1.3.3.2 Thick layer dielectric substrate	8
1.3.4 Conductivity of element	8
1.4 Conventional filtering geometries and relevant equivalent circuit	9
1.4.1 Strip grating	9
1.4.2 Square loop (SL).....	11
1.5 FSS Requirements	12
1.5.1 Miniaturization of the FSS	12
1.5.2 Angular stability characteristic	12
1.5.3 Polarization insensitive characteristic	12
1.6 Related work	13
1.6.1 Single layer FSS	13
1.6.2 Multilayer FSS.....	14
1.6.3 3-Dimensional FSS.....	15
1.6.4 2.5- Dimensional FSS.....	16
1.7 Applications of band stop FSSs	17
1.7.1 Spatial Filtering	17
1.7.2 Reconfigurable FSS.....	18
1.7.3 Isolation in MIMO Antennas.....	19
1.7.4 Electromagnetic Shielding.....	19
1.7.5 Performance enhancement of antennas	20
1.7.6 FSS radomes	21
1.8 Motivation	22
1.9 Research Problem Formulation.....	22
1.10 Research gaps.....	24

1.11 Research Objectives	25
1.12 Thesis Orientation	25

CHAPTER 2

Triple Band Notched FSS over entire UWB frequency range.....27-38

2.1 Introduction	27
2.2 Design analysis of the FSS unit cell.....	28
2.2.1 Unit cell model	28
2.2.2 Design principle and step wise making of FSS unit cell	29
2.3 Simulated and experimental results.....	30
2.3.1 Frequency response of the designed FSS	30
2.3.2 Surface current distribution	31
2.3.3 Frequency response curve at various incident angles.....	36
2.3.6 Parametric variations	37
2.3.7 Verification of the simulated results experimentally.....	38
2.3.8 Proposed FSS design compared with various other FSS design reported in literature.....	41
2.4 Conclusion.....	43

CHAPTER 3

Polarization Insensitive Triple Band Notched FSS over UWB frequency range.44-58

3.1 Introduction	44
3.2 Design analysis of FSS unit-cell	46
3.2.1 Unit cell model	46
3.2.2 Principle of operation and step by step development of unit cell.....	47

3.3 Simulated and experimental results.....	48
3.3.1 Frequency response of given unit cell	48
3.3.2 Surface current distribution	50
3.3.3 Equivalent circuit model (ECM)	52
3.3.4 Electromagnetic shielding	54
3.3.5 Frequency response curve at various incident and polarization angles.....	54
3.3.6 Parametric analysis.....	58
3.3.7 Verification of the simulated results experimentally.....	60
3.3.8 Proposed FSS design compared with various other FSS design reported in literature.....	61
3.4 Conclusion.....	64

CHAPTER 4

Dual Band Notched FSS using Single Resonant Element	66-74
4.1 Introduction	66
4.2 Design analysis of the FSS unit cell.....	67
4.2.1 Unit cell model	67
4.2.2 Principle of operation and step by step development of unit cell.....	68
4.3 Simulated and experimental results.....	68
4.3.1 Frequency response of the proposed unit cell	68
4.3.2 Surface current distribution	70
4.3.3 Equivalent circuit model (ECM)	71
4.3.4 Electromagnetic shielding	73
4.3.5 Frequency response curve at various incident and polarization angles.....	75

4.3.6 Parametric analysis	76
4.3.7 Verification of the simulated results experimentally.....	78
4.3.8 Comparison of various unit cell FSS	79
4.4 Conclusion	81

CHAPTER 5

Design and Analysis of UWB FSS using Modified SL..... 83-94

5.1 Introduction	83
5.2 Design analysis of UWB FSS unit cell	84
5.2.1 Unit cell model	84
5.2.2 Principle of operation and stages in the making of UWB FSS	85
5.3 Simulated and experimental results.....	86
5.3.1 Frequency response of the UWB FSS	86
5.3.2 Surface current distribution	88
5.3.3 Equivalent circuit model (ECM)	89
5.3.4 Frequency response curve at various incident and polarization angles.....	93
5.3.5 Parametric analysis.....	95
5.3.6 Verification of the simulated results experimentally.....	95
5.3.7 Proposed FSS design compared with various other FSS design reported in literature.....	100
5.4 Conclusion.....	102

CHAPTER 6

2.5D FSS for Sub 6 GHz 5G Communication System 103-108

6.1 Introduction	103
------------------------	-----

6.2 Design analysis of the FSS unit cell.....	104
6.2.1 Unit cell model	104
6.2.2 Principle of operation and development of FSS element	106
6.3 Simulated and experimental results.....	107
6.3.1 Frequency response of the proposed unit cell	107
6.3.2 Surface current distribution with circuit modeling.....	108
6.3.3 Frequency response curve at various incident and polarization angles.....	111
6.3.4 Parametric analysis	114
6.3.5 Comparison of proposed 2.5D FSS with FSSs in literature	117
6.4 Conclusion.....	120
CHAPTER 7	
Conclusion and Future Scope	121-111
REFERENCES.....	125
APPENDIX.....	147
LIST OF PUBLICATIONS	150

SUPERVISORS' CERTIFICATE

This is to certify that the work reported in the Ph.D. thesis entitled “**Design and Development of Frequency Selective Surface for Various Practical Applications**”, submitted by **Kanishka Katoch** in fulfillment of the requirement for the award of the degree of Doctor of Philosophy in Electronics and communication Engineering and submitted in the Department of Electronics and Communication Engineering of **Jaypee University of Information Technology, HP, India**, is a bonafide record of her original work carried out under my supervision.

This work presented in this thesis has not been submitted elsewhere for any other degree or diploma.



Prof. Samir Dev Gupta
Dean of Academics
Department of Electronics &
Communication Engineering
Jaypee University of Information
Technology
Waknaghat, Solan, 173234, India

Dr. Naveen Jaglan
Assistant Professor
Department of Electronics &
Communication Engineering
Jaypee University of Information
Technology
Waknaghat, Solan, 173234, India

ACKNOWLEDGEMENT

With the providential grace of “**Almighty God**”, the expedition of my Ph.D. came to an end and my heart is overflowing with appreciation towards each and every person who has lend a hand in the form of support, believe and efforts to accomplish this journey.

It is an immense pleasure to express my profound gratitude towards my supervisors **Prof. Samir Dev Gupta**, Dean of Academics and **Dr. Naveen Jaglan**, Assistant Professor, Department of Electronics and Communication Engineering who graciously gave me the opportunity to work under their guidance. I am thankful to both of them for their patience, continuous support, optimistic approach, never-ending deliberations, time to time guidance and liberty throughout this course. Their valuable motivation, help, suggestion, affirmative vision, magnificent supervision and enormous confidence in my abilities made me face tough circumstances during the progress of the research work. It is a great honor to work under their supervision.

I also owe my sincere thanks to the **Prof. Vinod Kumar**, Vice Chancellor, **Maj. Gen. (Retd.) Rakesh Bassi**, Registrar and JUIT administrations for providing all the amenities and infrastructure to finish this research work.

I am greatly indebted to HOD, **Dr. Rajiv Kumar**, Department of Electronics and Communication Engineering for his kind cooperation throughout the research. I extend my heartfelt thanks to all the DPMC members **Prof. Sunil Kumar Khah**, **Dr. Salman Raju Talluri** and **Dr. Vikas Baghel** for their help, constructive remarks and valuable suggestions in every phase of this study. I would also like to express my sincere thanks to all the faculty members of Department of Electronics and Communication Engineering for the same. My special thanks are to **Prof. B. K. Kanaujia**, JNU, Delhi and **Dr. Kumud Ranjan Jha**, Shri Mata Vaishno Devi University, Katra, J&K, for providing measurement facilities in their respective laboratories.

I cannot express enough gratitude to my family members for their unconditional love and support throughout the journey. I owe my success to my grand-parents, parents **Mr. Pradeep Katoch** and **Mrs. Asha**, and Sister **Shreya Katoch**. I also express my profound thanks to my Fiancé **Akshay Sharma** for his concern and support this whole time and for being a positive driving force behind me.

I cherish all the moments spent in JUIT and my friends made it happen. Therefore, I express my special thanks to **Dr. Jyotsna, Dr. Amit, Dr. Ashutosh, Dr. Prabhat, Dr. Charu, Dr. Urvashi, Dr. Keerti, Dr. Ankush, Dr. Vikrant, Dr. Ekta, Ratish, Diksha, Pooja, Achyut, Vishakha, Garima, Swati, Anuradha, Shikha, Arvind, Rohit, Neha** and **Sameer** who not only are my seniors or colleagues but are friends to rely upon and have been in my every thick and thins. Moreover I would like to thanks my dearest friends **Ashutosh, Rahul, Mandeep, Shefali and Sunayna** for the warmth, joy and laughter they have bestowed me with during this period. Without all of their support my journey would not have completed.

Lastly, I would like to thank all those people from the core of my heart who made this thesis possible.

Kanishka

ABSTRACT

The era of wireless technology has witnessed a great demand of high data rate for end users. Ultra wide band (UWB) which ranges from 3.1 to 10.6 GHz in the electromagnetic spectrum being the utmost important band has been studied for decades and with the commercialization of this band in 2002, enormous amount of the work is carried out in this band due to the magnificent features it owns, such as, high impedance bandwidth, low power consumption and low cost. UWB frequency band has been used in various applications such as imaging, sensor data collection, indoor position systems and high accuracy radars and many more. However, various devices work in the narrow bands such as mobile WiMAX, Sub 6 GHz 5th generation (5G) frequency band, Satellite communication X-band, WLAN and Satellite communication C-band cause the interference among the closely separated narrow band operation and with UWB system. To mitigate the effect of interference the implementation of spatial filter becomes mandatory. Therefore the concept of spatial filtration comes into existence and Frequency Selective Surface (FSS) is a preferential candidate in doing so. FSSs are commonly 2 D planar periodic structures which behave as a spatial filter. To electromagnetic shield the system, the band stop filtering feature is adopted. In this work, multiple-bands as well as single bands have been band-stopped using single FSS design in order to eliminate unwanted radiations and for better functioning of the system. Various methods to develop the design parameters of the conventional SL and SSRR, and their modified versions have been explored. Moreover, in communication system as the wave impinges from any direction, therefore, highly stable frequency response regardless of the widest angle of incidence and polarization of the incident plane wave is required. Therefore, for the improvement in the scattering parameters various techniques have been implemented. Angular stability is one such characteristic which defines a good FSS. Angular stability is improved with the miniaturization of the unit cell of the FSS design. Miniaturization has been achieved using square loop (SL) and square split ring resonator (SSRR) structures and their modified versions. Triple band notched characteristic is obtained using SL and two SSRR at the bottom and top layer of the FSS substrate over the entire UWB range.

The structure resonates at 3.4, 5.6 and 7.9 GHz with a decent angular stability up to 40°. Another characteristic which is highly desirable by FSS is polarization insensitivity towards the frequency response of the given FSS, i.e., at any impinging wave whether it is TE or TM polarized similar frequency response is obtained. Symmetrical structure assures high level of polarization stability and has been implemented in the given work. Asymmetrical structure such as SSRR has been modified to symmetric structure using the 90° rotational symmetric techniques to obtain the desired frequency response regardless of the polarization. Triple band notches with polarization insensitivity are extracted using SL and rotational symmetric SSRR. The structure resonates at 3.92, 5.68 and 7.92 GHz with a good angular stability up to 70°. Another novel FSS structure has been developed which makes use of single resonant element to procure dual narrow bands using single FSS. Modification in the SSRR structure is performed by adding a metallic patch at the center of the substrate and connecting all the four SSRRs. With this the electrical length of the element increases which helps in the miniaturization of the structure further. The structure resonates at 3.08 GHz and 10.2 GHz with a good angular stability up to 75°. Further, conventional SL is applicable in controlling the bandwidth of any structure. With increase in the arm width of the structure, the bandwidth of the structure increases and with increased perimeter, miniaturization of the design is possible. This approach has been used in the designing of other two FSS designs. To make an FSS work in the UWB frequency range to serve as performance enhancer of the UWB system, a modified SL structure is presented. The structure works in the desired UWB frequency range (3.1 to 10.8 GHz). The perimeter of the structure is increased by including the outer metallic arms to reduce the size of the structure. Moreover, the bandwidth is enhanced by incrementing the width of inner metallic arms which are inserted at the edges of the simple SL. With further increment in the perimeter of the SL, the miniaturization of the structure size occurs but at the cost of reduced bandwidth. For the implementation of sub 6 GHz 5G frequency band ranging from 3.3 to 3.8 GHz, the above given approach is applied using 2.5 D FSS structure. The miniaturization of the structure is performed by increasing the electrical length of the metallic element and by implementing metallic vias

which interconnects the S-shaped and inverted S-shaped metallic elements at both the sides of the substrate. The structure provides an ultra-miniaturized structure and resonates at 3.62 GHz. The -10 dB impedance bandwidth obtained is 7.7 GHz which is achieved in between 3.2 to 3.9 GHz frequency range. Structure shows an excellent frequency response towards the varying incident and polarization angles. All the designs have been simulated in the Ansoft HFSS simulator. The validation of the results has been experimentally performed inside anechoic chamber after fabrication of each design. Equivalent circuit model (ECM) has been extracted and verified by comparing the results of full wave simulator (HFSS) with circuit simulator advanced design system (ADS).

LIST OF SYMBOLS

λ_g	Guided Wavelength inside substrate (mm)
λ_0	Free space wavelength
Z_0	Characteristic impedance of free space, 120π
Z_d	Characteristic impedance of transmission line
Γ	Reflection coefficient
P	Period of FSS unit cell
c	Speed of light in free space = 2.99792458×10^8 (m/s)
C	Capacitance (F)
dB	Decibel
ϵ_r	Dielectric constant (Dimensionless)
ϵ_{eff}	Effective dielectric constant (Dimensionless)
ϵ_0	Permittivity of free space = 8.854×10^{-12} (F/m)
θ	Angle of incidence
ϕ	Polarization angle
E	Electric Field Strength (V/m)
D	Electric Flux density (C/m ²)
f_r	Resonance frequency (Hz)
f	Operating frequency (Hz)
f_c	Cut-off frequency (Hz)
f_z	Transmission zero frequency at normal incidence (Hz)
$f_{oblique}$	Oblique angle frequency (Hz)
GHz	Gigahertz
h	Thickness of the substrate (mm)
k	Wave vector

kHz	Kilohertz
MHz	Megahertz
Q	Quality factor
R	Resistance(Ω)
S_{ij}	Scattering matrix elements
L	Inductance (H)
$Tan(\delta)$	Dielectric loss tangent
μ	Absolute permeability = $\mu_0 \cdot \mu_r$ (H/m)
μ_0	Permeability of free space = $4\pi \times 10^{-7}$ (H/m)
ω_0	Angular frequency = $2\pi f$ (rad/sec)
$E_{incident}$	Incident electric field
$E_{transmit}$	Transmitted electric field

LIST OF ACRONYMS

1 D	One Dimensional
2 D	Two Dimensional
2.5 D	Two point five Dimensional
3 D	Three Dimensional
3G	Third Generation
4G	Fourth Generation
5G	Fifth Generation
ADS	Advanced Design System
BW	Bandwidth
DRA	Dielectric Resonator Antenna
EBG	Electromagnetic Band-Gap
ECM	Equivalent Circuit Model
EM	Electromagnetic
EMI	Electromagnetic Interference
GPR	Ground Penetrating Radar
GSM	Global System for Mobile Communication
IB	Impedance Bandwidth
ITU	International Telecommunication Union
IEEE	Institute of Electrical and Electronics Engineer
FBW	Fractional Bandwidth
FCC	Federal Communication Commission
FR	Flame Retardant
AFSS	Active Frequency Selective Surface

FSS	Frequency Selective Surface
HFSS	High Frequency Structure Simulator
LTE	Long Term Evolution
MIMO	Multiple Input Multiple Output
MM	Meta-material
MPA	Microstrip Patch Antenna
RCS	Radar Cross-section Reduction
SE	Shielding Effectiveness
SL	Square Loop
SRR	Split Ring Resonator
SSRR	Square Split Ring Resonator
TE	Transverse Electric
TEM	Transverse Electromagnetic
TM	Transverse Magnetic
UWB	Ultra-Wide Band
WiMAX	World Wide Interoperability for Microwave Access
WLAN	Wireless Local Area Network

LIST OF FIGURES

Figure 1-1 Identical placement of an infinite array	4
Figure 1-2 Functioning of FSS	4
Figure 1-3 Various shapes of FSS elements [1].....	6
Figure 1-4 Representation of oblique angle with respect to the normal incidence [16].....	7
Figure 1-5 Representation of E-field corresponding to its equivalent circuit and (b) Impinging incident wave on the surface of the FSS with incident angle θ and polarization angle ϕ	9
Figure 1-6 (a) Array of a SL and (b) ECM corresponding to conventional SL design	11
Figure 2-1 Triple notched FSS design (a) Upper layer (b) Lower layer of the substrate.	28
Figure 2-2 Stages in the making of main unit cell design.....	30
Figure 2-3 Simulated results of all stages used in the making of given unit cell.	31
Figure 2-4 Distribution of surface currents on each resonant element of FSS at the three resonant notches (a) 3.4 GHz (b) 5.6 GHz and (c) 7.9 GHz.....	32
Figure 2-5 Vector surface current distribution at (a) 3.4 GHz, (b) 5.6 GHz and (c) 7.9 GHz.....	33
Figure 2-6 Equivalent circuit model	35
Figure 2-7 Comparison of frequency response curves implemented in full wave simulator and circuit simulator	36
Figure 2-8 Frequency response at varying incident angles.....	37
Figure 2-9 Frequency response curve at varying D_3	38
Figure 2-10 Frequency response curve at varying G_1	39
Figure 2-11 Frequency response curve at varying G_2	39
Figure 2-12 Fabricated FSS prototype.....	40
Figure 2-13 FSS sheet inside the anechoic chamber for the measurement of the frequency response of the proposed FSS	40
Figure 2-14 Simulated as well as measured frequency response curve at normal incident angle.....	41
Figure 3-1 Unit cell configuration	46

Figure 3-2 Stages in the making of triple band notched FSS	48
Figure 3-3 Simulated results of all steps used in the implementation of given unit cell..	49
Figure 3-4 S-parameter with respect to frequency.....	50
Figure 3-5 Surface current distribution at (a) and (b) 3.92 GHz, (c) and (d) 5.68 GHz and, (e) and (f) 7.92 GHz, respectively.	51
Figure 3-6 ECM for the given FSS design.....	52
Figure 3-7 Comparison of frequency response curve using full wave simulator and circuit simulator	53
Figure 3-8 SE with respect to frequency at $\theta = 0^\circ$	54
Figure 3-9 Impinging incident wave representation	55
Figure 3-10 Frequency response at varying angle of incidence under (a) TE and (b) TM mode.....	56
Figure 3-11 Frequency responses at varying polarization angles at (a) TE and (b) TM incident mode of wave	57
Figure 3-12(a) Change in the width of W_1 and (b) W_3	59
Figure 3-13(a) Change in D_1 , (b) D_2 and (c) D_3	59
Figure 3-14 (a) Change in G_2 (b) G_3	60
Figure 3-15 Fabrication prototype (a) top layer, (b) bottom layer and (c) FSS sheet inside the anechoic chamber for the measurement of the frequency response.....	61
Figure 3-16 Measured frequency response curves under (a) TE and (b) TM incident mode, under normal and varying incident angles	62
Figure 4-1 Design of a dual band notched unit cell FSS	67
Figure 4-2 Stages in the making of dual notched FSS design	69
Figure 4-3 Simulated results of all steps used in the implementation of given unit cell..	69
Figure 4-4 S-parameters with respect to frequency	70
Figure 4-5 For TE incident polarized wave the surface current distribution at (a) 3.08 GHz and (b) 10.2 GHz.....	71
Figure 4-6 ECM with respect to surface current distribution for individual SSRR element at (a) 3.08 and (b) 10.2 GHz	72

Figure 4-7 ECM with respect to surface current distribution for proposed FSS design at (a) 3.08 and (b) 10.2 GHz	73
Figure 4-8 Comparison of frequency response curve for full wave and circuit simulator	74
Figure 4-9 Shielding effectiveness at $\theta = 0^\circ$	74
Figure 4-10 Frequency responses at varying angle of incidence at (a) TE and (b) TM mode.....	75
Figure 4-11 Frequency responses at varying polarization angles at (a) TE and (b) TM mode.....	77
Figure 4-12(a) Change in the width W_1 and (b) gap G_1	78
Figure 4-13 Fabrication prototype (a) top layer and (b) FSS sheet inside the anechoic chamber.....	80
Figure 4-14 Measured frequency response curves under (a) TE and (b) mode, under normal and varying incident angles	82
Figure 5-1 UWB FSS design	85
Figure 5-2 Stages in the making of UWB FSS design.....	87
Figure 5-3 Simulation of various stages of UWB FSS	88
Figure 5-4 Transmission and reflection coefficient curve with respect to frequency.....	89
Figure 5-5 For the TE incident polarized wave the surface current distribution at (a) 3.1 GHz (b) 6.7 GHz and (b) 10.8 GHz.....	90
Figure 5-6 (a) Vector surface current distribution and (b) ECM.....	90
Figure 5-7 Representation of the unit cell of given FSS.....	91
Figure 5-8 Comparison of frequency response of HFSS and ADS simulator	93
Figure 5-9 Frequency responses at varying incident angles under (a) TE and (b) TM polarization	94
Figure 5-10 Frequency responses at varying polarization angles under (a) TE and (b) TM polarization	97
Figure 5-11 Change in the parameters (a) d_1 , (b) d_2 and (c) w_1	97
Figure 5-12 Fabrication prototype (a) top layer and (c) FSS sheet inside the anechoic chamber for the measurement of the frequency response.....	98

Figure 5-13 Measured frequency response curves under (a) TE and (b) TM polarized incident wave, under normal and varying incident angles.....	99
Figure 5-14 Measured frequency response curves under (a) TE and (b) TM polarized normal incident wave, under normal and varying polarization angles	100
Figure 6-1 Sub 6 GHz 5G unit cell design (a) Top, (b) Bottom, (c) 3-D and (d) Side view	105
Figure 6-2 Stages in the making of main unit cell design.....	107
Figure 6-3 Simulation of all the stages implemented for a given unit cell of FSS.	108
Figure 6-4 S-parameters with respect to frequency	109
Figure 6-5 For the TE incident polarized wave the surface current distribution at 3.62 GHz.....	110
Figure 6-6 Lumped element representation and (b) ECM with respect to surface current distribution	111
Figure 6-7 Comparison of frequency response of HFSS and ADS simulator	112
Figure 6-8 Representation of impinging incident wave on the surface of FSS	112
Figure 6-9 Frequency response for varying angles of incidence under (a) TE and (b) TM polarized wave	113
Figure 6-10 Change in the parameters (a) <i>dia</i> , (b) <i>t</i> and (c) w_1 & w_2	114
Figure 6-11 Measurement setup inside anechoic chamber	115
Figure 6-12 (a) Top View and (b) Bottom view of the fabricated prototype	116
Figure 6-13 Measured response curves w.r.t. frequency under (a) TE polarized incident wave and (b) TM polarized incident wave, for normal and oblique incident angles.....	116

LIST OF TABLES

Table 2-1 List of parameters with all values (mm).....	29
Table 2-2 Comparison with various FSS structures in literature.....	42
Table 3-1 List of all the parameters	47
Table 3-2 Triple band notched FSS compared with FSS structure in literature	63
Table 4-1 Parameters' list.....	68
Table 4-2 Comparison of dual band FSS with FSS design in literature	81
Table 5-1 Parameters' list.....	85
Table 5-2 Various unit cell FSS compared with modified SL UWB FSS.....	101
Table 6-1 Parameters' list.....	106
Table 6-2 various unit cell FSS compared with the proposed FSS.....	117
Table 6-3 Comparison of all the FSS covered in the thesis.....	119

CHAPTER 1

Introduction

With the adaptation of wireless technology a constant surge in witnessed in the utilization of microwave frequency band. Every now and then more research is carried out and new devices or equipments are getting developed. Due to potential saturation of the spectrum with devices working in narrow bands and ultra wide band, a constant need to suppress the unwanted radiation is mandatory for proper working of the system. FSS plays a vital role in this situation and is studied widely in this work.

1.1 UWB Technology

To transmit the data digitally over a wide EM spectrum UWB wireless technology plays an important key role. Earlier UWB technology was known as ‘pulse radio’ and was recognized as one of the most capable technology which could be revolutionary in the field of communication. The power density of the UWB technology is -41.3 dBm/MHz and has a very short duration of pulse of the order of pico seconds. According to Federal Communication Commission (FCC) the UWB frequency range lies in between 3.1 to 10.6 GHz with -10 dB impedance bandwidth of 7.5 GHz and fractional bandwidth of 110%. Due to this wide bandwidth and low power consumption, a large amount of data can be carried forward over a short distance. The channel capacity with respect to bandwidth and signal to noise ratio is given by Shannon’s equation:

$$C = BW \times \log_2(1 + SNR) \quad (1.1)$$

where C is the transmission data rate, BW is the channel bandwidth and SNR stands for signal to noise ratio. It is observed that the channel capacity is totally dependent on the bandwidth of the system. Moreover, the channel capacity can get enhanced by increasing the signal power. The set back in the enhancement of signal power is that the portable devices works on batteries backed by power. Consequently the only way to increase the channel capacity is by increasing the bandwidth of the device.

In relation to emitted power and magnitude, UWB system is huge in comparison to the narrow band systems. Some of the benefits of UWB system is high data rate of more than 100Mbps, low cost, low power consumption and efficient in avoiding multipath interference. UWB can be used as a carrier frequency due to wide bandwidth, therefore it offers a carrier free transmission, thus avoiding additional mixers of radio frequencies. UWB provides high isolation to distorted pulses due to its short duration pulses at receiver end. Thus it can be used to provide multipath diversity. Based upon all the above features that an UWB frequency range offers, it has been emerging in various applications. For the indoor application, the transmission of 100 Mbps and beyond is obtained within the range of 20 meters in wireless Universal Serial Bus (USB) and Wireless Personal Area Network (WPAN) for the connectivity in computers and other peripherals. It is also used in tracking as well as medical applications with the help of wireless sensor network (WSN). Other applications where UWB technology works is ground penetrating radars, surveillance systems, vehicular radar systems, through wall imaging systems and many more.

1.2 Frequency Selective Surface: An Overview

Spatial filtering is considered as one of the most required characteristic in wireless communication system. FSSs are commonly 2 D planar periodic structures which behave as a spatial filter and have high selectivity towards polarization of the incident plane wave, angle of wave incident and frequency of operation [1]. These structures either passes a given frequency band and suppress the others or vice versa. FSS offers transmission and reflection characteristics fully or partially by implementing metal or aperture over the dielectric substrate. Low pass, high pass, band reject and band pass are some of the filtering features that FSS provides. Thus, it is useful in controlling the electromagnetic propagation of the energy. Owing to the above features, FSSs are employed in frequency scanning antennas, Cassegrain sub-reflector, antenna reflector, resonant beam splitter, microwave absorbers, radome, electromagnetic shielding, polarizer, absorbers, beam switching, frequency and pattern reconfigurability and currently in wireless communication system [2]–[13]. In ideal scenario, FSS structure exhibits total transmission and reflection at fundamental resonance frequency on the

grounds of radiating element being placed over the dielectric substrate which can be metallic type or aperture type. Parameters of the unit cell of FSS such as dielectric substrate, size, geometry, inter element spacing determines the overall impedance bandwidth and resonance frequency of the given FSS. Moreover, sensitivity towards the polarization and angle of incidence of the planar incident wave is also controlled by the parameters of the unit cell. Thus, appropriate geometrical parameters are necessary to acquire the desired frequency response, as they have the potential to vary the frequency response significantly. The conventional used of FSS is filtering. However, currently FSS serves as a multi-functional device due to the variety of features it presents in various applications, apart from filtering. Some of the features that FSS owns are simple design, low profile, ease of fabrication, low cost, angular stability with huge out of band rejections [14].

1.2.1 Periodic Structure

A periodic structure is a collection of identical elements in an infinite array. Basically, incident plane wave and generators to every element of FSS are used for the excitation of passive array and active array, respectively. Floquet theorem is the base in the implementation of a periodic structure like FSS. According to the theorem, when an impinging plane incident polarized wave falls on the surface of a planar structure of identical infinite array with identical inter-element spacing ($D_x = D_y$), as shown in Figure 1.1, the current and fields are distributed equally among all the elements of the structure. Considering the impinging wave in any particular direction of \hat{a} , it is given by

$$\hat{a} = x \hat{a}_x + y \hat{a}_y + z \hat{a}_z \quad (1.2)$$

The current remains identical in an infinite FSS sheet but phase variation occurs due to finite inter-element distance and is given by

$$I_{mn} = I_{oo} e^{-j\beta m D_x a_x} e^{-j\beta n D_z a_z} \quad (1.3)$$

Thus the reference unit cell voltage is given by

$$V_{oo} = \left[Z_L + \sum_{m=-\infty}^{\infty} \sum_{n=-\infty}^{\infty} Z_{0,mn} e^{-j\beta m D_x a_x} e^{-j\beta n D_z a_z} \right] I_{oo} \quad (1.4)$$

And the impedance is given by

$$Z_L = \sum_{m=-\infty}^{\infty} \sum_{n=-\infty}^{\infty} Z_{0,mn} e^{-j\beta m D_x a_x} e^{-j\beta n D_z a_z} \quad (1.5)$$

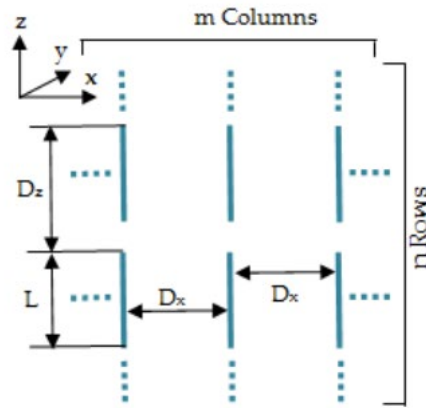


Figure 1-1 Identical placement of an infinite array

1.2.2 Principle of operational theory in FSS

When an impinging wave strikes the surface of FSS, the current gets excited inside the unit cells of FSS. Amplitude and phase of the produced current is generated in accordance with the coupling of incident wave with the FSS.

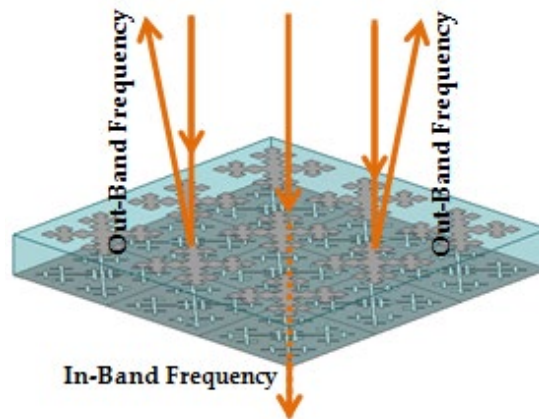


Figure 1-2 Functioning of FSS

The current generated ultimately works as electromagnetic source which produce scattered fields additionally. Incident fields and the scattered fields when combined together, produces final resultant fields. Therefore, to obtain the desired scattering parameters a proper designing of FSS is required. This is shown in Figure 1.2. For the bandstop characteristic, patch type FSS is designed and for the counterparts, aperture type FSS shows passband characteristics

1.3 Factors affecting the frequency response of FSS

The frequency response of an FSS is governed by the following the factors

1. Shape and size of element
2. Angle and polarization of the incident plane wave
3. Dielectric substrate
4. Conductivity of element

1.3.1 Shape and size of element

To obtain a desired frequency response, the shape and size of the FSS plays an important role [15]. The composition of metallic pattern over a dielectric substrate defines the type of application for which it has to be used. Various types of FSS have been studied in the literature. The FSS has been segregated in four basic groups [1]. Group-1 is the FSS elements connected through the center, thus involves dipoles, Jerusalem cross and cross dipoles. In Group-2, loop type elements are included such as square loop, circular loop and hexagonal loop. Patch type elements come under solid interior type FSS and are included in Group-3. In the last category of Group-4 combination type FSS are involved which have the combination of all the aforementioned types. All the four category of FSS elements are shown in Figure 1.3. Every shape has its own advantages and disadvantages which rests on the working application. The main characteristic of FSS is to provide a stable frequency response at various incident angles. Group-1 provides narrow impedance bandwidth. However, with adjustment in the inter-element spacing, bandwidth can be improved. Thus, selection of Group-2 is more beneficial as it provides wide impedance bandwidth. Moreover, the wavelength at the resonance is approximately equal to perimeter of the loop. In Group-3 the size of element is quiet large, therefore an

unstable frequency response is procured using the elements of Group-3. Thus size reduction of the elements is an important aspect. For this convoluted or meander line elements can be used, which falls in the category of Group-4.

Other parameters on which the resonance depends are the periodicity (P), width of the slot or patch (w) and inter-element spacing (g) [1]. The bandwidth of the structure can be increased simply by reducing the inter-element spacing. But it should be kept in mind that after a particular decrease in spacing, capacitive behavior builds up in between the closely spaced elements which drastically drags the resonance frequency to the lower part of the spectrum. Thus with the variation of the shape, size and spacing the required bandwidth and resonance can be achieved.

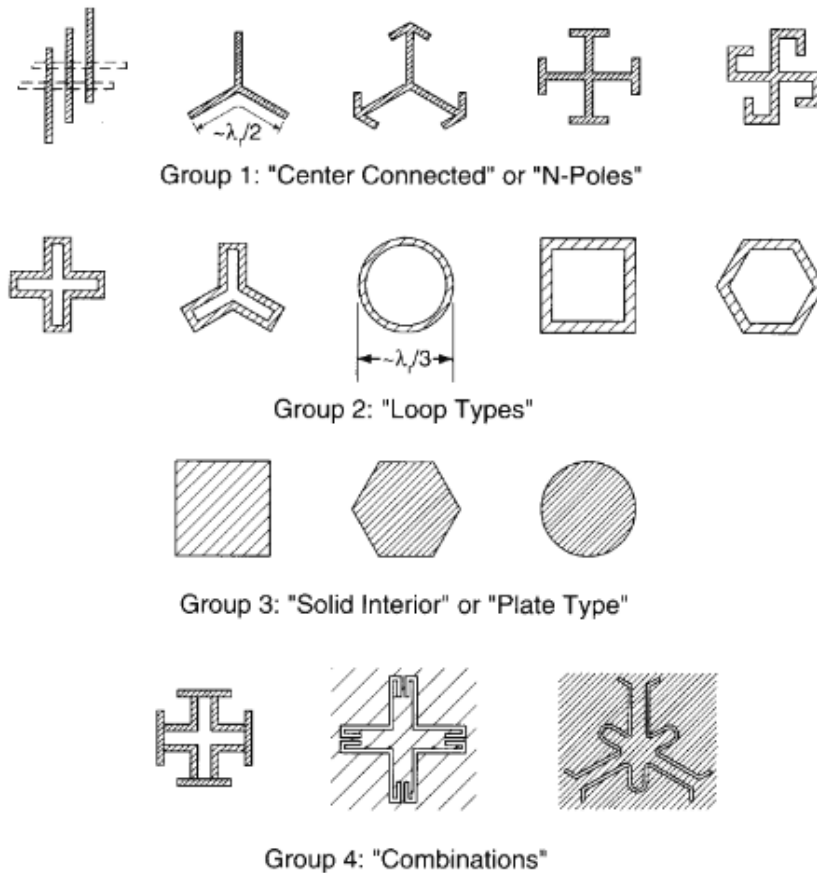


Figure 1-3 Various shapes of FSS elements [1]

1.3.2 Angle and polarization of the incident plane wave

1.3.2.1 Effect of angle of incidence

The width of the metallic element of unit cell and inter element gap between the unit cell changes by a factor of $\cos\theta$, when an incident plane wave impinges under TM or TE polarization on the surface of the FSS at varying angles, as shown in Figure 1.4 [16]. Thus, the geometrical parameter of FSS changes at varying oblique angles with respect to normal incidence [17]–[19]. In practical situation under varying environmental conditions, the wave can be impinged from any angle of incidence and thus the structure is sensitive towards varying incident angles. It is required to reduce the angular sensitivity of the FSS for better performance.

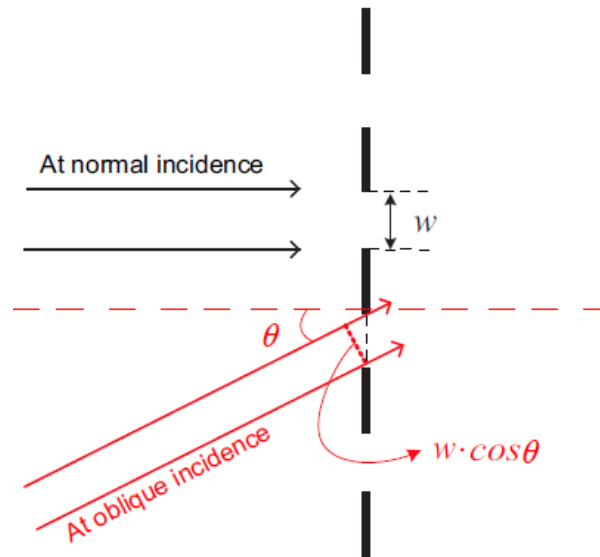


Figure 1-4 Representation of oblique angle with respect to the normal incidence [16]

1.3.2.2 Effect of incident wave polarization

The performance of the FSS also depends upon the polarization state of the incident plane wave. In this work, two polarizations, i.e., perpendicular and parallel polarization is mainly focused. When the E-field is perpendicular to the plane of incidence, then the wave is perpendicular polarized. Moreover, when the E-field is parallel to the plane of incidence, then the wave is parallel polarized [16]. Thus, if the metallic pattern or aperture pattern is not symmetrical then the structure will appear different under both the polarizations and different frequency responses will be obtained.

1.3.3 Dielectric substrate

The dielectric substrate provides angular stability with mechanical strength to the FSS structure [20], [21]. The effect of thickness of the substrate and dielectric material are interrelated on the resonant frequency of the FSS. These are divided into two sub category:

1.3.3.1 Thin layer dielectric substrate

Thin layer dielectric substrate has thickness less than 0.05λ , where λ is the corresponding resonant wavelength. When a thin layered dielectric substrate which contains the metallic pattern is excited, evanescent modes of higher order remains significantly at air-dielectric boundary. The storage energy near the FSS changes under the influence of these modes which results in varying resonant frequency and complex structure modeling. However, the effect of loss tangent is negligible at resonant frequency.

1.3.3.2 Thick layer dielectric substrate

Thick layer dielectric substrate has the thickness greater than 0.05λ , where λ is the corresponding resonant wavelength. As the dielectric permittivity increases, the resonant frequency shifts towards the lower part of the spectrum by a factor of $\sqrt{\epsilon_{eff}}$, where ϵ_{eff} is the effective permittivity and equal to $(\epsilon_r + 1)/2$

1.3.4 Conductivity of element

The surface currents are induced on the conducting metallic pattern with impinging incident wave. From the metallic patterns these induced current gets reradiated in the same way as the conductive strips inside rectangular waveguide [22]. In ECM, for the perfect electric conductor (PEC) no losses occur due to the conductor, therefore the circuit is represented by a combination of LC. However, the losses due to power dissipation occur in lossy metallic pattern which affects the frequency response of the FSS. The ECM gets changed and resistive lumped element is added to showcase the lossy behaviour of conductivity of element. In this thesis, copper of the thickness of 0.035mm have been implemented.

1.4 Conventional filtering geometries and relevant equivalent circuit

Full wave circuit simulators have been used in for the extraction of the frequency response accurately, but to understand the physical insight of the given design, the development of ECM is essential. Inductive strip grating and SL is the most common geometry to design a bandstop FSS.

1.4.1 Strip grating

One of the basic structures of FSS is a strip grating structure. Inductive and capacitive strip grating is extracted when the E-field is along and perpendicular to the metallic strip, respectively, as represented in Figure 1.5. When the E-field is polarized parallel and perpendicular to the plane of incidence, transverse electric (TE) and transverse magnetic (TM) incident polarization occurs, respectively. Thus the structure is modeled for TE and TM incident polarization.

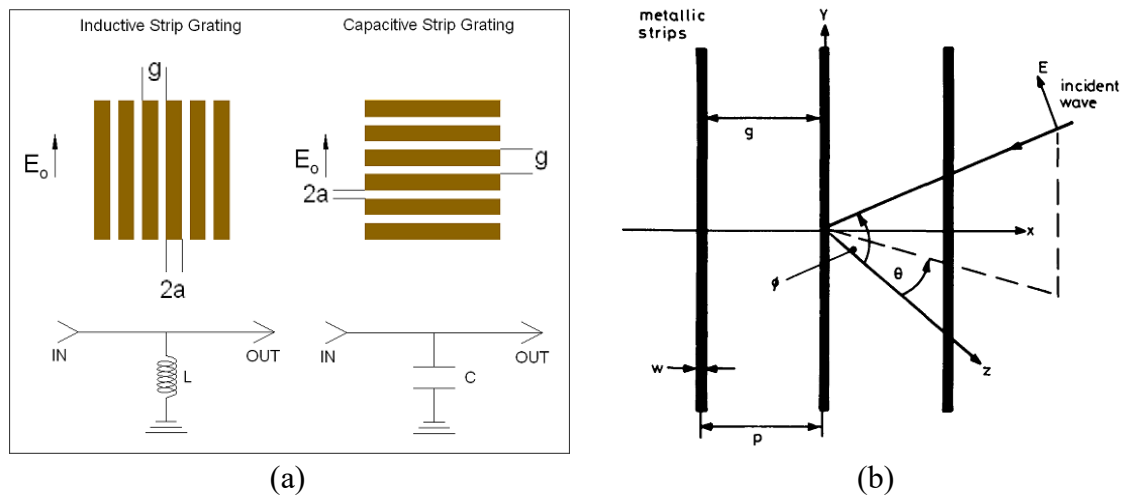


Figure 1-5 Representation of E-field corresponding to its equivalent circuit and (b) Impinging incident wave on the surface of the FSS with incident angle θ and polarization angle ϕ

For the inductive strip under TE polarization, the normalized shunt inductance is given by [23]:

$$X_{TE} = \frac{w_r L}{Z_o} = F(p, w, \lambda) = \frac{p}{\lambda} \cos \theta \left[\ln \left(\cos ec \left(\frac{\pi w}{2p} \right) \right) + G(p, w, \lambda, \theta) \right] \quad (1.6)$$

Further for the capacitive strip, the normalized shunt capacitance is given by

$$B_{TE} = \frac{w_r C}{Y_o} = 4F(p, g, \lambda) = 4 \frac{P}{\lambda} \sec \theta \left[\frac{p}{\lambda} \ln \left(\csc \left(\frac{\pi g}{2p} \right) \right) + G(p, w, \lambda, \theta) \right] (\epsilon_{eff}) \quad (1.7)$$

where correction factor is given by

$$G(p, w, \lambda, \theta) = \frac{(1 - \beta^2) \left[\left(1 - \frac{\beta^2}{4} \right) (A_+ + A_-) + 4\beta^2 A_+ A_- \right]}{\left(1 - \frac{\beta^2}{4} \right) + \beta^2 \left(1 + \frac{\beta^2}{2} - \frac{\beta^4}{8} \right) (A_+ + A_-) + 2\beta^6 A_+ A_-} \quad (1.8)$$

$$A_{\pm} = \frac{1}{\left[1 \pm \frac{2p \sin \theta}{\lambda} - \left(\frac{p \cos \theta}{\lambda} \right)^2 \right]^{1/2}} - 1 \quad \text{and} \quad \beta = \frac{\sin \pi w}{2p} \quad (1.9)$$

Since in a periodic structure, there is discontinuity in the inductive strip and capacitive strip, thus the reactance' are decreased by d/p factor and shown as follows

$$X_{TE} = \frac{d}{p} F(p, w, \lambda) \quad \text{and} \quad B_{TE} = 4 \frac{d}{p} F(p, g, \lambda) \quad (1.10)$$

The effective permittivity is given by:

$$\epsilon_e = \frac{\epsilon_r + 1}{2} + \frac{\epsilon_r - 1}{2} \cdot \frac{1}{\sqrt{1 + \frac{12t}{w}}} \quad (1.11)$$

The grating lobes are eliminated by:

$$p(1 + \sin \theta) < \lambda \quad (1.12)$$

where g , w , p , Z_o , Y_o and d are the gap in between two adjoining FSS unit cells, width of each arm of the metal, periodicity of FSS, characteristic impedance and admittance, and length of the arm, respectively. λ is the corresponding resonant wavelength and θ is the impinging angle of incidence.

1.4.2 Square loop (SL)

With the help of ECM, SL is segregated into inductive and capacitive part with E-field along single direction. When the incident E-field is parallel to the metallic strip, the electrons inside the metallic strip starts to oscillate. As a result surface current flows and the structure shows inductive behaviour. Further, when the E-field is perpendicular to the horizontal metallic strip, due to the separation of charges over the surface of the metal, the structure behaves as a capacitor [16]. The SL is modeled as shunt connection of series LC circuit, as shown in Figure 1.6.

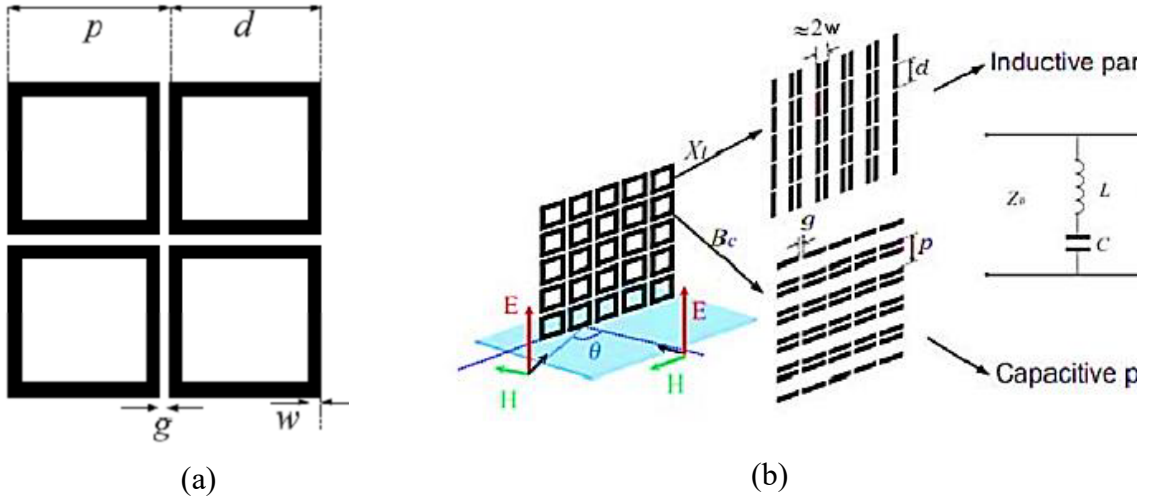


Figure 1-6 (a) Array of a SL and (b) ECM corresponding to conventional SL design

The normal shunt inductive reactance and capacitive susceptance for the discontinuous arm lengths is given by [24]:

$$X_{TE} = \frac{X_f}{Z_o} = \frac{d}{p} F(p, 2w, \lambda) = \frac{d}{p} \times \frac{p}{\lambda} \cos \theta \left[\ln \left(\cos \operatorname{ec} \left(\frac{\pi w}{p} \right) \right) + G(p, w, \lambda, \theta) \right] \quad (1.13)$$

$$B_{TE} = \frac{w_r C}{Y_o} = 4 \frac{d}{p} F(p, g, \lambda) = 4 \frac{d}{p} \times \frac{p}{\lambda} \sec \theta \left[\frac{p}{\lambda} \ln \left(\operatorname{csc} \left(\frac{\pi g}{2p} \right) \right) + G(p, w, \lambda, \theta) \right] \epsilon_{eff} \quad (1.14)$$

The correction factor is given in the equation 1.8 and 1.9.

1.5 FSS Requirements

For the implementation of a good performing FSS, three major requirements are as follows:

1.5.1 Miniaturization of the FSS

The implementation of the FSS design is done by considering it as an infinite set of unit cells arranged in a periodic manner. However, in practical case only finite number of unit cells is involved in the creation of FSS sheet in a given space. To obtain an ideal filtering behaviour in the practical FSS, miniaturization of FSS is required. Moreover, the occurrence of grating lobes gets reduced with the implementation of miniaturized unit cells with edge diffraction avoidance. The techniques such as meta-materials (MM), fractal, meander lines, convoluted structures are useful in the miniaturization of unit cell. Moreover the implementation of multilayer, 3D and 2.5 D FSS structures are also effective in size miniaturization.

1.5.2 Angular stability characteristic

All of the applications which make use of FSS require high angular stability. With angular stability, it is meant to have highly stable frequency response at varying angle of incident plane wave. The property of the FSS is influenced by the geometry it carries. Therefore, with the miniaturization of the FSS and confinement of large unit cell in a limited area angular stable characteristic of the FSS is assured.

1.5.3 Polarization insensitive characteristic

As defined earlier, the direction of polarization of a given plane incident wave is defined by the orientation of E-field in the free space. The plane incident wave can be Transverse Magnetic (TM) or Transverse Electric (TE) in orientation. In most of the applications identical frequency curves with respect to TE and TM incident polarized wave is demanded because FSS deployed practically can get excited by the wave of any orientation. It is required to produce similar responses to any incident wave mode. Conventional structures such as dipole have high level of polarization sensitivity.

Therefore, the implementation of symmetrical geometry of the unit cell is highly required to obtain a polarization insensitive behaviour.

1.6 Related work

FSS is a multifunctional device which offers various featured applications from microwave frequency to terahertz regime in the whole electromagnetic spectrum [25]–[31]. It is used in the performance enhancement of an antenna, elimination of EM interference and designing of radomes and many more. Additionally, it is helpful in the satellite communication[32]. FSS is also used in the segregation of the closely separated bands by isolating a given band with high level of attenuation [33]. In optical frequency range FSS have been used as solar energy collector, beam splitter and polarizer [34], [35]. However in microwave frequency for a significant functioning, steady response curves with respect to frequency is required at varying incident angles under varying wave polarizations [36]. This disparity is controlled by implementing miniaturized and symmetric structures. To obtain the ideal characteristic of FSS, a complete knowledge of transmission and reflection through the FSS is required. In this section different approach to obtain angularly stable and polarization insensitive behaviour of the FSS has been studied. The impedance bandwidth of the structure for stop band and pass band is quantified by considering the reference threshold of -10 dB for both the transmission and reflection coefficient curve, respectively, in the entire thesis.

1.6.1 Single layer FSS

Single layer FSS is a combination of two-dimensional array of planar periodic structure, in which only single layer of substrate is used. The space is limited in this approach to the top and bottom layer of the substrate, thus structure such as meander lines and convoluted elements provides miniaturization [37], [38], [39]. Circular and square loop elements are printed over the RO3010 dielectric substrate to decrease the EMI in S-, C- and X-bands by more than 20 dB [40]. The dimension of the structure is 0.15λ which is 90% compact than the conventional FSS structure. λ is the center wavelength of the desired frequency bands. The angular stability of 80° is achieved under both the polarizations and a fractional bandwidth of 120% is obtained. A convoluted swastika structure is used in the

miniaturization of the structure to the dimension of 0.095λ to provide a stable frequency response till 60° and fractional bandwidth of 9 % under both TE and TM polarization [41]. An interwoven convoluted element of cross dipole is implemented to shift the resonant frequency 15 times for a single layer surface [42]. In [43], the unit cell dimension is reduced to 4.84% of the λ at resonant frequency. The structure provides dual bandpass at 2.5 GHz and 4.95 GHz with high quality of polarization insensitivity and angular stability. In [44], tri-band pass convoluted FSS design is implemented to operate at 3.28, 4.2 and 5.4 GHz with the unit cell dimensions of 0.066λ . At the top layer, four branched triangles are used and interconnected at the center whereas in the bottom gridded tortuous cross-dipole is implemented to produce highly stable frequency response under both the polarizations. In [45], meander lines are imprinted at both the layer of substrate to provide a miniaturized structure of 0.017λ dimensions. The structure exhibits a pass band at 750MHz.

Another approach to reduce the FSS size is the implementation of metamaterial (MM) which with the help of negative permeability and permittivity reduces the size of the FSS [46]. In [47], a MM based on swastika shaped metallic element is presented which shows negative permeability and permittivity at distinct frequency range. In [48], to band reject the WLAN at 2.45 GHz and 5 GHz, at both the layers of the dielectric substrate folded edges mirrored C-shaped element and mirrored C-shaped element is imprinted. The structure shows angularly steady response for the structure up to 50° regardless of polarization of the incident wave. To obtain triple band rejection at 2.4, 5.2 and 5.9 GHz, an F-type resonant element antipodal to each other are implemented with a SL at the top layer [49]. The structure provides an angular stability of 60° in both the polarizations.

1.6.2 Multilayer FSS

It is a challenge to obtain a desired operating bandwidth with high angular stability at wide incidence angle. This problem can be solved by stacking multiple layers in FSS together [50]. For the improvement of the impedance bandwidth the use of multilayer FSS become a better option. Wideband response is obtained using multilayer FSS because of the discontinuity in between the layers of FSS. With higher order multilayer FSS, faster roll-off and better frequency response can be acquired in comparison with

single-layer FSS. In [51], two dielectric substrates are sandwiched between three metallic layer. The upper and lower metallic layer consists of metallic patches and the middle layer comprises of a metallic grid. The given structure band rejects the frequency ranging from 5.85 to 18.45 GHz and has an -10 dB impedance bandwidth of 12.6 GHz. Cross and square patch metallic elements have been implemented on the metallic layers to band stop 3.49 to 12.13 GHz frequency band and also provides has a good angular stability towards various impinging incident angles [52]. Two substrate layers are stacked in between three metallic layers, in which top and bottom metallic layer comprises of metallic square patch whereas the middle layer consists of split ring shaped aperture. The design provides resonant notches at 2.5, 5 and 6 GHz. Meanwhile the structure also works as pass band at 3.6 GHz and is polarization independent [53]. In [54], a multilayer resonant element is implemented which comprises of inductive meandering grid and circular rings. A fifth order ECM is extracted over the band of 0.1 to 8 GHz. The dimension of the structure is 0.0263λ at the start of resonant frequency. A variety of dielectric material have been cascaded together to make a multilayer novel FSS structure [55]. The structure is miniaturized to $0.012\lambda \times 0.012\lambda$, thus produces a high level of angular stability till 75° for dual polarized bandpass FSS at 1.96 GHz. A second order bandpass FSS has been developed to obtain fast roll-off and flat in band frequency response [56]. With a non resonant inductive layer, compact resonant surfaces are coupled to operate at 3.8 GHz with highly stable frequency response. The dimension of the given design is $0.076\lambda \times 0.076\lambda$ with the thickness of material less than $\lambda/24$. The main issue with the multilayer FSS is that the thickness of the substrate in most of the cases is of the order of $\lambda/4$, which is not at all applicable. Thus a tradeoff occurs in between the size and frequency response. As the number of layers increases a much wider bandwidth and smooth roll off is achieves but at the cost of complex, costly and bulky structure.

1.6.3 3-Dimensional FSS

To obtain fast roll off with miniaturized design, 3D FSS are of great advantage [57], [58]. 3D FSS are the modification to the 2D FSS structures which adds extra layer of structures and cavities over a simple FSS design for the miniaturization of the structure[59]. 3D

FSS provides high angular stability towards the frequency response with high level of polarization insensitivity [60]. In [61], 3D FSS is designed over a multilayer printed circuit board using via holes. The structure provides a highly stable frequency response till 60° at dual polarization. A reconfigurable 3D FSS is developed from concentric threaded cylinder [62]. The structure bandstop L- and S- band and by sliding the inner cylinder, reconfigurability is obtained from 1.86 to 3.10 GHz. A high degree of freedom in bandwidth adjustment and frequency is obtained using dual band 3D FSS [63]. In [64], a simple square coaxial waveguide is used, and center gaps, H-shaped slots and via holes have been deployed to obtain multiple transmission poles and zeros. A sharp roll off is obtained in between the two pass bands with a transmission zero in between. A stable frequency response is obtained under both the polarization. In [65], water transfer printing technology is used to implement a high quality metallic pattern layer of a 3D FSS. The use of water surface tension technique in absence of solid planar structure, keeps the metallic pattern floating flat. However, the structure is polarization selective in nature. It is observed from all the aforementioned designs that the maximum frequency deviation of resonant frequency at normal incidence and widest angle of incidence is almost negligible in comparison to single layer FSS. However, the design and fabrication of the 3D FSS are quiet complex and expensive.

1.6.4 2.5- Dimensional FSS

2.5 D FSS are the new class of FSS which has been extensively studied in the literature. The setback of the 2D FSS is the limitation of element space over one side of the substrate, which does not allow further miniaturization [66]–[70]. 2.5 D FSS structures make use of metallic vias etched inside the substrate to interconnect the metals placed at both the sides of the substrate to enhance the path length of the element for further miniaturization of the FSS structure [71]. An ultra-miniaturized design is developed by making use of 2.5 D closed loop structure. Four metallic vias have been used to interconnect the metals at both sides of the substrate with a dimension of $0.048\lambda \times 0.048\lambda$ [72]. A highly stable frequency response is obtained. A knitted double square loop are realized in a $0.072\lambda \times 0.072\lambda$ 2.5D geometry, to bandstop 900 and 1790 MHz band [73]. A high shielding effectiveness of 41.9 dB and 49.2 dB is obtained for GSM 900/1800 band.

The resonant notches are highly stable at wide incidence angles under varying polarization till 60° . An active multifunctional 2.5D FSS consisting of four similar sub cells based on unitary element is designed to miniaturize the unit cell to $0.63\lambda \times 0.63\lambda$ dimensions [74]. Due to this, these structures provide a very high level of stability in the frequency response. With the help of PIN diodes, four independent operating states are realized. In [75], a hexagonal shaped metallic arms are interconnected using vias to obtain an UWB ranging from 1.97 to 8.08 GHz. In [76], surface integrated waveguide is used to design 2.5 D FSS to improve the angular stability and bandwidth. Square loop and Jerusalem cross are the two shapes realized in this work. In [77], an ultra-miniaturized design is developed using convoluted segments at both the side of the substrate and connected with metallic vias. The structure provides the degree of freedom in multiband performance and size. In [78], the design is made of knitting a square loop structure using both the metallic surfaces. The structure resonates at 1.9 GHz with an angular stability of 60° . In [79], a closed loop meander line pattern is presented in which the vias are connected at the corner of the lines. The dimension of the design is $0.053\lambda \times 0.053\lambda$ and resonates at 1.6 GHz with a narrow band characteristic. A similar approach of using tapered meander lines and knitting it using vias at both the side of the substrate provides a 2.5 D FSS structure [80]. The structure is ultra-miniaturized to $0.026\lambda \times 0.026\lambda$ with resonance at 2 GHz. The structure provides a highly stable frequency response at widest incident angle. In [81], convoluted lines in the spiral shape are implemented in a 2.5D structure by the use of vertical vias. The size of the structure is reduced to 2.7% of resonant wavelength at 2.8 GHz. The structure shows an excellent angular stability till 75° with negligible deviation in the resonant notch. 2.5D FSS is a fair compensation between 2D and 3D FSS structures, as 2.5D FSS provides ultra miniaturized design with better frequency response, and lesser bulky structure with less complex design than 2D FSS and 3D FSS, respectively.

1.7 Applications of band stop FSSs

1.7.1 Spatial Filtering

Spatial filtering finds a special place in the implementation of antennas and radomes. However, one of the most important features is to avoid any unwanted radiation from

other working systems. FSS provides band stop and band pass characteristics using metal and aperture over the substrate, respectively [82]. Various systems work in the narrow bands, and single bands and multiple bands are obtained using FSS filtering. A swastika shaped metallic element is used to band reject WLAN frequency range to provide an impedance bandwidth of 400 MHz [83]. To obtain dual bandstop behaviour, a metallic square patch with L-shaped arms is implemented over a dielectric substrate [84]. Upper resonant frequency is obtained by horizontal arms, and vertical arms are responsible for lower resonant frequency. An SL and modified SL with attached metallic arms is imprinted at both the layers of the substrate to provide triple band rejection [85]. Further, penta band rejection is obtained using multi-resonant structure at both sides of the substrate [86]. The structure band rejects PCS, Wi-Fi, CBRS, WLAN and X-band downlink satellite communication band. For the designing of band pass filter, Babinet's principle is applied which provides complementary operation towards the band stop filter [87].

1.7.2 Reconfigurable FSS

For the futuristic wireless communication the need of switching in between different generations of communication system is necessary for easy adaption of any system using less complex system. Considering this, reconfigurability is a smart option [88]–[93]. Reconfiguration works on the principle of changing the current distribution of the radiating element. With the change in the field distribution, the radiation properties and impedance of the structure changes eventually, this ultimately changes the frequency response of the structure. Frequency response [94], polarization [95] and radiation pattern [96] are some type of reconfigurations. Reconfigurable FSS works by integrating the given FSS with active devices such as PIN diode, which uses external DC bias source to rapidly switch ON and OFF the FSS accordingly [97]. FSS becomes a source of incident wave transmission in ON state whereas highly reflective surface in OFF state [98]–[100]. A cylindrical active FSS (AFSS) is surrounding a dipole antenna in [101]. AFSS comprises of 10 circular metallic loops per column and are inserted with metallic strips. During the OFF state, two stop bands are obtained due to the metallic strip and metallic loop. However in the ON state, only a single stop band is obtain because of the presence

of the metallic loop. A similar structure of using cylindrical AFSS made of discontinuous split-ring resonator (SRR) is designed to cover omnidirectional antenna to obtain frequency reconfigurability [102]. For dual band reconfigurability an AFSS is designed in [103]. To avoid the complex bias network in PIN diodes, a hexagonal shaped cantilever enabled FSS is mounted over a cylindrical DRA for dual plane beam sweep [104]. In [105] Eutectic gallium indium (EGaIn) is poured inside the micro-channels of elastomeric substrate which is of a meander line shape to obtain pattern reconfigurability.

1.7.3 Isolation in MIMO Antennas

MIMO has been chosen in 4G and beyond communication to reduce the effect of multipath fading. Moreover, reliability and data rate enhances by sending multiple data streams. However, the coupling in between the ports and closely placed MIMO antennas increases, which require low correlation level and high port isolation [106]–[114]. A Jerusalem cross and FAN shaped metallic elements is inserted on the upper and bottom side of the dielectric substrate. The given design provides resonant frequency at 48 GHz and 60 GHz [115]. The FSS when used with 60 GHz dielectric resonator antenna reduces the effect of mutual coupling to a great extent. An FSS wall is mounted in between the MIMO antennas in [116] to provide isolation of 30 dB by reducing free space radiation. The gain gets enhanced by 1.5 dB using the FSS design. A good isolation of 20 dB is attained by a Y shaped slot and FSS structure implemented over a MIMO antenna [117]. To avoid the overlapping of radiation pattern in a closely placed two-element Fabry-Perot cavity MIMO antenna, practical reflective surface (PRS) have been used [10]. For decorrelation in four element DRA MIMO system, two DRs are placed at the top of the substrate whereas two below the substrate orthogonally [118]. PRS of triangle shape is implemented as the superstrate to all the DRAs to provide a gain of 7.2 dB, ECC up to 0.1 and efficiency of 81%. Port isolation of 20 dB is also obtained. Without the use of PRS layer, the structure produced a gain of 4.9 dB, ECC of 0.31 and efficiency of 89%, which are not acceptable enough.

1.7.4 Electromagnetic Shielding

Electromagnetic shielding becomes necessary in order to reduce the interference in between the devices [119]. The shielding effectiveness is given by [120]:

$$SE(dB) = 20 \log_{10} \left| \frac{E_{incident}}{E_{transmitted}} \right| \quad (1.14)$$

and is defined by the ratio of incident E-field to transmitted E-field. Due to the good reflection and transmission property, FSS is best suited for the given application. With an attenuation of signal more than 56 dB, a modified SL is designed to band reject entire X-band [121]. The structure shows a stable frequency response and high degree of isolation from the neighboring frequency bands. On both the sides of dielectric substrate ring and cross shaped metallic elements are imprinted [122]. The structure resonates at 7.5 GHz and provides shielding effectiveness of 20 to 35 dB.

1.7.5 Performance enhancement of antennas

Applications such as ground penetrating radars (GPR), high resolution medical imaging and communication require narrow beam and high gain antennas. However, conventional antennas cannot provide enough gain. Thus, many techniques have been implemented in improving the gain and the use of FSS is one of its kinds. When an antenna is collaborated with FSS, the gain and impedance bandwidth of the antenna increases with high level of filtration [123]–[126]. The gain of the antenna with FSS gets enhanced due to the constructive interference created by reflection of the EM wave in between antenna and FSS layer. In [127], FSS is implemented as a back reflector in order to extend the operating frequency band range. The gain gets enhanced due to the constructive addition of wave reflections in between antenna and FSS. Moreover, impedance bandwidth of the antenna does not get disturbed. In [128], a high gain of 9.5 dB is attained in UWB frequency range by mounting dual- polarized radiator over FSS back reflector surface. To improve the gain with good front to back ratio, FSS is positioned in between ground plane and connected dipole antenna array [129]. Multilayer FSSs have also been used in attaining high gain. Below antenna, dual layer of FSS has been implemented in which one layer reflects at lower frequency band and other at higher frequency to provide a wide impedance bandwidth at UWB frequency range with high gain [130]. An average gain of 7.8 dB is obtained with 122% fractional bandwidth. In [131], four layers of FSS have been used below a patch antenna for the improvement of gain from 4 dBi to 9.3 dBi.

Without FSS the bandwidth of 145 % is obtained in comparison to 149 % obtained with the use of the FSS, which is well inside the substantial limits.

Various conformal FSS have also been used for the performance enhancement of the antennas [132]. A hybrid monopole DRA is surrounded by a conformal FSS which works as a parabolic reflector and placed at a distance of half wavelength from the antenna [133]. The structure provides an improved gain of 5-6 dBi and impedance bandwidth of 27% in 4-6 GHz frequency band. Other method of the placement of FSS is as a superstrate to a given antenna [132][59]. The peak gain of 22.5 dB with improved impedance bandwidth of 145% is attained by inserting an FSS as superstrate over electromagnetic band-gap (EBG) antenna [132]. Moreover, integration of FSS with antenna also reduces the inference which occurs due to the presence of feedline in a given antenna system [134].

1.7.6 FSS radomes

To hinder the vulnerability of antennas and radar system from physical environment, radome came into being, which is placed around these systems for the protection against physical wear and tear through its protective layer [135]–[139]. In various commercial and military applications, FSS radome can work as passband, absorption band and reflection band [140]–[142]. Radar cross section (RCS) reduction is one of the most important features required by the FSS radomes in stealth technology and detection. The unique dome shape of the radome, reflect backs the signal in different direction making the signal strength weak. FSS radomes can also be used in telemetry, weather forecast, surveillance and radio astronomy. In [137], the results of dielectric radome with monostatic RCS of FSS radome are compared. It is observed that FSS radome controls the RCS of the antenna better than dielectric radome. Over a monopole antenna, a conical thick screen FSS radomes is positioned to control RCS and to achieve narrow frequency response [138]. For RCS reduction reconfigurable AFSS are also developed [143]. PIN diode is used to switch between the ON (bandpass) and OFF (bandstop) state to enable FSS reflector around 3.8 GHz. Therefore, it is inferred that the RCS reduction using hybrid FSS is way better than the dielectric radomes.

1.8 Motivation

In the current era of adapting new techniques and technology in the field of communication, high data rate has become an ultimate goal. UWB frequency range which lies in the microwave frequency regime provides a very high impedance bandwidth of 7.5 GHz and various UWB, wideband and narrowband antennas work in this particular frequency range. The idea is to work upon this wide impedance bandwidth is to obtain high data rate with short latency. Therefore, UWB frequency range is much better option to work and due to its commercialization any researchers can work upon this frequency band without any hassle. Owing to this various narrow band applications are working in the frequency range of UWB band, such as WiMAX, WLAN and various satellite communication bands have also been in use such as, Satellite communication C-band and Satellite communication X-band. Recently, sub 6 GHz 5th generation (5G) communication band is also allocated in the frequency range of UWB. These narrow band applications are very important in the aspect of wireless communication. Hence, a massive research has been carried out in the field of communication with numerous devices working over the entire UWB frequency range, which makes the band congested. Therefore, to work upon the entire UWB frequency and narrow band applications without any disturbance created by each other on one another's work, electromagnetic shielding of each device is mandatory for the performance enhancement of each application.

1.9 Research Problem Formulation

With the implantation of various electrical and electronic devices and many getting implanted to work in the major narrow band applications such as, WiMAX (2.5 – 2.7 GHz and 3.3 – 3.6 GHz), Sub 6 GHz 5G band (3.3 – 3.8 GHz), Satellite communication C-band (3.7 – 4.2 GHz), WLAN (5 – 6 GHz), Satellite communication X-band (7.2 – 8.4 GHz), the risk of UWB overburdening has exponentially increased and is in the way of saturation. Apart from narrow band radiating sources, various wide band and UWB antennas are also implemented for the performance enhancement for all the applications working in UWB regime. Due to this clustering of devices in a confined band, the devices works at very closely separated narrow band frequency ranges. Therefore, with more number of operating devices and radiating sources, the EMI among the sources

increases. Further it leads to increased mutual coupling in between the devices. Overall, the major impact of this situation occurs upon the functioning of any system and resultant is performance degradation. The peaking urge of EMI reduction in between the devices operating in narrow bands as well as entire UWB band and efficient utilization of UWB has demanded the need of electromagnetic shielding or to obtain bandstop characteristic. Multi-resonant 2D FSS elements with multi bandstop feature are a great option in eliminating the disturbance created by the narrow band devices in UWB system. It can also be used in providing isolation among narrow band systems and the systems which operates at multiple frequency bands. Moreover, frequency response of conventional FSS is sensitive towards polarization and incident angle of the plane wave, which is highly undesirable. Theoretically FSS is an infinite sheet thus provides a steady response at varying angle of incidence but in actual case the space is confined and therefore if the largely sized unit cell is implemented, the effective size of FSS sheet becomes large and due to the edge diffraction, a steady response curve at wide varying angle of incidence is not possible. Large number of miniaturized unit cell when placed in a given array behaves as an infinite array and high angularly stable response is procured. This miniaturization can be performed with the help of the modified structures, which increases the effective inductance and capacitance of the structure and further helps in the attainment of lower resonant frequency and smaller dimensioned structure. Another aspect is to incorporate polarization insensitive behaviour of FSS under TE or TM polarization, i.e., to obtain identical response for the impinging incident TE or TM polarized signal under varying environmental conditions. For this symmetric structures are implemented as they present isotropic medium behaviour which means that the designed prototype will appear similar from any impinging angle of incidence. Many structures make use of multi-resonant elements to obtain multiple stop bands. However to ease out the fabrication and cut the cost, multiple stop can be obtained using single resonant element with design modification. There are many recent applications such as 5th generation communication system which require a very precise angular stability curve with very narrow frequency band. Therefore, an ultra-miniaturized FSS is required in which with increase in the inductance, the resonant frequency shifts downwards and band becomes narrower. However, the element length in conventional FSS stagnate over one

side of the substrate. With the use of 2.5 D closed loop FSS, the elements at both the layers get interconnected using metallic vias etched inside the substrate and ultra-miniaturized structure with narrow bandwidth can be obtained.

1.10 Research gaps

With the aforementioned techniques and extensive study of the literature some of research gaps are listed below.

1. The main set back is the EMI among the various narrow band devices separated by a very close proximity, with UWB system and the systems which operates at multiple frequency bands. There is need to avoid the interference created by unwanted radiation or leakage from a given system. Therefore, a single multi-resonant FSS structure is required to bandstop few highly used frequency bands such as Satellite communication X-band (7.2 – 8.4 GHz), WLAN (5 – 6 GHz) Satellite communication C-band (3.7 – 4.2 GHz) and WiMAX (2.5 – 2.7 GHz and 3.3 – 3.6 GHz).
2. To achieve angularly stable and polarization insensitive frequency response from a given FSS design, miniaturization and implementation of a symmetric structure are the major requirement, respectively. This problem can be resolved by implementing a square loop (SL) and rotational symmetric square split ring resonator (SSRR), as resonating elements.
3. Another challenge is to extract multiple resonant bands using single resonant element. To achieve this rotational symmetric SSRR structure is used with metallic patch attached at the center of the structure connecting all the four SSRRs.
4. For all in one performance enhancement of UWB antennas and various narrow band applications such as Satellite communication X-band, WiMAX, WLAN and Satellite communication C-band, an UWB FSS is required.
5. Some recent applications such as sub 6GHz 5G communication system require a highly stable frequency response with very narrow bandwidth. For this, an ultra-miniaturized structure is required which can be achieved using closed loop 2.5 D FSS

structure.

1.11 Research Objectives

Based on these research gaps, different objectives are framed as follows:

1. To design a compact triple band notched FSS using SL and SSRR at UWB frequency range.
2. To design a compact polarization insensitive triple band notched FSS using SL and rotational symmetric SSRR at UWB frequency range.
3. To design a compact polarization insensitive dual band notched compact FSS using a modified rotational symmetric SSRR over single sided substrate
4. To design a simple yet miniaturized polarization insensitive UWB FSS for improvement in the UWB antenna performance.
5. To design ultra – miniaturized 2.5 D FSS for sub 6 GHz 5G communication system.

1.12 Thesis Orientation

The reset of the presented work is listed below:

Chapter 2 discusses implementation of conventional SL and SSRR structure to bandstop narrow bands such WIMAX, WLAN and Satellite Communication X-band from closely separated bands and with UWB frequency band. The principle of operation has been discussed. Ansoft HFSS is used as the full wave simulators and fabrication of 18×18 elements over a 190×190 mm² substrate is performed. The design is experimentally validated inside anechoic chamber.

Chapter 3 enables the polarization insensitive behaviour of the FSS. With SL, 90° clockwise rotational symmetric SSRRs have been implemented over either sides of the substrate to triple bandstop WIMAX/ Satellite Communication X-band, WLAN and Satellite Communication X-band over UWB frequency range. The working mechanism is further studied and has been supported by the extraction of surface current distribution followed by an equivalent circuit model (ECM). The frequency response in

correspondence to incident angle and polarization angle variation is procured. The results are observed for TE and TM polarization as well. The fabricated prototype and the measured results are also observed in this study.

Chapter 4 shows further miniaturization of the effective dimensions of the unit cell. Rotational symmetric SSRR has been implemented over one side of the substrate with metallic patch attached in the middle of the substrate connecting all the four SSRRs. The design is supported with working mechanism using surface current distribution and ECM. The simulation is performed to obtain response curves of frequency for varying angles of incidence and polarizations. The validation of the results has been performed after fabrication and testing under anechoic chamber.

Chapter 5 showcases a modified SL structure. The designing of the structure is done to cover the UWB frequency range. The modification of SL is performed by inserting identical outer and inner arms at the edges of the conventional SL structure. The working principle of the given design is illustrated. ECM is extracted by studying the effect of surface current distribution over the design and the ECM is then developed in circuit simulator software. The comparison of the S-parameters of HFSS and advanced design system (ADS) has been shown in the presented work for the verification. Further, the results of measurement are also illustrated in the chapter.

Chapter 6 shows another SL modification with the help of four metallic vias in a 2.5 D FSS structure for ultra-miniaturization of the unit cell. S-shaped and inverted shaped metallic element is implemented at either side of the substrate. Both the layers are interconnected with metallic vias etched inside the substrate. The working mechanism is presented with surface current distribution and ECM. The simulated results of developed ECM in ADS and that of HFSS are also compared. The frequency response for varying polarization and incident angle, and TM and TE polarization is illustrated.

Chapter 7 finally concludes all the chapter of this thesis and a significant future work is recommended.

CHAPTER 2

Triple Band Notched FSS over entire UWB frequency range

2.1 Introduction

Researchers have witnessed a sharp inclination towards UWB frequency since the time it has been liberated by the FCC for commercial applications for the users'. Some of the key features owned by this frequency range are wide impedance bandwidth, high data rate, less power consumption and low spectral density. Currently, it is widely used in short range and low power communication. Hence UWB is a promising frequency band for wireless communication also. However, there are many devices and systems operating in some particular bands, such as satellite communication X-band (7.2-8.4 GHz), WLAN (5-6 GHz) and WiMAX (3.3-3.6 GHz) that creates interference problem [144]–[148]. Hence, FSS comes into existence. FSS has the tendency to bandstop a particular frequency while passing the other and vice versa and which totally depends upon the design of the array. FSS works as bandpass and bandstop filter and a wide research has been done for the same. Spiral shaped elements, convoluted SL and bionical elements are some of the structures which provides a band notched resonance at the desired frequency [149]–[151]. With the advent in the wireless technology, the demand to extract multiband using single FSS is increasing. By incorporating multiband in a single FSS, the overall system becomes less complex and bulky. Structure involving convoluted elements, fractal elements and multi-resonant elements, are used to achieve multiband characteristic of the FSS. Convoluted structure and fractal structures provides better results but at the cost of design complexity. Thus, the use of multi-resonant element over a single FSS is more reliable option. Cross and ring shaped metallic element are imprinted on both the sides of the dielectric substrate to obtain the bandstop characteristic at Ka-band and X-band [122]. In [152] shorted square loop us implemented to band reject triple notches. Triple band notches are obtained using a circular loop and two square loops [153]. The structure resonates at 2.45, 3.5 and 5.5 GHz. These structures do not provide a steady response curve of frequency at various impinging angle of incidence due to large sized FSS unit cells.

Consequently, to provide optimum results and to obtain triple band rejections, a miniaturized single layer FSS has been designed. The structure works in the frequency range of UWB and provides a steady response corresponding to frequency. This chapter is thus segregated into different section as given below: The triple band notched FSS design and its analysis is illustrated in Section 2.2. It is followed by results and discussion which is shown in Section 2.3. Finally in Section 2.4, the chapter is concluded.

2.2 Design analysis of the FSS unit cell

2.2.1 Unit cell model

The design of individual unit cell which is named as Design 1 is shown in Figure 2.1. Two square loop split ring resonators named SSRR₁ and SSRR₂ which are having the gaps in opposite sides of each other is imprinted over one side of the dielectric substrate.

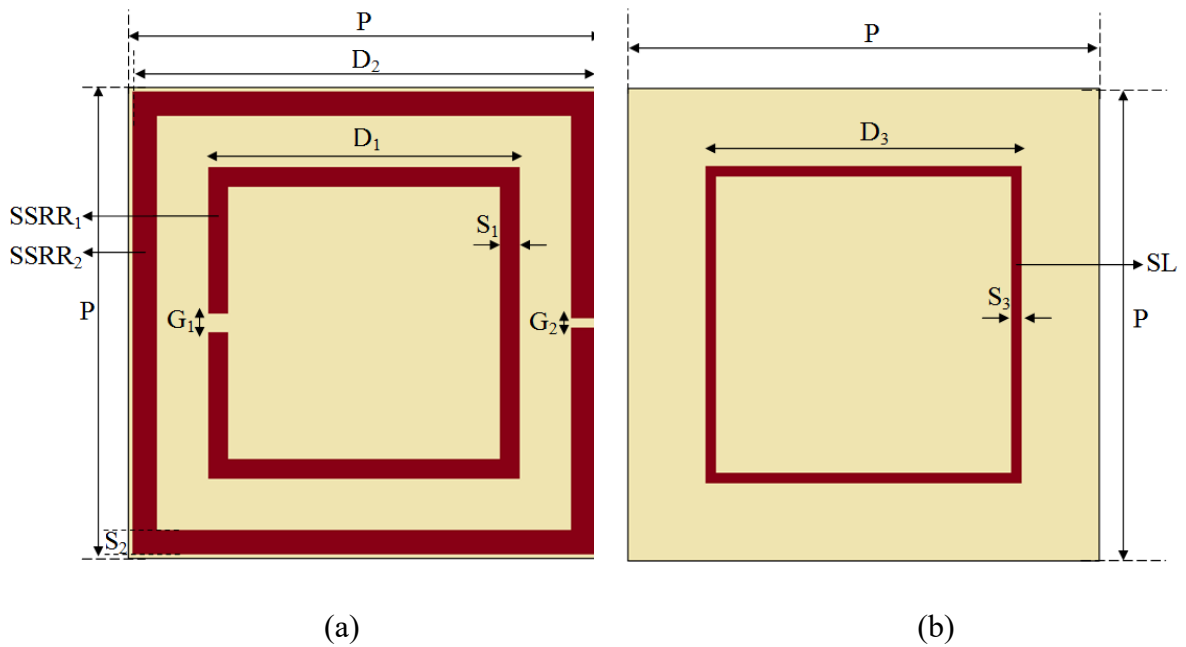


Figure 2-1 Triple notched FSS design (a) Upper layer (b) Lower layer of the substrate.

On the other hand an SL metallic element is placed at the other side of substrate. FR-4 is used as a dielectric substrate which is having dielectric constant of 4.4, loss tangent of 0.02 and thickness of 1.6 mm. $10 \times 10 \text{ mm}^2$ is the dimensions of single cell and the parameters associated to the design are illustrated in Table 2.1.

Table 2-1 List of parameters with all values (mm).

Parameter	P	G ₁	G ₂	S ₁	D ₁	S ₂	D ₂	S ₃	D ₃
Value	10	0.4	0.2	0.4	6.6	0.5	9.8	0.2	6.7

2.2.2 Design principle and step wise making of FSS unit cell

The design of any given FSS depends upon its periodicity P as FSS is a collection of array of unit cells arranged periodically. The structure is effectively homogeneous when the value of P is less than the guided wavelength. Moreover, for the structure to be refractive P should be less than $\lambda_g/4$ [154]. With respect to the given FSS design, the periodicity is equal to $\lambda_g/4.29$. Here λ_g is equivalent to the guided wavelength with respect to middle frequency of UWB frequency range which is equal to 6.8 GHz. The response curve of conventional FSS with respect to frequency is sensitive towards angle of incidence of the plane wave, which is highly undesirable. Small structures are required so that the phase variation is very less over the entire FSS sheet to obtain stable frequency response under wide incident angles. Here SSRR and SL are used to obtain the required results. SL is conventional structure which is symmetrical and simple to design. It resonates at a single frequency. SSRRs provide narrow band characteristics and resonate at lower frequencies. The SSRRs miniaturizes the structure with the influence of the gap capacitance which resides in between the metallic element. The capacitance varies with the variation of the gap and thus the resonance frequency shifts downwards. Figure 2.2, illustrates all the stages used in the making of given FSS unit cell design.

The unit cell is evolved in such a way that an SSRR₁ is imprinted over one side of the dielectric substrate at the initial stage. In stage 2, second SSRR₂ is implemented at the outer surroundings of the SSRR₁ but has the gap bearing side is opposite direction to that of the SSRR₁. Finally, in stage 3, an SL is implemented at the other side of the substrate to make the complete unit cell design.

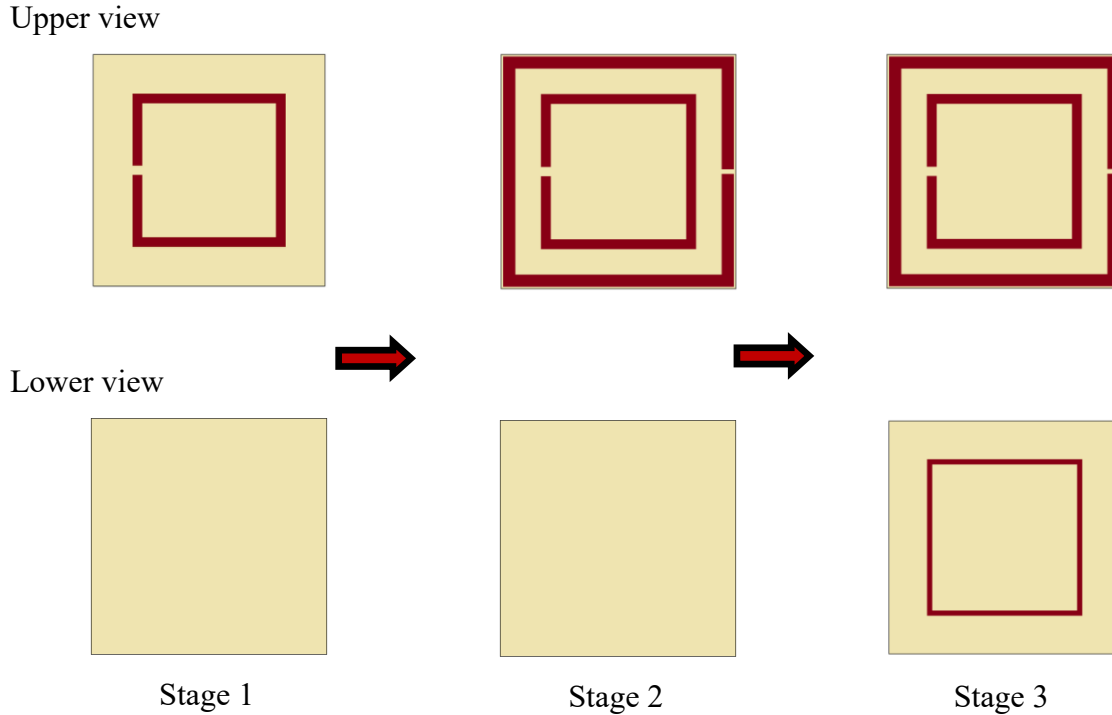


Figure 2-2 Stages in the making of main unit cell design

2.3 Simulated and experimental results

2.3.1 Frequency response of the designed FSS

After the designing of FSS, the response curve of frequency is obtained by the simulation of the design in Ansoft HFSS v.13 software. For TE polarization transmission coefficient has been studied as a function of frequency. The simulation is performed in stages. In stage 1, using $SSRR_1$ the unit cell resonates at 4GHz. By implementing both the SSRRs in stage 2, the structure resonates at 3.9 and 5.6 GHz. In the last stage, three resonant notches are obtained at 3.4, 5.6 and 7.9 GHz. It is thus inculcated from this result that individual metallic element is responsible for individual resonances. A slight variation in the frequency response is observed with the implementation of all the three metallic elements. This occurs because of the mutual coupling among FSS elements, as all the elements are closely spaced. Thus, the structure band rejects WiMAX, WLAN and satellite communication X-band, which ranges from 3.3 to 3.6 GHz, 5.1 to 6 GHz and 7.2 to 8.4 GHz, respectively. Figure 2.3 shows response curve of frequency corresponding to the FSS designing stages.

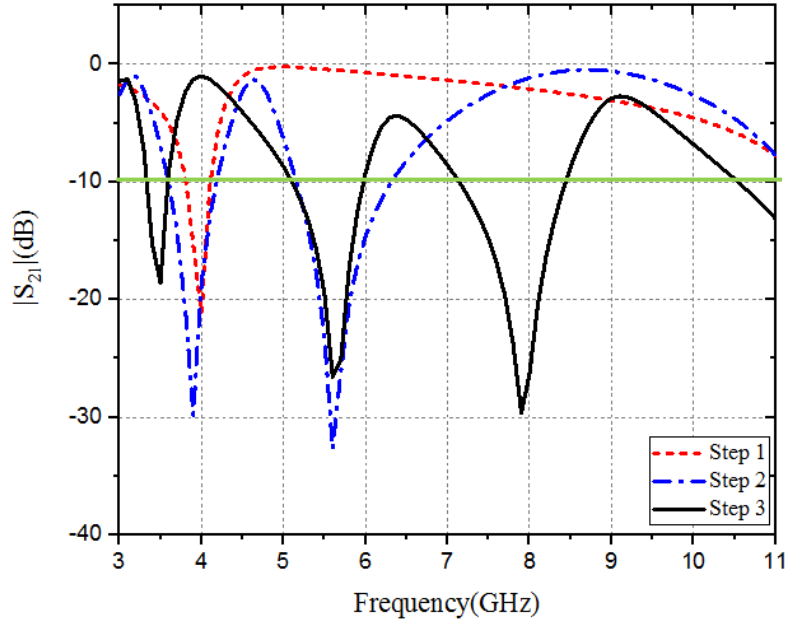


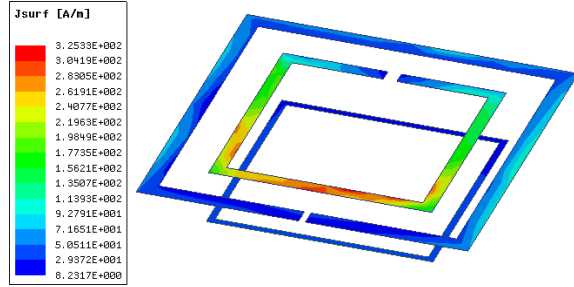
Figure 2-3 Simulated results of all stages used in the making of given unit cell.

2.3.2 Surface current distribution

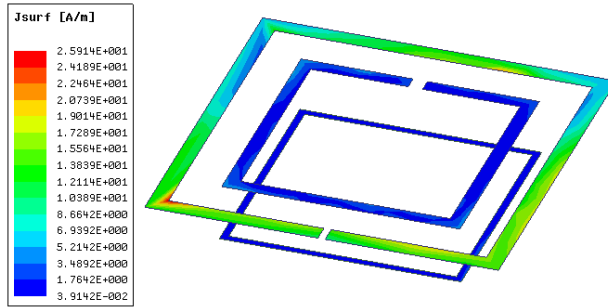
To verify whether each resonant element is responsible for its own resonance, the surface current distribution of the structure has been studied. At 3.4 GHz it is observed that maximum current intensity is obtained in SSRR₁. At 5.6 GHz maximum current intensity is concentrated in SSRR₂ structure and at 7.9 GHz maximum current intensity is concentrated in SL. The surface current distribution at all the three resonant notches is shown in Figure 2.4.

2.3.3 Equivalent circuit model

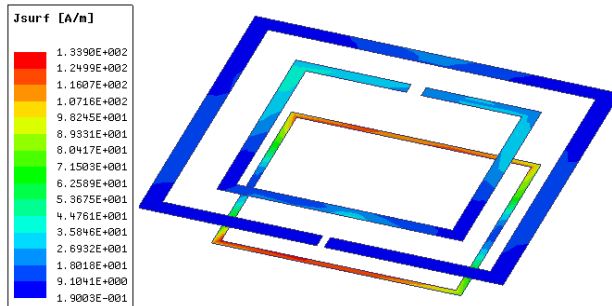
To understanding the working of the triple band notched design an equivalent circuit model has been deduced. The direction of surface current is showcased using the vector distribution, as examined in Figure 2.5 and ECM is extracted using it. The ECM is illustrated in Figure 2.6 and the evaluation of the current path is done for TE polarized wave. Here the ECM has been shown for each resonant element at its own respective resonance for the ease of understanding. The current bearing metallic part is represented as inductors and the gaps are represented as capacitors. At 3.4 GHz, it is observed that full current paths have been formed from a₁ to a₂. This means that the current is flowing



(a)



(b)



(c)

Figure 2-4 Distribution of surface currents on each resonant element of FSS at the three resonant notches (a) 3.4 GHz (b) 5.6 GHz and (c) 7.9 GHz

in one direction. Since it contains the gap bearing side, the lumped circuit becomes the parallel combination of inductance and capacitance. Here the capacitance is the gap capacitance in addition to the adjoining unit cell capacitance. The inductance of the loop is represented by L_1 and the capacitance by C_1 . In case of 5.6 GHz resonant frequency, it

is observed that two currents have been formed in which the current is moving from point b_1 to b_2 and from b_3 to b_4 in same direction, however, the current moves in opposite direction from point b_1 to b_4 . This also forms a parallel path. Therefore, the inductance from b_1 to b_2 path and b_3 to b_4 is added and represented by L_{21} and the inductance from b_1 to b_4 is represented by L_{22} . C_2 is the capacitance of $SSRR_2$. In case of 7.9 GHz resonant frequency, two equal current paths have been formed in between c_1 and c_2 of SL, therefore, the lumped circuit becomes the parallel combination of inductance and capacitance. Thus, two parallel inductances get formed in a series LC circuit. Each inductance is represented as L_{31} and L_{32} and gap among two corresponding unit cell as C_3 . The mutual capacitance is presented as C_{1m} , C_{2m} and C_{3m} .

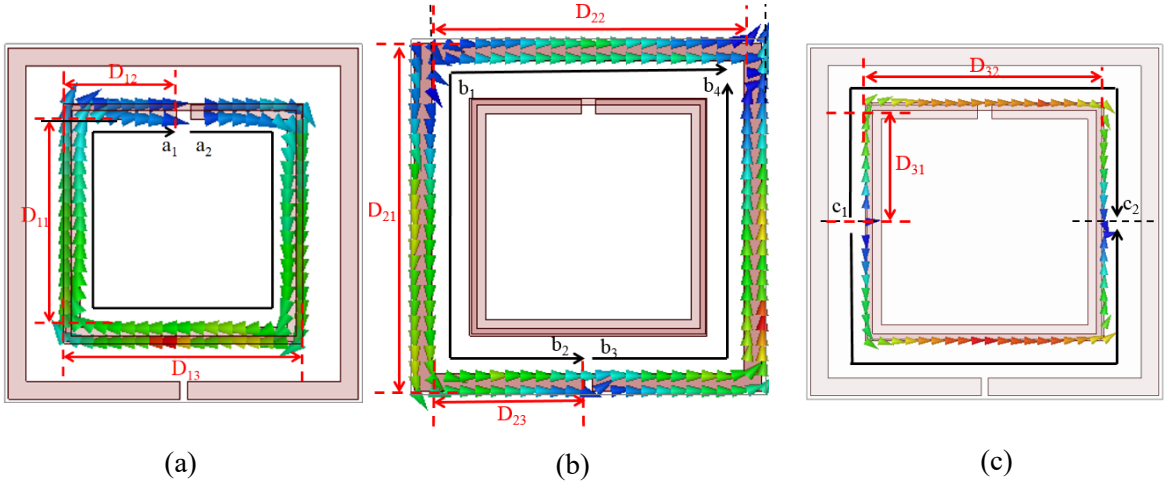


Figure 2-5 Vector surface current distribution at (a) 3.4 GHz, (b) 5.6 GHz and (c) 7.9 GHz

The values of the inductance has been extracted using the equations given by Marcuwitz [23], for each metallic part. Each metallic part is considered as a strip and for an infinite array under TE polarization. The inductive reactance for strip grating is given by the equation (1.6) as:

$$\frac{X_L}{Z_0} = F(P, w, \lambda) = P \frac{\cos \theta}{\lambda} \left[\ln \left(\cos ec \left(\frac{\pi S}{2P} \right) \right) + G(P, S, \lambda) \right] \quad (2.1)$$

where λ is wavelength of the resonating frequency, S is each strip width, P is period and θ is angle of incidence of impinging wave. The values of inductance is calculated at normal incidence angle ($\theta = 0^\circ$), therefore $\cos\theta = 1$. The inductance of each strip is calculated using the equation (1.10)

$$\frac{wL}{Z_o} = \frac{d}{P} F(P, S, \lambda) \quad (2.2)$$

Under TE polarization, the shunt susceptance is given by the equation (1.10). The susceptance of the given structure is reduced by d/p factor. Therefore, the capacitance is given by:

$$C_a = 4 \frac{Y_o d}{P w_r} F(P, g, \lambda) \quad (2.3)$$

The gap capacitance in between the SSRR loop is obtained using the formula given as:

$$C_g = \epsilon \frac{St}{G} \quad (2.4)$$

At 3.4 GHz resonant frequency SSRR₁ is illustrating the maximum current intensity. The width of each arm is 0.4 mm. However, the length of each arm is divided into three parts D_{11} , D_{12} and D_{13} for the calculation of inductance. Therefore,

$$L_1 = 2L_{D_{11}} + 2L_{D_{12}} + L_{D_{13}} \quad (2.5)$$

C_1 is the combination of C_g and C_a .

$$C_1 = C_a + C_g \quad (2.6)$$

At 5.6 GHz resonant frequency SSRR₂ is illustrating the maximum current intensity. The length of each arm is divided into three parts D_{21} , D_{22} and D_{23} for the calculation of inductance. The width of each arm is 0.5 mm. From point b_1 to b_2 and b_2 to b_4 the current is moving in same direction, therefore, the inductance is given by L_{21} .

$$L_{21} = 2L_{D_{21}} + 2L_{D_{23}} \quad (2.7)$$

From b_1 to b_4 the current is moving in opposite direction the inductance is denoted by L_{22} . The overall inductance is the parallel combination of L_{21} and L_{22} . The capacitance C_2 is given by:

$$C_2 = C_{a2} + C_{g2} \quad (2.8)$$

At 7.9 GHz resonant frequency, SL is showing the maximum current intensity. The width of each arm is 0.2 mm. Here the current path is equally divided into two parts. Therefore,

$$L_{31} = L_{32} = 2L_{D_{31}} + L_{D_{32}} \quad (2.9)$$

Since the thickness of the dielectric substrate is of a very short electrical length, thus impedance of transmission line is given by $Z_d = Z_0 / \sqrt{\epsilon_r} = 179.7\Omega$, where $Z_0 = 120\pi$.

The lumped circuit elements are then modeled in advanced design system (ADS) for the extraction of reflection and transmission characteristic response curves. Optimization of the values has been done to produce the similar frequency response as that by the full wave simulator using curve fitting method. The values are given by $L_1 = 14.4041$ nH, $C_1 = 0.9775$ pF, $C_{1m} = 0.0473$ pF, $L_{21} = 17.4155$ nH, $L_{22} = 4.6579$ nH, $L_2 = 3.675$ nH, $C_2 = 0.21428$ pF, $C_{2m} = 0.01848$ pF, $L_{31} = L_{32} = 9.8818$ nH, $C_3 = 0.05861$ pF and $C_{3m} = 0.0259$ pF. Figure 2.7 shows the comparison of the curve obtained by HFSS and ADS and almost similar response curves are obtained in both the simulator.

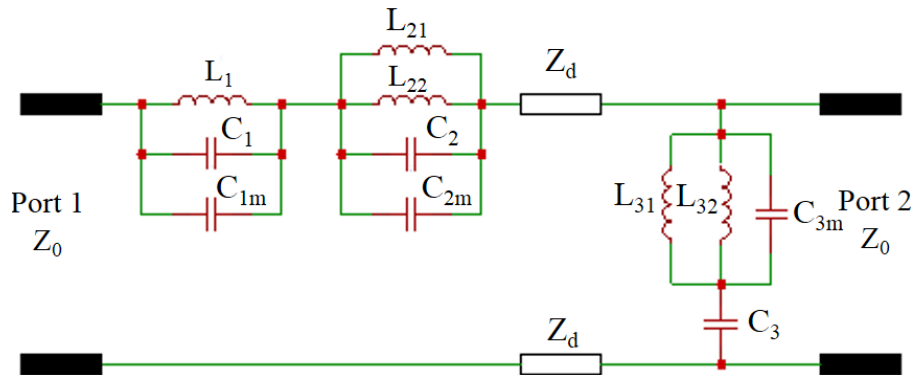


Figure 2-6 Equivalent circuit model

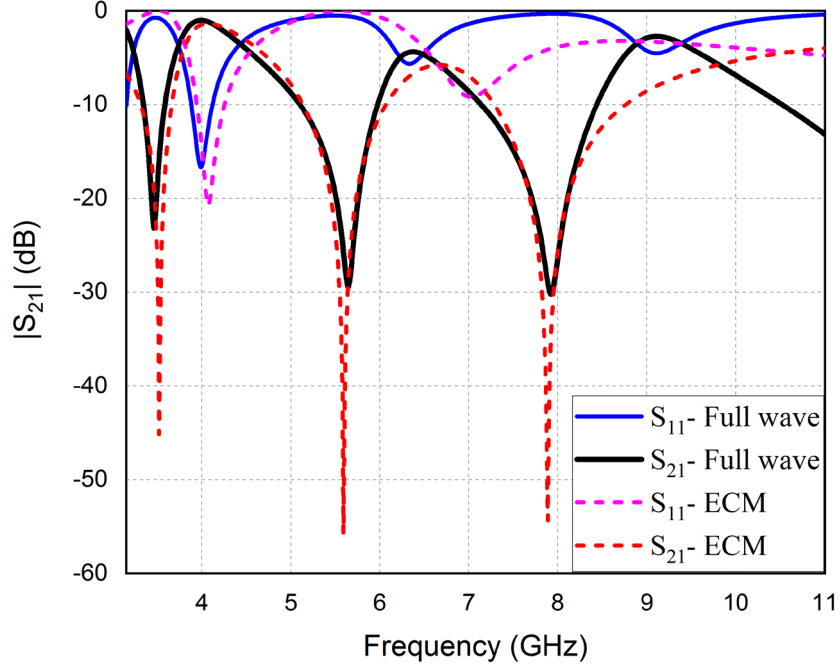


Figure 2-7 Comparison of frequency response curves implemented in full wave simulator and circuit simulator

2.3.3 Frequency response curve at various incident angles

For a FSS to be stable, the frequency response should remain same even at different impinging incident angles under varying environmental conditions. Figure 2.5 shows the transmission coefficient frequency response curve at various angles of incidence under TE polarized wave. The graph has been studied for the variation of the angles up to 60° . It is observed that the response curves for transmission coefficient remains steady for the first and third stop band, with a slight variation in third band. However, with varying incident angles, the second resonant notch gets shifted and more variation is seen after 40° . Thus, the overall structure remains stable up till 40° .

The resonant frequency deviation at $\theta = 40^\circ$ from the resonant frequency at normal incidence is 0.06, 0.3 and 0.2 GHz. The maximum relative deviation is thus given by [120] as:

$$\Delta f = \left| \frac{f_z - f_{oblique}}{f_z} \right| \times 100 \quad (2.10)$$

Here, f_z represents the resonant frequency at $\theta = 0^\circ$, $f_{oblique}$ represents the resonant frequency at oblique angles and maximum relative deviation is given by Δf . From $\theta=40^\circ$ incident TE polarized wave, the maximum relative deviation from normal incidence curve is 1.8%, 5.3% and 2.5%.

Stability towards varying incident angles is also dependent upon the periodicity, P, of any FSS [86] and is given by:

$$P < \frac{\lambda}{1 + \sin \theta} \quad (2.11)$$

Here, θ is the incident angle of the plane wave and λ is the wavelength corresponding to the resonant frequency. For the incident angle at $\theta = 40^\circ$, the maximum tolerance of P is 0.608λ . Therefore, for the first and third resonant frequency, the maximum tolerable limit of P should be 44 mm and 19 mm, respectively. The given FSS has the value of P lower than the tolerable limit. Thus a good stability towards varying incident angle is observed till 40°

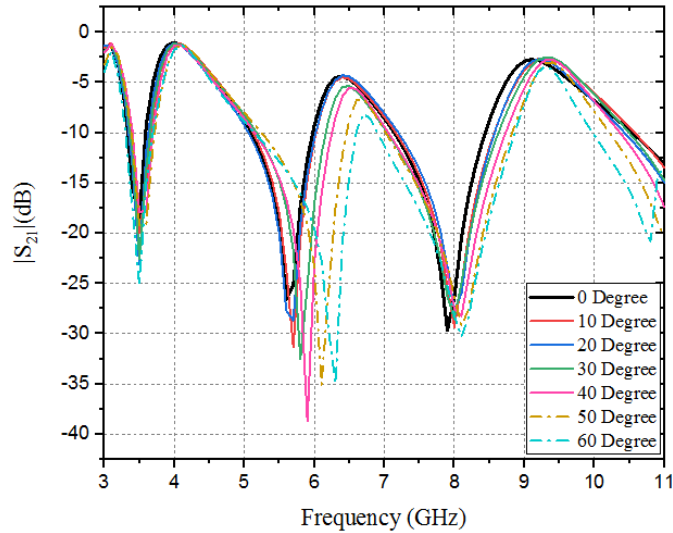


Figure 2-8 Frequency response at varying incident angles

2.3.6 Parametric variations

The changes in the parameters of any structure signify the dependency of the frequency response over the corresponding parameter. The length D_3 is varied in Figure 2.6 to check the response of the given FSS. It is studied that as D_3 increments while other parameters

remain the same, there is increase in the inductance of the loop. Hence, as the inductance increases the resonant frequency decreases. Figure 2.7 and Figure 2.8 illustrates the dependency of frequency response upon the change in gap width of each element of SSRR₁ and SSRR₂, respectively. With the increment in the gap width, the resonant frequency increases because the capacitance decreases, while keeping all the other parameters constant. It is also observed that when D_3 , G_1 and G_2 vary, the resultant variation in the frequency response is obtained at third, first and second resonant frequency, respectively. Thus it is inculcated that each metallic part is responsible for its own resonant notch.

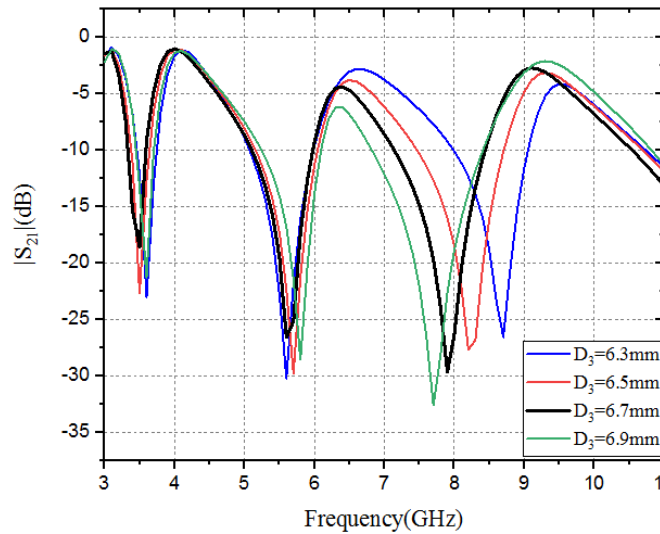


Figure 2-9 Frequency response curve at varying D_3

2.3.7 Verification of the simulated results experimentally

The given design is implemented over a FR-4 substrate. A periodic array of 18×18 unit cells is implemented over a $190 \times 190 \text{ mm}^2$ dimensioned substrate, as shown in Figure 2.9. The structure is then verified by measuring the results inside the anechoic chamber. In the measurement setup, the positioning of the FSS is done in such a way that it lays in between two multi waveguide horn antennas with similar distance. One of the horn antenna works as transmitter while the other works as receiver, as shown in Figure 2.10. Free space measurement technique is used in which in step 1 the transmission curve without FSS is measured using vector network analyzer (Anritsu-MS2038C VNA master). In step 2, FSS is positioned at the center of the two horn antennas and the

measurement is taken again. Finally, normalization is performed using both the transmission curves to obtain the actual measured result. The measured result is obtained at normal incident angle, i.e., $\theta = 0^\circ$. Figure 2.11 illustrates that an approximate match has been confirmed in between the simulated result and measured result.

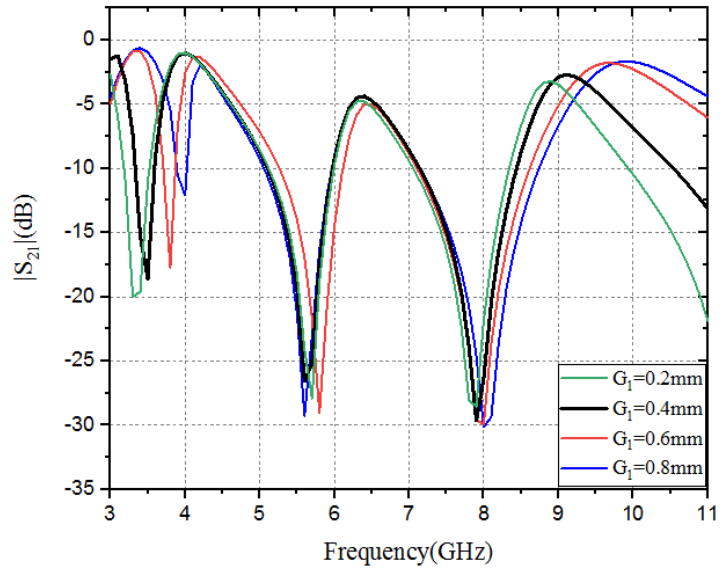


Figure 2-10 Frequency response curve at varying G_1

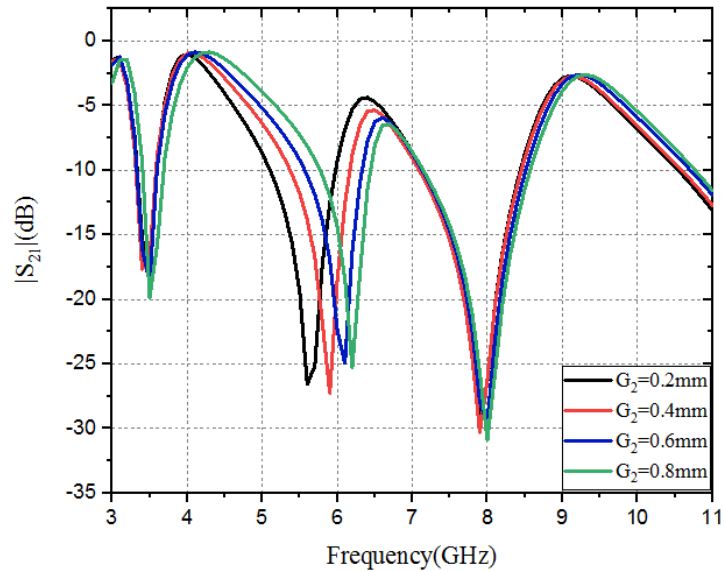


Figure 2-11 Frequency response curve at varying G_2

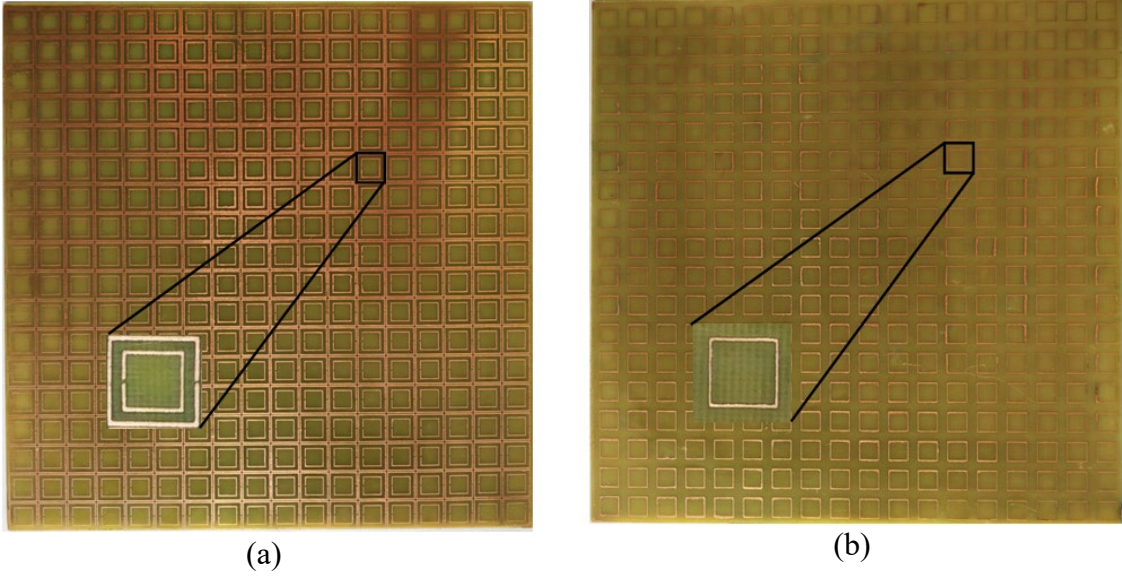


Figure 2-12 Fabricated FSS prototype

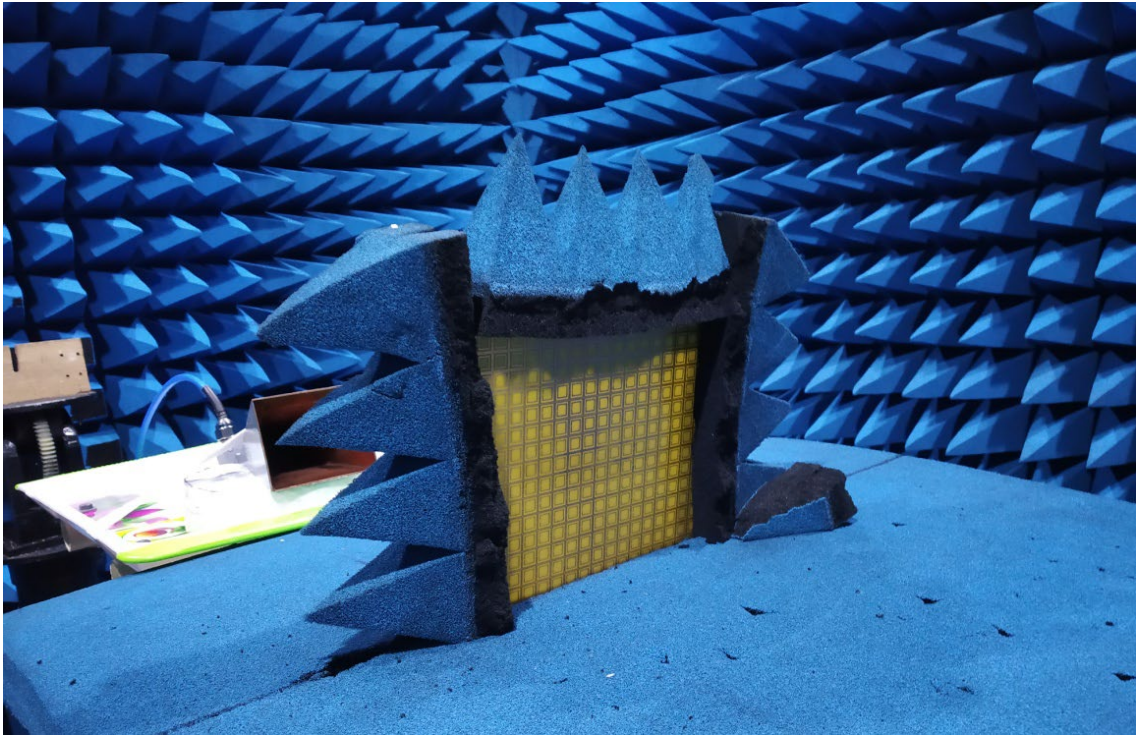


Figure 2-13 FSS sheet inside the anechoic chamber for the measurement of the frequency response of the proposed FSS

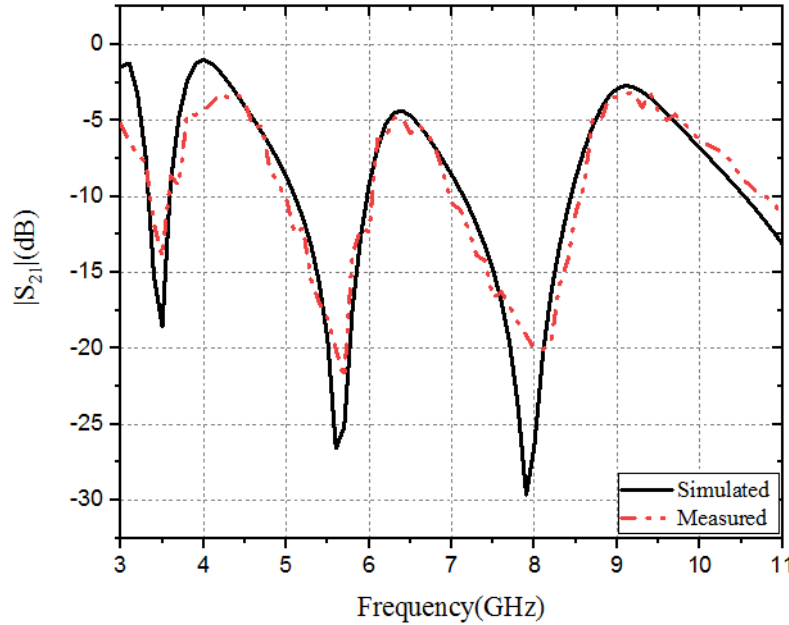


Figure 2-14 Simulated as well as measured frequency response curve at normal incident angle

2.3.8 Proposed FSS design compared with various other FSS design reported in literature.

Table 2 contains the data of various FSS unit cell designs and are then compared with the given unit cell design. Dimensions of the unit cell, rejection bandwidth, number of operational bands, resonant frequency angular stability and polarization insensitivity are the parameters on which the given FSS is compared with various FSS implemented in the literature. In the comparison table it is observed that individual frequency response is obtained for the design of [83] and [121], and dual frequency response is obtained for the designs of [84] and [119]. When these designs are compared with the proposed one, the proposed design provides triple band rejection using a single unit cell design. The design in [85] band rejects WiMAX, WLAN and X-band and has similar physical dimensions as that of the proposed one and works over the entire UWB frequency range. The proposed FSS design avoids the band wastage and improves the angular frequency response over the design of [85].

Table 2-2 Comparison with various FSS structures in literature

Ref.	Size of unit cells (mm^3/λ)	Band	No.	f_z	Operational bands	Freq. Ratio (f_h/f_l)	-10 dB Bandwidth, GHz (Freq. range)	MFD % TE TM (AS in Deg.)	PI
[83]	$7 \times 7 \times 1.6$ $0.116\lambda \times 0.116\lambda$	Stop	1	5	WLAN	-	1.5 (4.2-5.7)	- - (0°-60°)	Yes
		Pass		-		-	-		
[121]	$6.8 \times 6.8 \times 0.127$ $0.22\lambda \times 0.22\lambda$	Stop	1	10	X-band	-	5.2 (7.8-13)	1.9 1.9 (0°-60°)	Yes
		Pass		-		-	-		
[84]	$8.8 \times 8.8 \times 0.762$ $0.21\lambda \times 0.21\lambda$	Stop	2	8.47, 10.45	Wideband X-band	1.23	1.9 (7.5-9.4), 0.4 (10.4-10.8)	- - (0°-60°)	Yes
		Pass		9.6		-	0.2 (9.5-9.7)		
[119]	$20 \times 20 \times 2$ $0.16\lambda \times 0.16\lambda$	Stop	2	2.45, 5.5	Wi-Fi and WLAN	2.24	0.63, 1.43	< 2 < 2 (0°-45°)	Yes
		Pass				-	-		
[85]	$10 \times 10 \times 1.6$ $0.114\lambda \times 0.114\lambda$	Stop	3	3.5, 5.2, 10.2	WLAN, WiMAX, X- band	1.48, 1.96	0.5 (3.2-3.7), 1.9 (4.1-6), 4.1 (8-12.1)	- - (0°-30°)	Yes
		Pass		-		-	-		
Design 1	$10 \times 10 \times 1.6$ $0.113\lambda \times 0.113\lambda$	Stop	3	3.4, 5.6, 7.9 -	WiMAX, WLAN, X- band Satellite comm.	1.64, 1.41	0.3 (3.3-3.6), 0.9 (5.1-6), 1.2 (7.2-8.4)	1.8, - 5.3, 2.5 (0° - 40°)	No
		Pass	-	4.02		-	0.3 (3.9-4.2)		

* MFD – Maximum Frequency Deviation, AS – Angular Stability, PI – Polarization Insensitivity

2.4 Conclusion

Two SSRRs with gap bearing sides at opposite direction is positioned on one side of the FR-4 substrate while on the other side an SL is inserted. Triple band notches are obtained at 3.4, 5.6 and 7.9 GHz covering WiMAX, WLAN and satellite communication X-band while ranging from 3.3 to 3.6 GHz, 5.1 to 6 GHz and 7.2 to 8.4 GHz with -10 dB as reference in the transmission coefficient curve, respectively. A single pass band is obtained at 4.02 GHz, with -10 dB impedance bandwidth ranging from 3.9 to 4.2 GHz obtained at reflection coefficient curve. Simulated angular stability curve is observed for the given FSS design and a steady response curve is obtained upto 40° angle of incidence under TE polarization. It is observed that at normal angle of incidence under TE polarization, the simulated and measured results with respect to the bandstop behaviour of the given design is approximately the same, thus the given FSS structure is can be used in the various communication applications.

CHAPTER 3

Polarization Insensitive Triple Band Notched FSS over UWB frequency range

3.1 Introduction

With the inclination towards the wireless communication system, UWB is used extensively. Since humongous devices commercially and for military purpose operates at some particular bands, such as, WiMAX, WLAN, satellite communication C-band and Satellite communication X-band, the interference increases among these devices. As the number of devices increase it results in more saturation of the frequency spectrum. Since the devices are at close proximity, mutual coupling prevails which results in unacceptable frequency response. Moreover, various antennas work in these frequencies and resonate at multiple bands. Some of the conventional techniques such as reduction in the coverage area and point to point communication are used to handle the degradation of the signal, however to shield the closely separated frequency bands within device or in between various devices, a bandstop filter is required. FSS is proposed here as it works as spatial filter which hinders the systems from unwanted radiations meanwhile it also helps to avoid leakage of the signal from a given system.

It is necessary to make a compact unit cell design such that more unit cells can be incorporated in a given space to make FSS sheet which strongly resemble ideal filtering characteristics. Moreover, multi-band feature is in high demand in multi-functional devices, mostly in very tightly positioned bands [153], [155]. Therefore, in current scenario miniaturized structure with multiband characteristic is desired from an individual FSS sheet. Multi resonant elements, convoluted elements, fractal elements, multilayer FSS elements and perturbed elements, are some techniques used in implementation of multiband and miniaturized FSS. Structure such as perturbed element [156], fractal element [157] and convoluted element[158] has the complexity in the design and thus the fabrication is difficult with high manufacturing cost.

FSS structures such as multilayer has far better frequency for wide incident angles than single layer FSS with fast roll-off [159]. Two substrate layers are stacked in between three metallic layers, in which top and bottom metallic layer comprises of metallic square

patch whereas the middle layer consists of split ring shaped aperture [53]. The design provides resonant notches at 2.5, 5 and 6 GHz. Meanwhile the structure also works as pass band at 3.6 GHz and is polarization independent. In [160], two layer FSS is implemented to band rejection at X, K and Ka. SL and four metallic arms are used at both the layers of the substrate and the two FSS layers are separated by Rohacell foam. The structure provides a decent angular stability up to 45° regardless of the polarization. But the main issue with this kind of design is bulkiness of overall structure with high manufacturing cost. Other technique to compact the size of the FSS is to use multiple resonating elements in single FSS unit cell. Using the aperture type combination of U-, T- and rectangular- shaped alignment, resonant frequency is obtained at 8.1, 9.8 and 11 GHz [161]. In [162], triple band rejection is obtained at 1.81, 2.44 and 3.81 GHz using crossed dipoles and Matryoshka ring geometry.

To increase the angular stability, there is a need to reduce the size of the FSS further. Therefore, MM based FSS is appropriate for the same. Conventional MM structure provides narrow impedance bandwidth with reduced unit cell size but the whole layout becomes asymmetrical. The current requirement in the wireless communication system is of a polarization and angularly stable FSS. Polarization dependency occurs with asymmetrical structures and hence does not provide the required results. In [163], an asymmetric four arm star geometry provides dissimilar response curve at both the polarizations. In [164], T-type SRR and a rectangular shaped SRR is used to band stop dual bands. However, the frequency response for TM and TE mode came out to be different. Thus symmetry in the resonating element is necessary. Various MM based symmetric structures have been studied in the literature. On both the layers of the substrate, F-type resonators are implemented and they are placed antipodal to each other, whereas on the top layer an SL is also inserted [49]. The structure provides resonant notches at 2.4, 5.2 and 5.9 GHz and it also provides a pass band at 4.1 and 5.5 GHz under the influence of TM and TE incidence. In [165], two loop shaped resonator and one rectangle shaped resonator are used to band reject triple frequency bands.

By all the above discussions, it becomes evident that a miniaturized, symmetrical yet simple FSS structure is required to be implemented to ease out in designing and fabrication to cut down fabrication costs and also to provide high angular as well as

polarization stability. It is more important to acquire the exact narrow band notches to protect the devices from the interfering signal with high attenuation level. Thus, in this chapter a simple FSS design is implemented which is compact and is also polarization independent. SL and 90° rotational symmetric SSRR has been implemented at either side of FR-4 substrate to band reject three major bands under both the polarizations regardless of angle of incidence. This chapter is thus arranged as: In section 3.2 analysis and design of triple band notched FSS is included with its design principle. Section 3.3 compares the resultant curves of simulation as well as measurement. Moreover, a comparative study of triple band notched FSS with various FSS in the literature has been done. Conclusion of the chapter has been done in section 3.4

3.2 Design analysis of FSS unit-cell

3.2.1 Unit cell model

Figure 3.1 presents the configuration of triple notched FSS. Brown color here represents metallic part over dielectric substrate. Four SSRRs ($SSRR_1$ and $SSRR_2$) are positioned at either side of the dielectric substrate.

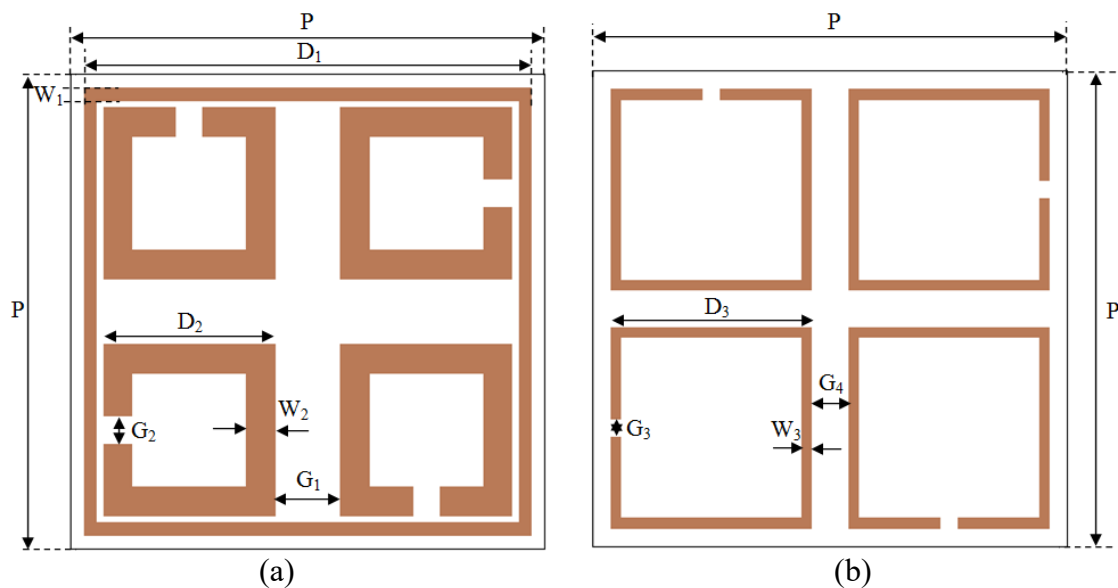


Figure 3-1 Unit cell configuration

All the four SSRRs are placed in such a way that the gap bearing sides are 90° rotationally symmetric in clockwise manner. Moreover, an SL is also implemented at the outer periphery of $SSRR_1$ over FR-4 substrate. $10 \times 10 \text{ mm}^2$ is the size of the unit cell with

a height of 1.6 mm. With respect to λ which is wavelength with respect to first f_r , the dimensions are $0.13\lambda \times 0.13\lambda$. The list containing all the values of parameters is presented in Table 3.1.

Table 3-1 List of all the parameters

Parameter	P	W ₁	W ₂	W ₃	G ₁	G ₂	G ₃	D ₁	D ₂	D ₃	G ₄
Value (mm)	10	0.25	0.6	0.2	1.4	0.6	0.4	9.4	3.6	4.2	0.8

3.2.2 Principle of operation and step by step development of unit cell

The proposed FSS unit cell is of an average size of $P=\lambda_g/4.3$, which is way smaller than the mentioned limiting value of P. λ_g represents wavelength corresponding to its counter frequency which is equal to 6.85 GHz, which is the middle frequency of operational band of 3.1 to 10.6 GHz. Since response curves of FSS is sensitive towards polarization and angle of incidence, miniaturized as well as symmetrical structures are required so that the phase variation is very less over the entire FSS sheet to obtain stable frequency response under wide incident angles and the structure is polarization insensitive. Both SSRR and SL can provide lower resonant frequency bands. SL provides high impedance bandwidth and symmetrical structure. On the other hand, SSRR provides low impedance bandwidth. Moreover, SSRR is polarization sensitive as it is asymmetric in design. For any impinging plane wave on the surface of a rotationally symmetric structure, the overall structure appears to be as an isotropic homogeneous medium. From this it is inferred that the design appears to be the same irrespective of the position from where the wave is incident. Thus the given design presents four SSRRs in which gap bearing sides are 90° clockwise rotationally placed making the structure symmetric. In stage 1, over one side of the substrate four similar 90° rotational symmetric SSRR₁ is imprinted. In stage 2, at that layer itself SL is added. Finally in stage 3, another four similar 90° rotational symmetric SSRR₂ has been imprinted at the bottom layer of the dielectric substrate. The evolution is illustrated in Figure 3.2.

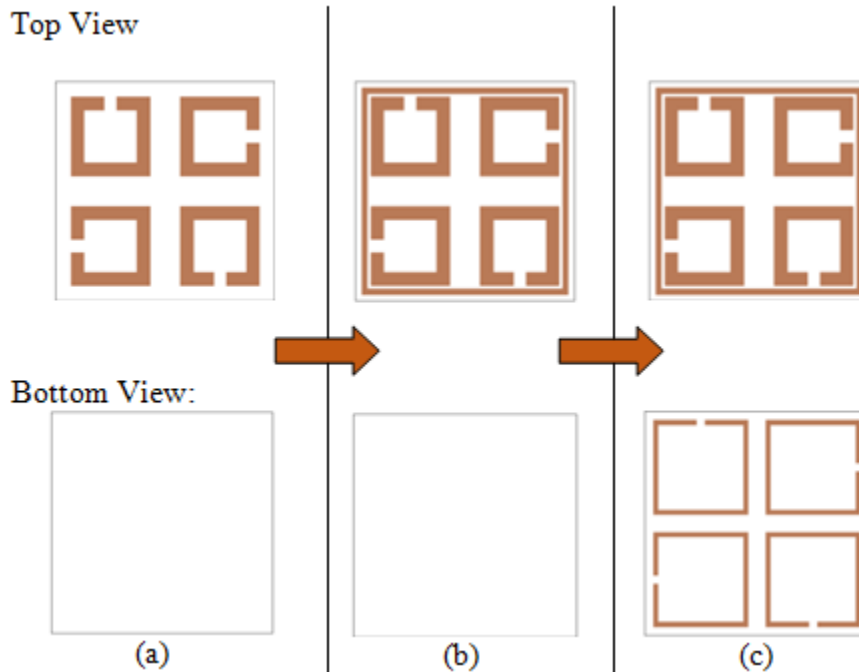


Figure 3-2 Stages in the making of triple band notched FSS

3.3 Simulated and experimental results

3.3.1 Frequency response of given unit cell

The simulated response curves of triple band notched FSS are observed for transmission and reflection coefficient under both the polarizations as a function of frequency. Each individual resonating elements, i.e., SL, SSRR₁ and SSRR₂ resonates at 4.2, 5.5 and 7.93 GHz, respectively, under both the polarized waves. The impedance bandwidth of the structure is quantified by considering the reference threshold of -10 dB for both the transmission and reflection coefficient curve. These resonating elements resonate at a particular frequency over the UWB frequency range. Figure 3.3 shows the stage by stage simulation to the given design. In stage 1, using SSRR₁ the unit cell resonates at 7.93 GHz covering -10dB impedance bandwidth from 7.68 to 8.11 GHz. In stage 2, with the implementation of SL at the outer periphery of the substrate, the resonance is obtained at 3.99 GHz (3.28 - 4.44 GHz) and 8.15 GHz (7.05 - 9.11 GHz). Finally, in last stage three notches are obtained at 3.92, 5.68 and 7.92 GHz. The triple band notched FSS thus works upon satellite communication X-band (7.2 - 8.4 GHz), WiMAX/satellite communication downlink C band (3.3 - 4.2 GHz) and WLAN (5.1 - 5.9 GHz). A slight variation is

examined in resonant frequency with the implementation of all the three resonating element in single unit cell which is the resultant of mutual coupling.

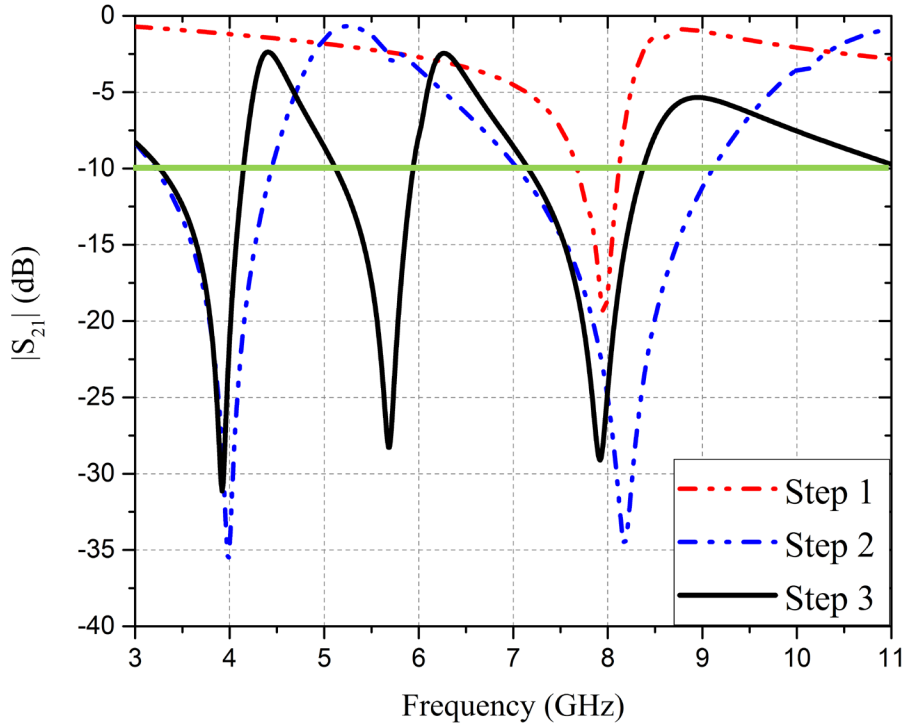


Figure 3-3 Simulated results of all steps used in the implementation of given unit cell.

The curves representing the reflection and transmission characteristic of triple band notched FSS at normal incident angle under both polarizations is presented in Figure 3.4. It is evident from Figure 3.4 that the structure is polarization insensitive as the frequency response under both the polarizations is same. It is also observed that in between two transmission zeros, a transmission pole is acquired. The structure band passes 4.37 and 6.22 GHz resonant frequencies, ranging from 4.31 to 4.44 GHz and 6.14 to 6.33 GHz, respectively.

The structure produces closely separated frequency bands. The ratio of separation from higher resonant frequency to lower resonant frequency for first and second transmission zero frequency is 1.44 and for second and third transmission zero frequency is 1.39, whereas for the transmission poles the ratio is 1.42. It is observed that SSRR₂ and SL are placed at different layers of the substrate. This is done to avoid the overlapping of the resonating elements so as to avoid mutual coupling in between first and second rejection bands. This helps in the emergence of pass band among stop bands.

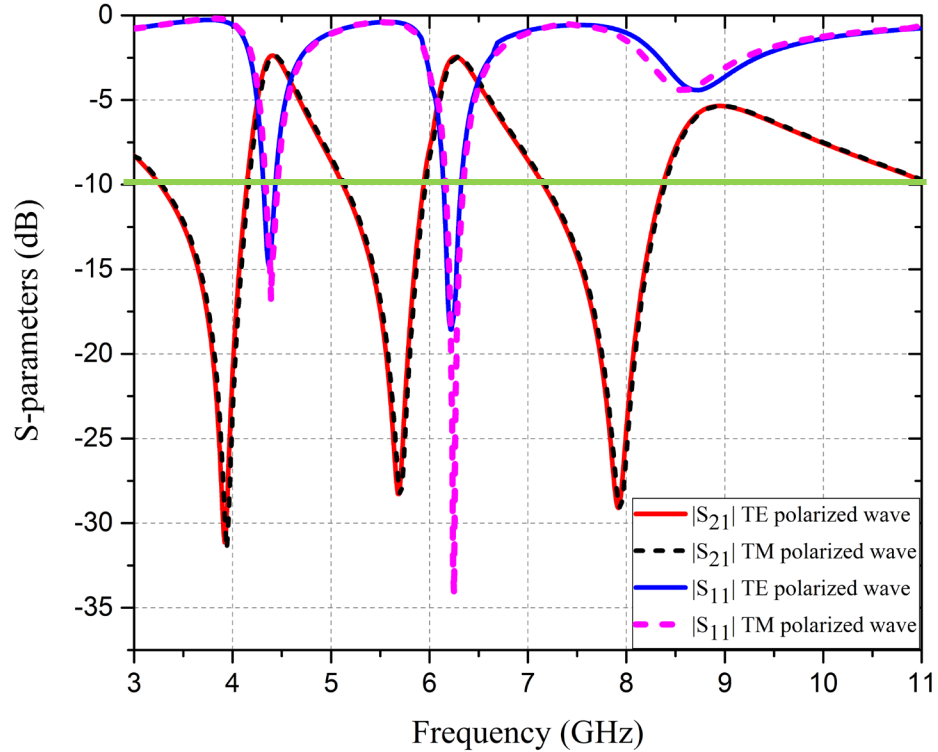


Figure 3-4 S-parameter with respect to frequency

3.3.2 Surface current distribution

Surface current distribution has been checked at all the three transmission zeros frequencies, i.e., at 3.92, 5.68 and 7.92 GHz under both polarizations at normal incidence and is shown in Figure 3.5. To explain the resonance mechanism easily, the current paths for each resonating element with respect to its resonance frequency are presented. For 3.92 GHz resonant frequency, it is observed that two current maximas are obtained in between two current minimas which is located in between point a_1 and a_2 of SL under both the polarized waves, dividing its wavelength path into two with respect to obtained resonant frequency. This is represented in Figure 3.5 (a) and (b). Each element of SSRRs has been simulated individually to check the surface current distribution (not shown here) and the structure resonates at different frequencies under TE and TM polarization. Thus rotational symmetric SSRR₁ and SSRR₂ have been studied at 5.68 and 7.92 GHz respectively. The surface current distribution for SSRR₁ and SSRR₂ is illustrated in Figure 3.5 (c) and (d), and Figure 3.5 (e) and (f), respectively. It is observed that under TE polarization the first and fourth element of the SSRR₁ and SSRR₂ shows maximum

current intensity, whereas under TM polarization the second and third element of the SSRR₁ and SSRR₂ shows maximum current intensity. Since at a time two opposite elements of SSRRs resonates with similar current intensity at TE and TM mode, thus both the SSRRs show polarization insensitive characteristics.

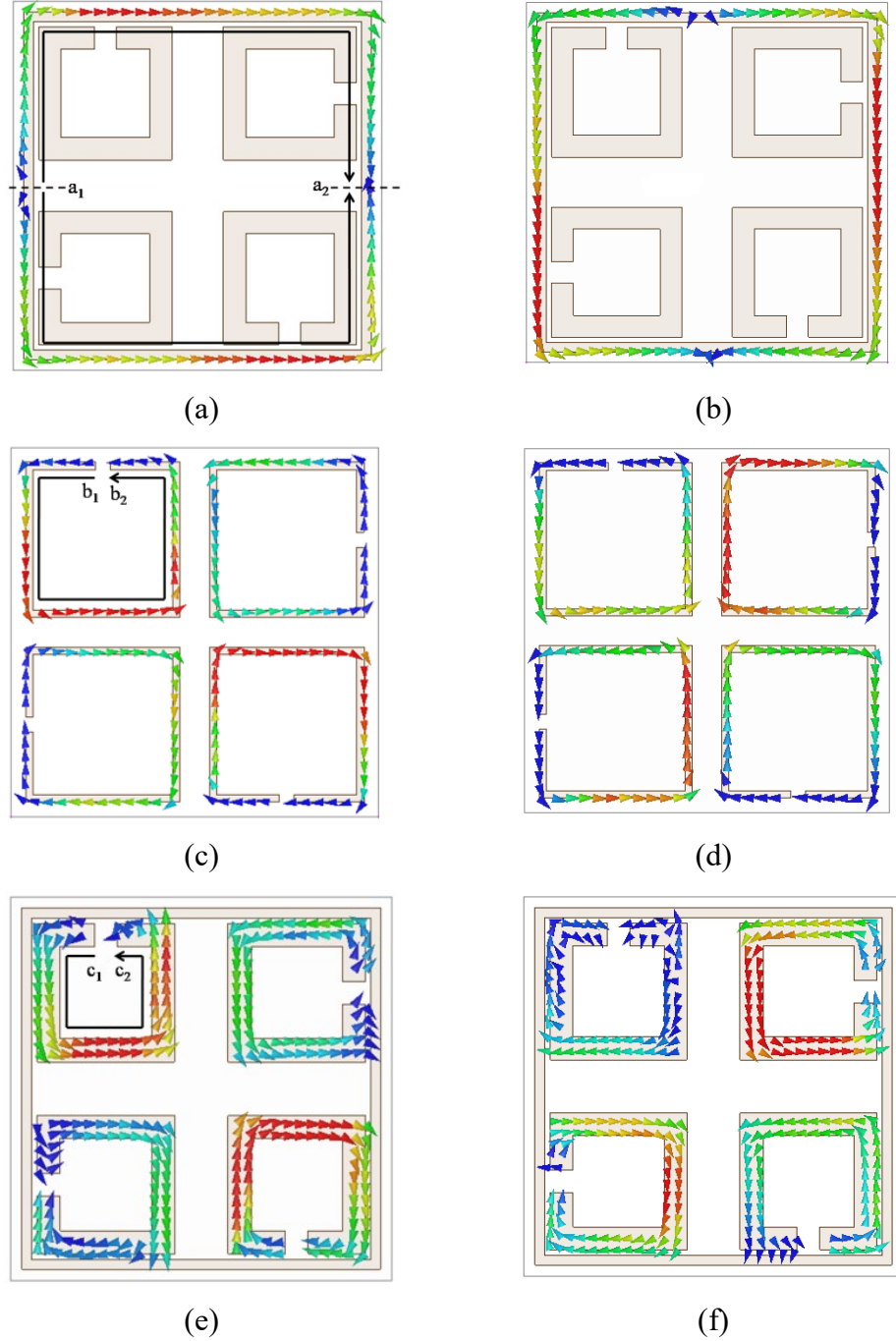


Figure 3-5 Surface current distribution at (a) and (b) 3.92 GHz, (c) and (d) 5.68 GHz and, (e) and (f) 7.92 GHz, respectively.

3.3.3 Equivalent circuit model (ECM)

The direction of surface current is showcased using the vector distribution, as examined in Figure 3.5 and ECM is extracted using it. The ECM is illustrated in Figure 3.6 and the evaluation of the current path is done for TE polarized wave. The current bearing metallic part is represented as inductors and the gaps are represented as capacitors. At 3.92 GHz, it is observed that two equal current paths have been formed. Thus, two parallel inductances get formed in a series LC circuit. Each inductance is represented as L_{11} and gap among two corresponding unit cell as C_1 . From Figure 3.5 (c) and (e), it is observed that full current paths have been formed from b_1 to b_2 and c_1 to c_2 in the case of SSRR₁ and SSRR₂, respectively. This means that the current is flowing in one direction in both the cases. Since it contains the gap bearing side, the lumped circuit becomes the parallel combination of inductance and capacitance. L_2 represents the inductance of SSRR₁ and L_3 represents the inductance of SSRR₂. Moreover, the metallic arm gap capacitance is given by C_2 and C_3 for SSRR₁ and SSRR₂, respectively. The mutual capacitance is presented as C_{1m} , C_{2m} and C_{3m} .

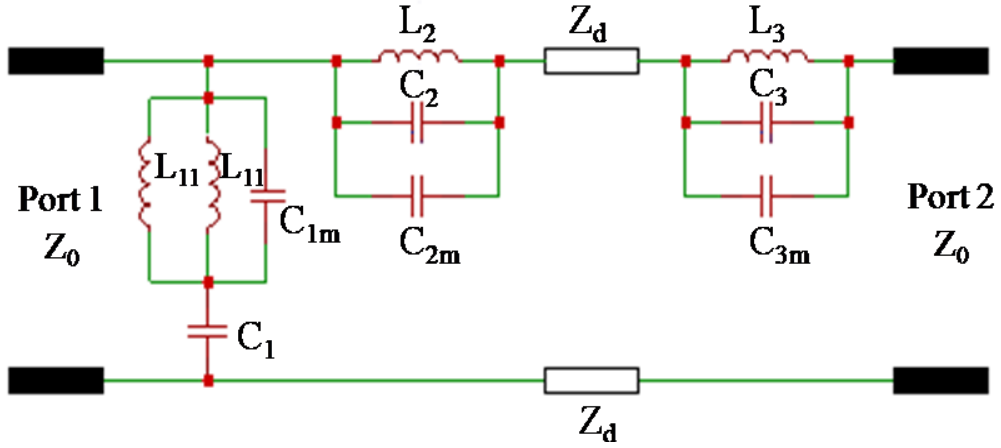


Figure 3-6 ECM for the given FSS design

The individual resonant frequency of SL, SSRR₁ and SSRR₂ is as follows:

$$f_{SL} = \frac{1}{2\pi\sqrt{L_1(C_1 + C_{1m})}}, \quad \text{where } L_1 = L_{11} \parallel L_{11} \quad (3.1)$$

$$f_{SSRR_1} = \frac{1}{2\pi\sqrt{L_2(C_2 + C_{2m})}} \quad (3.2)$$

$$f_{SSRR_2} = \frac{1}{2\pi\sqrt{L_3(C_3 + C_{3m})}} \quad (3.3)$$

All the values of SL, SSRR₁ and SSRR₂ are calculated from ref. [24] and [166] which is similar to that performed in Chapter 2. The calculation has been done at normal incidence under TE incident polarization. Since dielectric substrate height is very less, thus it is modelled as a simple transmission line which has the characteristic impedance equivalent to $Z_d = Z_0/\sqrt{\epsilon_r} = 179.7\Omega$ with respect to the characteristic impedance of free space Z_0 .

The lumped circuit elements are then modelled in advanced design system (ADS) and has been optimized to extract similar reflection and transmission characteristic response curves as that of full wave simulator. Thus, the calculated values of all the elements listed are: $L_1 = 6.305\text{nH}$, $L_2 = 7.866\text{nH}$, $L_3 = 11.6776\text{nH}$, $C_1 = 0.2053\text{pF}$, $C_2 = 0.0496\text{ pF}$, $C_3 = 0.0561\text{pF}$, $C_{1m} = 0.0634\text{nH}$, $C_{2m} = 0.00275\text{ pF}$, and $C_{3m} = 0.013785\text{pF}$. Figure 3.7 shows the comparison of the curve obtained by HFSS and ADS and almost similar response curves are obtained in both the simulator.

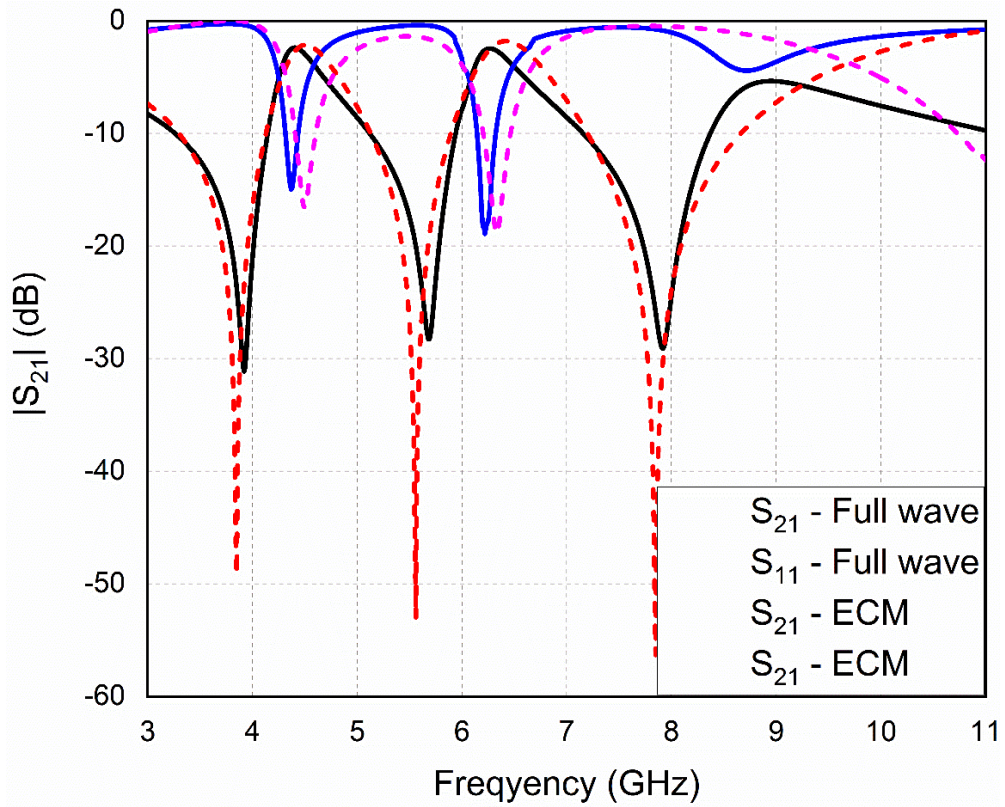


Figure 3-7 Comparison of frequency response curve using full wave simulator and circuit simulator

3.3.4 Electromagnetic shielding

Using the equation 1.14, shielding effectiveness of the triple band notched FSS is calculated and is presented Figure 3.8.

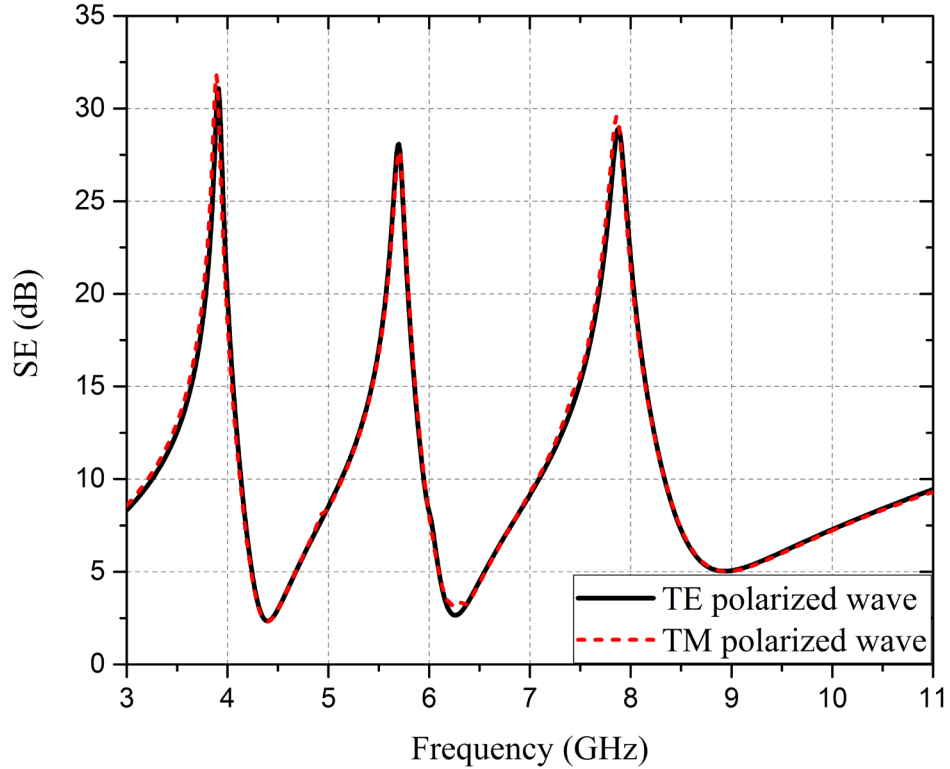


Figure 3-8 SE with respect to frequency at $\theta = 0^\circ$

For the response curves of frequency obtained under both the polarizations, attenuation of more than 10 dB is procured. It is also observed that at normal incident wave maximum attenuation of 32 dB is attained.

3.3.5 Frequency response curve at various incident and polarization angles

For an FSS to be stable under varying environmental conditions, the frequency response should remain same even at different impinging incident angles as well as polarization angles. Figure 3.9 illustrates the phenomenon of incident wave impinging on the surface of triple band notched FSS with the representation of varying θ and ϕ .

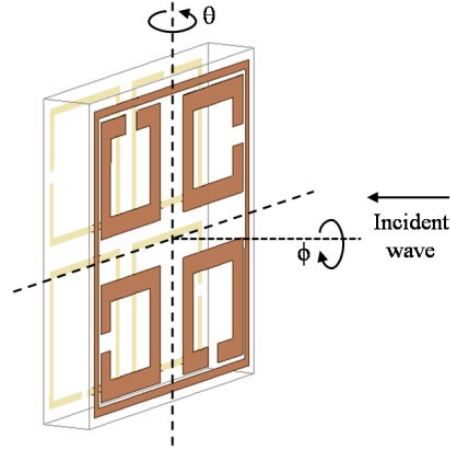
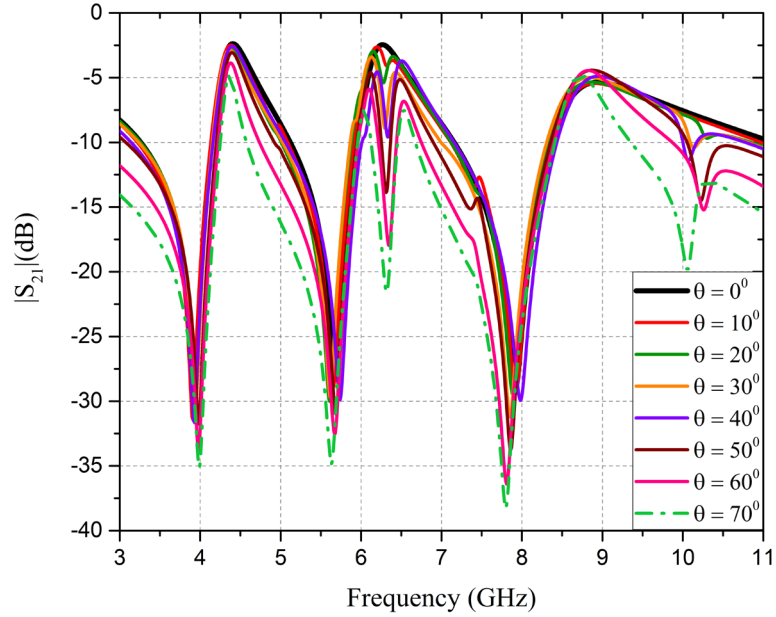
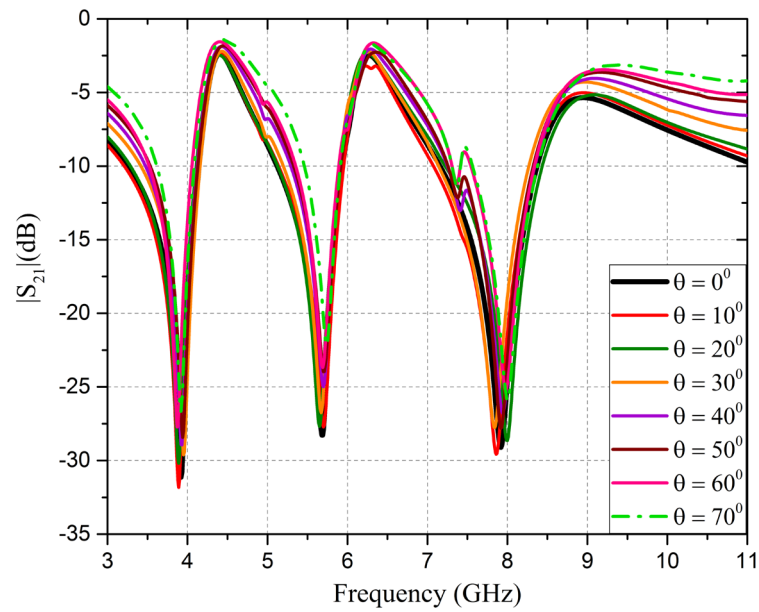


Figure 3-9 Impinging incident wave representation

Transmission behaviour of the triple band notched FSS with respect to the frequency is studied at varying incident as well as polarization angle. Frequency response under wide incident angle (θ) at $\phi=0^\circ$ for both the TE and TM polarization is illustrated in Figure 3.10 (a) and (b). From the curves it is clear that all the three resonant notches are insensitivity towards varying incident angles till 70° . For the frequency response under TE polarization additional resonant notches are obtained at 6.4 GHz and 10.2 GHz after 40° . However, frequency response curve of TM polarized wave shows full isotropic behaviour for all the incident angles. Under the influence of both the polarization first and second resonance remains stable till 80° , however, a slight variation in magnitude and resonance is observed in third resonant notch. Overall the structure shows a stable frequency response till 70° for all the resonant notches. It is observed that at $\theta = 70^\circ$, the resonant frequencies shows the variation of 0, 0.03 and 0.08 GHz under TM mode and 0.08, 0.03 and 0.11 GHz under TE mode when compared to that of normal incidence resonant frequency. From equation 2.1, it is observed that the maximum relative deviation of the triple notched frequency at normal incidence to that of oblique angle incidence at $\theta = 70^\circ$ is 0%, 0.5% and 0.08% under TM mode and 2%, 0.5% and 1.3% under TE mode.



(a)

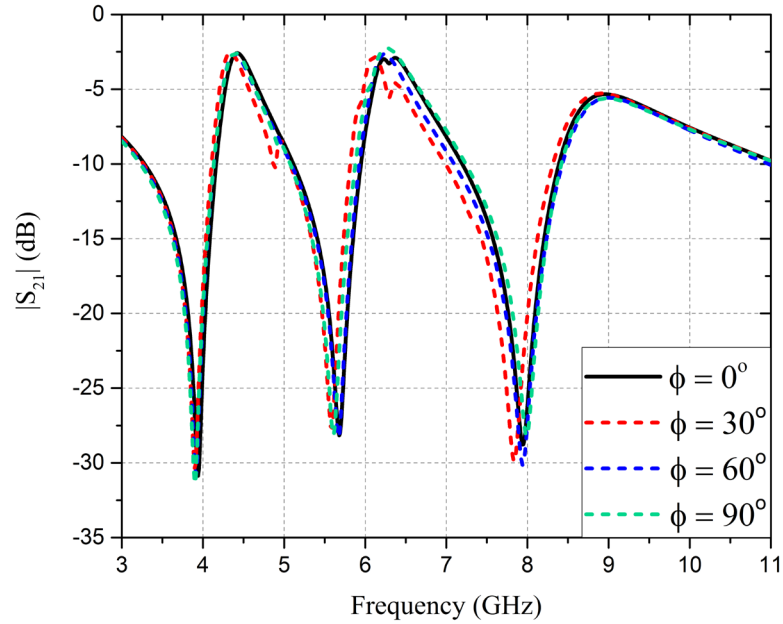


(b)

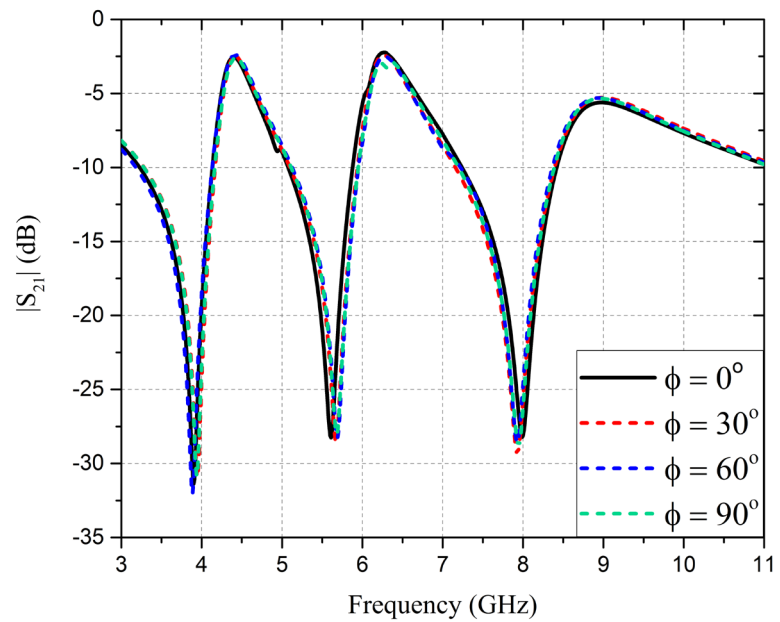
Figure 3-10 Frequency response at varying angle of incidence under (a) TE and (b) TM mode.

It is inferred that the triple band notched FSS provides better angular stability under both the polarizations. It is also observed that under TM and TE polarization, the bandwidth of the structure decreases and increases with wide angle of incidence, respectively. This occurs due to reduction of wave impedance under TM polarization by the amount

$Z_{TM} = Z_0 \cos \theta$ and increment in wave impedance under TE polarization by the amount $Z_{TE} = Z_0 / \cos \theta$. Frequency response under wide polarization angle (ϕ) at $\theta=0^\circ$ is presented in Figure 3.11.



(a)



(b)

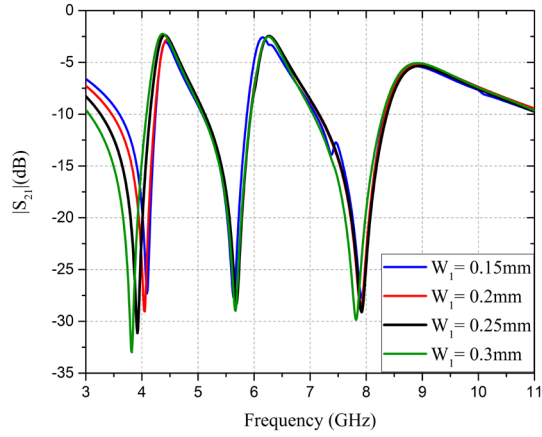
Figure 3-11 Frequency responses at varying polarization angles at (a) TE and (b) TM incident mode of wave

The maximum relative deviation is obtained from equation 2.1. It is observed that at $\theta = 30^\circ$, the frequency deviation from the obtained transmission zero frequencies are 0.2%, 0.5% and 0.5% under TM mode and is 0.2%, 1% and 0.7% under TE mode. Because of symmetric nature of resonating metallic element, the structure assures approximately similar response curves at wide polarization angles. Therefore, it is inferred that the triple band notched FSS structure attains steady response curve for both the polarizations under varying incident and polarization angles.

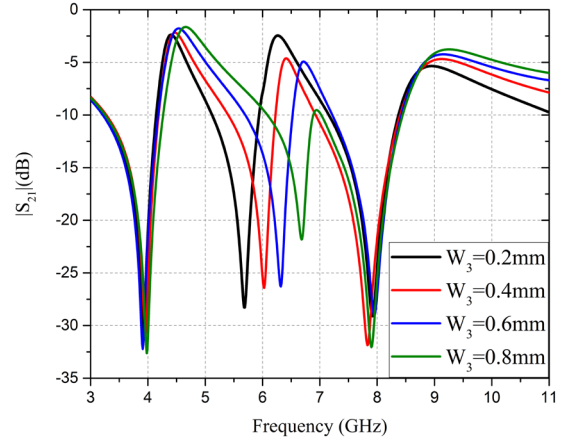
From equation 2.2, it is evident that for first and third resonant frequency, highest tolerable limit of P is 39 mm and 19 mm, respectively. The given FSS has the value of P lower than the tolerable limit. Thus a good stability towards varying incident angle is observed till 70°

3.3.6 Parametric analysis

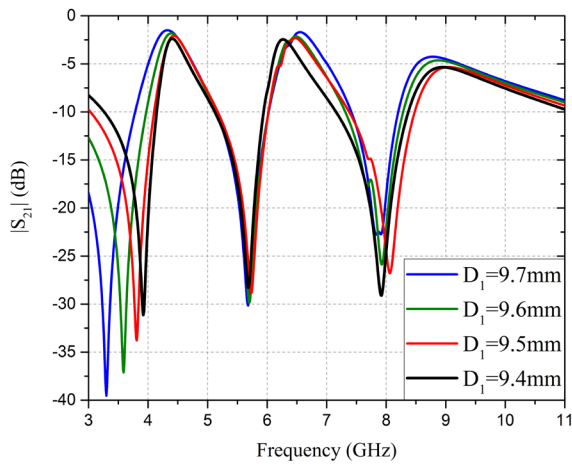
At 3.92, 5.68 and 7.93 GHz, this triple band notched FSS design resonates. Parametric analysis of the FSS shows the dependency of resonance over the change in the dimensions of structure. The width W_1 and W_3 is increased initially, as illustrated in Figure 3.12. In case of W_1 , the width is increased towards the outer side of the unit cell, whereas the inner length of D_1 remains the same to 8.4 mm. As W_1 increases the outer perimeter of the loop increases, which means that the inductance of the loop increases. Increase in inductance leads to the shift in the resonant frequency towards the left side of the spectrum. However, in case of W_3 the width is increased towards the inner side of the unit cell which means that D_3 remains same as 4.2mm. As the width increases the inner perimeter of the structure decreases, the inductance of the structure also decreases, thus the resonant frequency shifts to higher side of the spectrum. The similar effect is observed in Figure 3.12 (b). It is observed that the major shift in the resonance frequency is obtained at their respective resonant notch. In Figure 3.13, the arm length D_1 , D_2 and D_3 is changed while the other perimeters remain the same. In case of D_1 as the length of D_1 increases with respect to its original value of 9.4 mm, the perimeter of the loop increases which leads to increased inductance and reduced resonance frequency. With the decrement in the length in D_2 with respect to its original value of 4.2 mm, the resonance shift upwards in the spectrum. This happens because as the length decreases the perimeter



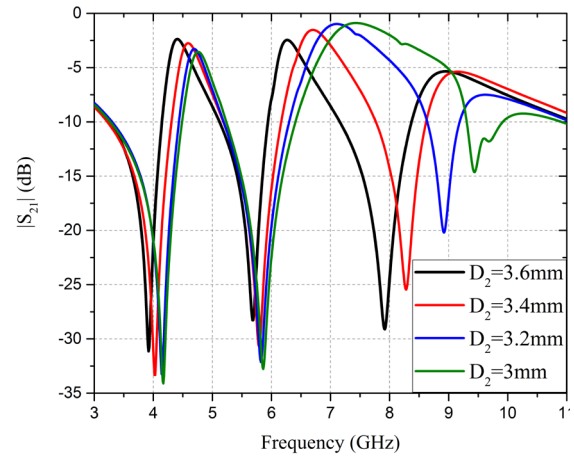
(a)



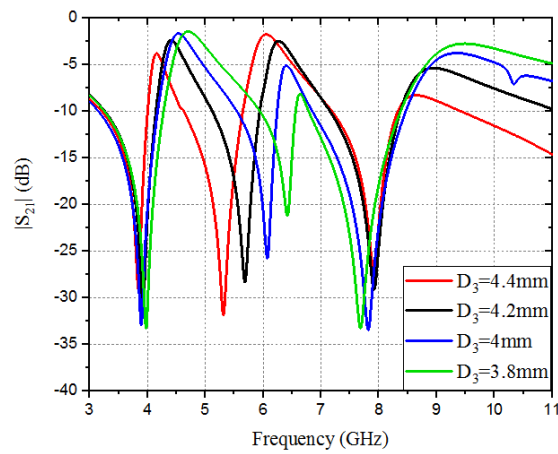
(b)

Figure 3-12(a) Change in the width of W_1 and (b) W_3 

(a)



(b)



(c)

Figure 3-13(a) Change in D_1 , (b) D_2 and (c) D_3

of the loop decreases which results in decrease in effective inductance, thus the resonance shift upwards. Similar is the case with the change in length D_3 . As the length decreases from 4.4 to 3.8 mm, the perimeter of the loop decreases, which shifts the resonant frequency to higher side of the spectrum. By changing the lengths, their respective resonant notches only shifts. Further the values of G_2 and G_3 is changed in Figure 3.14. The resonant notches shift upwards in the spectrum, with the increase in the width of the gap as the capacitance of the gap decreases. A slight deviation in other resonant notches has been noticed with the change in particular parameter. However these changes are negligible.

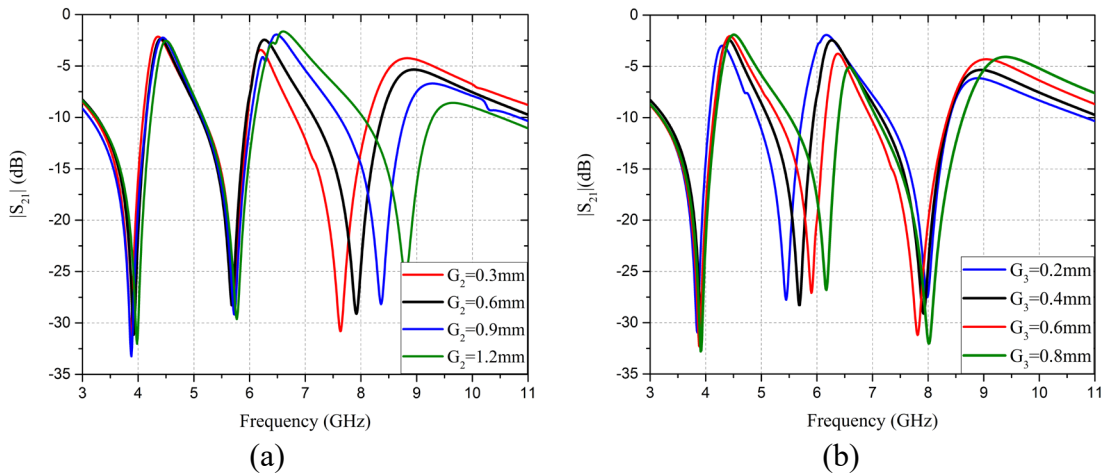


Figure 3-14 (a) Change in G_2 (b) G_3

3.3.7 Verification of the simulated results experimentally

For the validation purpose, triple band notched FSS is fabricated over a FR-4 substrate. A periodic array of 18×18 unit cells is implemented over a $180 \times 180 \text{ mm}^2$ dimensioned substrate. The fabricated design is presented in Figure 3.15. The response curve of the fabricated design is validated by measuring the results inside the anechoic chamber. The measurement setup is shown in Figure 3.15(c).

The measurement method used here is similar as that presented in chapter 2. The measured result is obtained at normal as well as varying incident angle till 60° . A good match has been confirmed in between the resultant response curves of simulation and measurement under both the polarizations, as shown in Figure 3.16 (a) and (b).

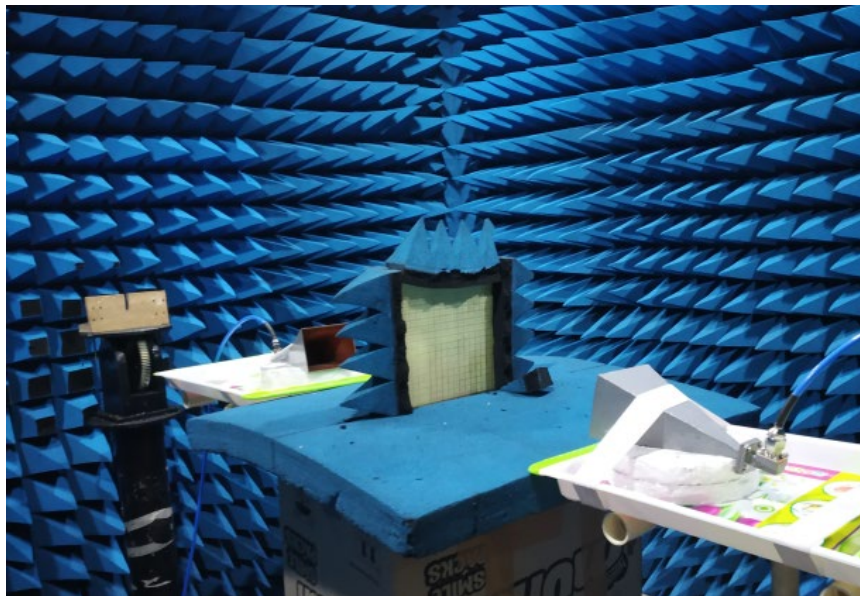
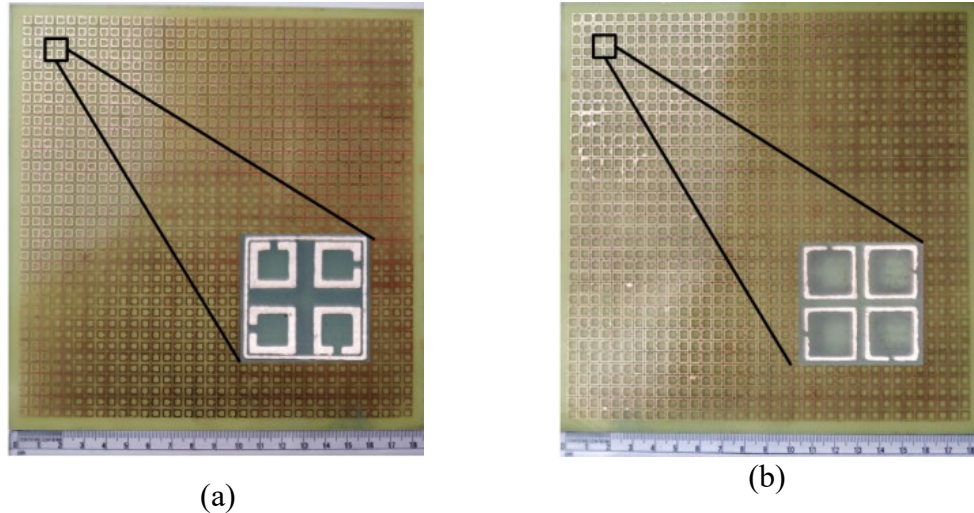


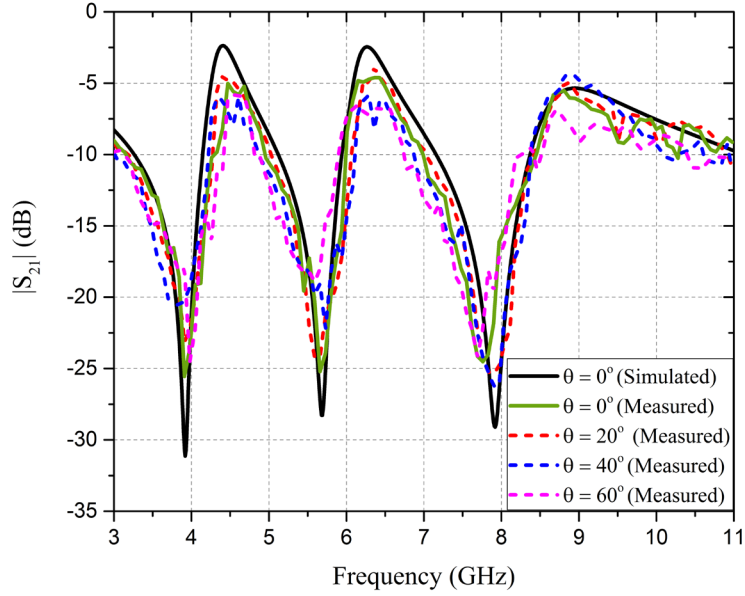
Figure 3-15 Fabrication prototype (a) top layer, (b) bottom layer and (c) FSS sheet inside the anechoic chamber for the measurement of the frequency response

It is inferred that small variations are present in transmission curves of the measured results but appears because of the limitation in measurement and fabrication error.

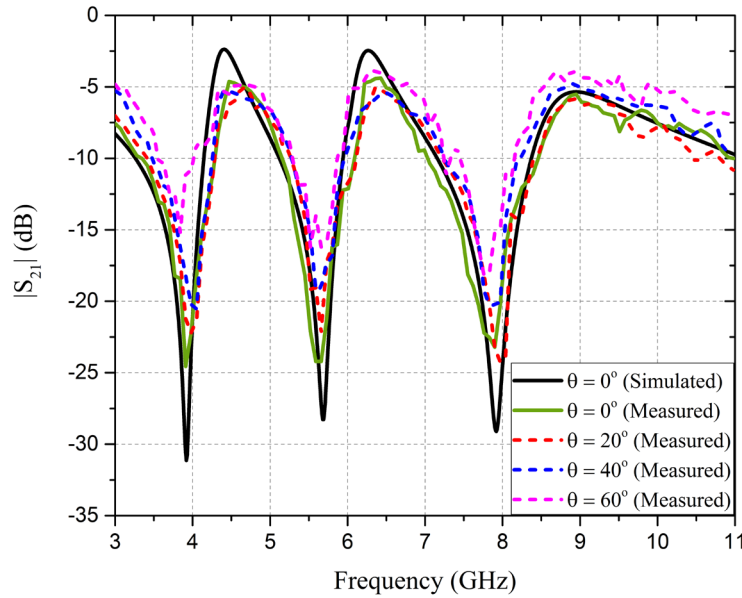
3.3.8 Proposed FSS design compared with various other FSS design reported in literature.

Table 3.2 contains the data of various FSS unit cell designs and are then compared with the given unit cell design. Dimensions of the unit cell, frequency ratio, number of bands,

resonant frequency, polarization stability and angular stability are the parameters on which the FSS is compared with various FSS implemented. The design of [83] and [167] resonates at one resonant frequency and design of [120], [119] and [164] resonates at dual



(a)



(b)

Figure 3-16 Measured frequency response curves under (a) TE and (b) TM incident mode, under normal and varying incident angles

Table 3-2 Triple band notched FSS compared with FSS structure in literature

Ref.	Size of unit cell $\text{mm}^3 \lambda$	Band	No. of bands	f_z TE TM (GHz)	Operational bands	Freq. Ratio (f_h/f_l)	-10 dB Bandwidth (Freq. range)	MFD % TE TM (AS in Deg.)	PI
[83]	$7 \times 7 \times 1.6$ $0.116\lambda \times 0.116\lambda$	Stop	1	5	WLAN	-	1.5 (4.2-5.7)	- - (0° - 60°)	Yes
		Pass		-		-	-		
[167]	$8 \times 7 \times 1.524$ $0.28\lambda \times 0.24\lambda$	Stop	1	10.5 -	3-30 GHz	-	-	- - (0° - 60°)	No
		Pass		-		-	-		
[120]	$46 \times 46 \times 0.5$ $0.14\lambda \times 0.14\lambda$	Stop	2	0.93, 1.72	GSM	1.84	0.3(0.75-1.25), 0.6(1.6-2.2)	- - (0° - 60°)	Yes
		Pass		1.35		-	0.1(1.3-1.4)		
[119]	$20 \times 20 \times 2$ $0.16\lambda \times 0.16\lambda$	Stop	2	2.45, 5.5	Wi-Fi and WLAN	2.24	0.63, 1.43	< 2 < 2 (0° - 45°)	Yes
		Pass		-		-	-		
[164]	$10 \times 10 \times 0.27$ $0.24\lambda \times 0.24\lambda$	Stop	2	7.23, 13.83	X and Ku band	1.91	-	- - (0° - 75°)	Yes
		Pass	2	9, 14.5		1.61	-		
[85]	$10 \times 10 \times 1.6$ $0.114\lambda \times 0.114\lambda$	Stop	3	3.5, 5.2, 10.2	WLAN, WiMAX, X- band	1.48, 1.96	0.5 (3.2-3.7), 1.9 (4.1-6), 4.1 (8-12.1)	- - (0° - 30°)	Yes
		Pass		-		-	-		
Design 1	$10 \times 10 \times 1.6$ $0.115\lambda \times 0.115\lambda$	Stop	3	3.45, 5.5, 8 -	WiMAX, WLAN and Satellite com., X-band	1.59, 1.45	0.3 (3.3-3.6), 0.9 (5.1-6), 1.2 (7.2-8.4)	1.8, - 5.3, 2.5 (0° - 40°)	No
		Pass	1	-		4.02	0.3(3.9-4.2)		
Design 2	$10 \times 10 \times 1.6$ $0.13\lambda \times 0.13\lambda$	Stop	3	3.92, 5.68, 7.93	WiMAX/downli nk satellite C band, WLAN, Satellite comm. X-band	1.44, 1.39	0.9 (3.3-4.2), 0.8 (5.1-5.9), 1.2 (7.2-8.4)	2, 0.5, 0.5, 0.5, 1.3 0.08 (0° - 70°)	Yes
		Pass	2	4.37, 6.22		1.42	0.2 (4.32-4.52), 0.22(6.18-6.4)		

* MFD –Maximum Frequency Deviation, AS – Angular Stability, PI – Polarization Insensitivity

resonant frequencies. The given design resonates at triple frequencies with better frequency band separation ratio and higher angular stability when compared with all the above given designs. The design represented in [164] is of the same physical dimensions as that of the given FSS design but the former only acquires dual bands with high resonant frequency band. The design represented in [85] and design 1 with respect to the given FSS design have the same physical dimensions and rejects almost same resonating bands. The design in [85] has an issue of side band wastage and has low angular stability. Design 1 eliminates the issue of side band wastage and provides better angular stability related to ref [85]. However, it works as a triple band rejection FSS only for TE incident polarized wave.

In comparison to design 1, the proposed design 2 is polarization insensitive for varying incidence angles and polarization angles. The maximum frequency deviation in design 1 is higher than design 2. Due to the symmetric nature of the design 2, it provides better angular stability than design 1. The given FSS design 2 separates the frequency bands residing in a very close proximity efficiently. The proposed design 2 have pass bands in between two stop bands and provide higher angular stability than the above mentioned unit cells.

3.4 Conclusion

In this chapter a polarization insensitive FSS design is presented which is simple to design and is compact in structure. The given structure band rejects WiMAX/downlink Satellite C-band, WLAN, Satellite communication X-band which resides in the frequency range of UWB. In the given structure, 90° rotational symmetric SSRRs and SL is printed on one side of FR-4 dielectric substrate and at other side another four 90° rotational symmetric SSRRs are imprinted. The unit cell size is of $10 \times 10 \text{ mm}^2$, which is $0.13\lambda \times 0.13\lambda$, where λ represents the wavelength corresponding to the first resonant frequency. An angular stability up to 70° is achieved. The structure also obtains -10 dB impedance bandwidth of 0.22 and 0.2 GHz for pass band ranging from 6.18 to 6.4 GHz and 4.32 to 4.52 GHz, respectively. The attenuation of the signal is reported to be more than 30 dB at resonant notches. At $\theta = 70^\circ$, the maximum relative deviation from the resonant frequency at normal incidence is reported to be of 2%. With -10 dB as reference, the

closely spaced bands are efficiently separated by the ratio of 1.42 at pass band, and 1.44 and 1.39 at stop band. A good degree of similarity is obtained in the resultant response curve of measurement and simulation. Therefore, the given FSS can become a suitable candidate in future communication systems.

CHAPTER 4

Dual Band Notched FSS using Single Resonant Element

4.1 Introduction

In many multifunctional devices which are operating commercially in the wireless communication, FSS has been used intensively. In current scenario, the need of multiple resonant elements is increasing to demolish bulky structure with high manufacturing and maintenance cost. Since most of the devices operate in microwave frequency range, there is a need to isolate the systems from one another, i.e., to electromagnetically shield the devices within the system. Multi-resonant FSS is thus considered. FSS helps in the achieving multiband resonant performance using individual FSS sheet. The mandatory requirement from an FSS is incident angle and polarization stability at varying communication path. The miniaturizing of the structure helps in attaining a steady response curves. This can be achieved by effectively increasing the metallic element length to increase the perimeter of the structure which further increases the inductance of FSS [10]. Yet another approach to attain low resonant frequency using compact structure is to increment the inductance and capacitance of structure as well. This can be done with the use of metamaterial (MM) [168]–[173]. The size of a conventional MM is one tenth the size of its guided wavelength. MM such as split ring resonators are self-resonant structure which provides negative permeability characteristics with narrow bandwidth but at the cost of asymmetric structure. Asymmetric structures make the design polarization sensitive. Thus, there is a need to make the structure symmetric. Various studies have shown symmetric designs with respect to the MM. In [165] two looped resonators and one rectangular resonator is used to extract triples bands with similar responses for both polarized plane wave. To make the SSRR structure symmetric, four SSRRs and T shaped resonators are positioned in 90° clockwise fashion. The structure resonates at dual resonant frequency for TE and TM polarized incident wave.

Thus in this chapter to obtain a smaller dimensioned structure two of the above approaches have been used. A simple and miniaturized FSS has been proposed to attain similar response curve under both polarizations. In this chapter, rotational symmetric

SSRR structure been used to eliminate polarization sensitivity. Moreover to make the design more compact for a given frequency range, a metallic patch at the center is implemented to connect all the four rotational symmetric SSRRs. The reset of this chapter is given as: In section 4.2 analysis and design of FSS is included with its design principle. Section 4.3 contains the simulated results as well as measured results and comparative study of dual notched FSS with FSS in literature has been done. Conclusion of the chapter has been done in section 4.4.

4.2 Design analysis of the FSS unit cell

4.2.1 Unit cell model

The prototype of the proposed unit cell FSS is illustrated in Figure 4.1. The brown color represents the metallic element placed over dielectric substrate. Four SSRRs are connected from the center with a metallic square patch. The modified SSRR is implemented at top layer of the FR-4 substrate having the dimension of $8 \times 8 \text{mm}^2$ and thickness of 1.6mm. With respect to λ which is wavelength with respect to the first resonant frequency, the dimensions are $0.081\lambda \times 0.081\lambda$. The values of all the parameters are presented in Table 4.1.

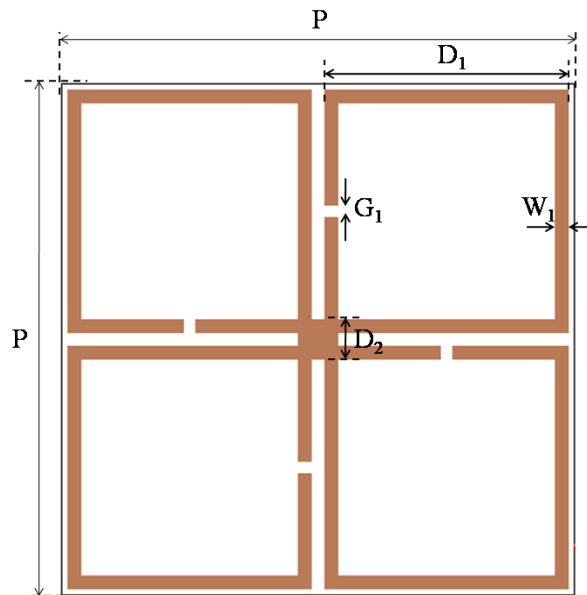


Figure 4-1 Design of a dual band notched unit cell FSS

Table 4-1 Parameters' list

Parameter	P	D ₁	D ₂	G ₁	W ₁
Value (mm)	8	3.8	0.6	0.2	0.2

4.2.2 Principle of operation and step by step development of unit cell

For a structure to remain refractive than diffractive and homogeneous, the periodicity for this structure is also taken to be less than $\lambda_g/4$. The proposed FSS unit cell is of an average size of $P=\lambda_g/5.05$, which is way smaller than the mentioned limiting value of P. λ_g is equal to 7.4 GHz, which is the centre frequency of operational band of 2.5 to 12.3 GHz. Rotational symmetric structure helps in achieving polarization insensitive behavior for every FSS design. With the implementation of gap in between the metallic loop of the SSRR, the overall capacitance of the FSS increases which results in decreased resonant frequency. In rotational symmetric SSRR, since all the four SSRRs are not connected together, there is no direct current flow from one SSRR to another. Therefore, a certain resonant frequency can only be attained. To obtain smaller resonant frequency from a given design, a metallic patch is imprinted at the center of the FSS connecting all the four SSRRs. The resultant is direct current flow from one SSRR to another which further increases the perimeter of the metallic arm with increase in inductance. The resonant frequency increases with the enhancement of inductance. Thus, physically the structure becomes miniaturized. Therefore, the evolution of the unit cell is as follows: in stage 1 four identical 90° clockwise rotational symmetric SSRR are implemented and in second step at the middle portion of the unit cell, a metallic square patch is implemented which connects all the edges of the four SSRRs, as shown in Figure 4.2.

4.3 Simulated and experimental results

4.3.1 Frequency response of the proposed unit cell

The simulated response curves of FSS are observed for transmission and reflection coefficient under both the polarized wave. The design has been simulated in Ansoft HFSS v.13 software. Figure 4.3 thus illustrates the response curves at different stages.

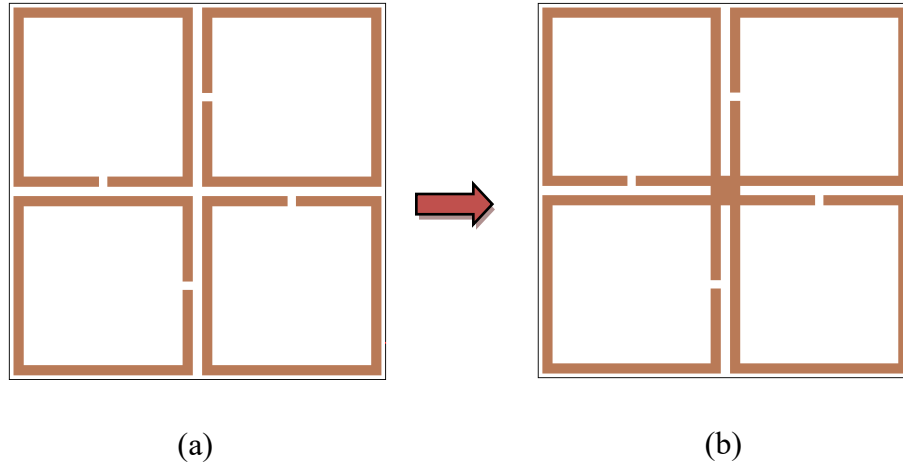


Figure 4-2 Stages in the making of dual notched FSS design

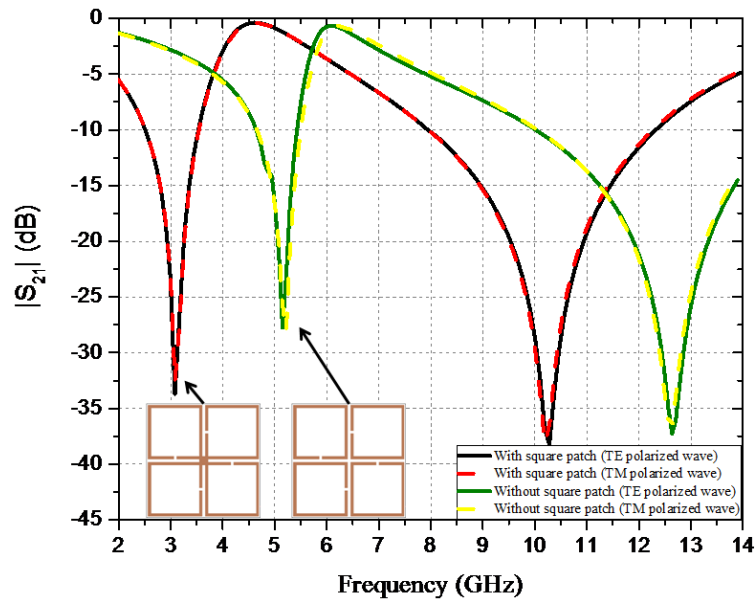


Figure 4-3 Simulated results of all steps used in the implementation of given unit cell

In stage 1, using the rotational symmetric SSRR the unit cell resonates at 5.15 GHz and 12.6 GHz. In stage 2 which is the final stage, both the resonant frequencies shift downwards to 3.08 GHz and 10.2 GHz with the implementation of metallic loop. This happens due to the increment of effective inductance of the structure.

The curves representing the transmission and reflection characteristic of the design under both the polarizations is illustrated in Figure 4.4. From Figure 4.4 it is evident that the structure is polarization independent as the frequency response under both the polarization is same. The given structure produces resonance at 3.08 and 10.2 GHz under both the incident polarized wave with -10dB impedance bandwidth of 1.1 and 4.3 GHz,

respectively. The given structure band-rejects dual frequency bands, i.e., mobile WiMAX band ranging from 2.5 to 2.7/3.3 to 3.6 GHz and X-band ranging from 8 to 12 GHz. A transmission pole is obtained in between the first and second stop bands. A resonant dip is obtained at 4.6 GHz ranging from 4.3 to 5 GHz. 3.31 is the ratio of closely separated dual bandstop. For the dual band stop frequency bands the fractional bandwidth is 35.71% and 43%, respectively and for the pass band the fractional bandwidth is 15.21%.

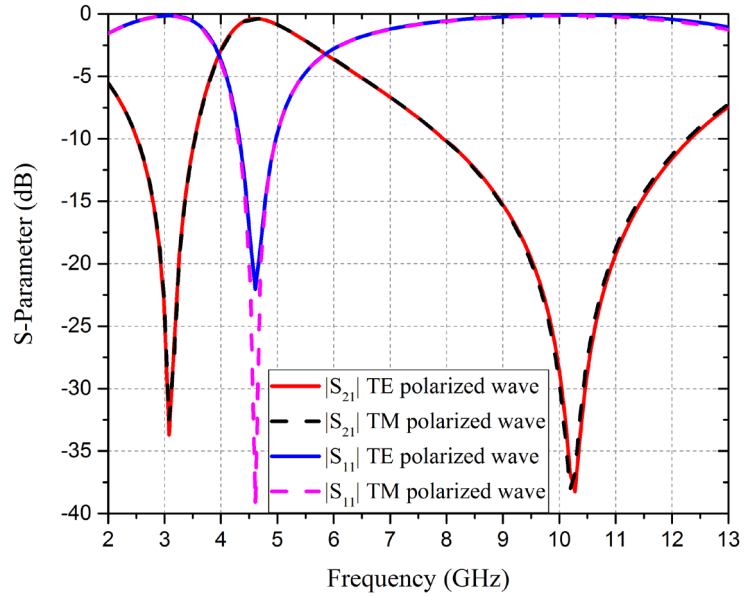


Figure 4-4 S-parameters with respect to frequency

4.3.2 Surface current distribution

At 3.08 GHz and 10.2 GHz for TE polarized incident wave, the surface current distribution is presented, as shown in Figure 4.5. Surface current distribution helps in analyzing the mechanism of any structure visually. The given FSS design produces resonance at two different frequencies due to the excitement of metallic elements at two different current paths. The flow of the current in two different paths is shown using the vector surface current distribution, shown in Figure 4.5. To distinguish the current paths, a black line is represented as the direction of flow of current in between the SSRRs at 3.08 GHz and 10.2 GHz. At 3.08 GHz, the current flows in one direction in between adjoining SSRR elements, i.e. from one end of the first element of SSRR to other end of the third element of the SSRR, as presented in Figure 4.5(a).

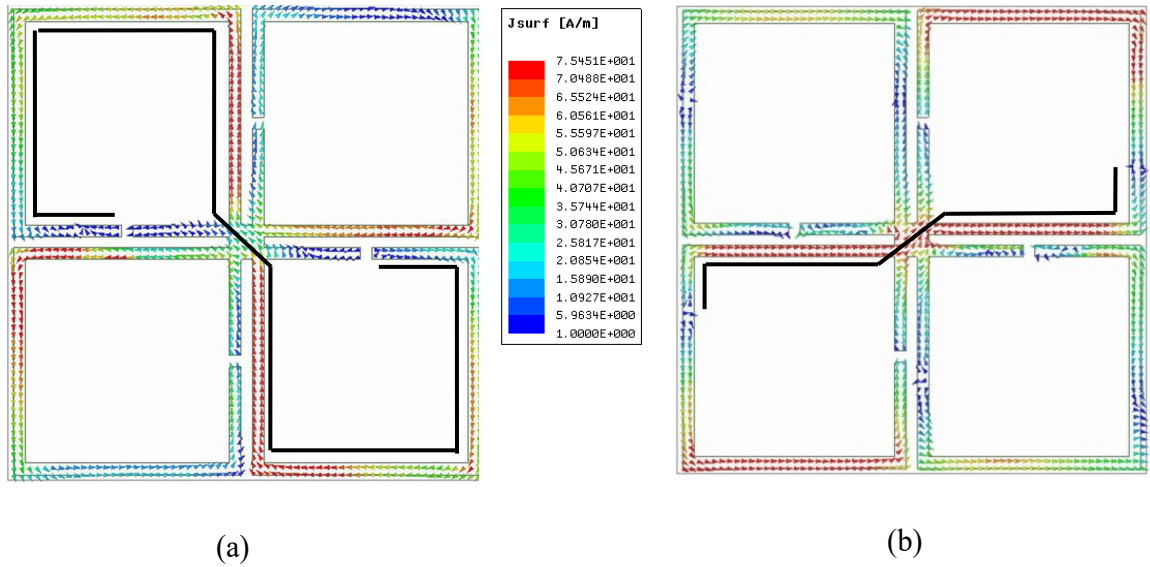


Figure 4-5 For TE incident polarized wave the surface current distribution at (a) 3.08 GHz and (b) 10.2 GHz

From examining Figure 4.5(a) it is clear that the overall perimeter of the structure increases with respect to the increase in electrical length, thus given structure resonates at lowest resonant frequency. At 10.2 GHz, the current path in each SSRR elements divides into two different parts. Thus the formation of short current path is observed in between SSRRs which results in resonance at higher end of the spectrum. It is also observed that with the connection of metallic patch, a high intensity path is formed among SSRRs using metallic patch.

4.3.3 Equivalent circuit model (ECM)

Figure 4.6 illustrates the ECM for individual SSRR element at 3.08 and 10.2 GHz. The evaluation of the current path is done for TE incident polarized wave. The current bearing metallic part is represented as inductors and the gaps are represented as capacitors. At 3.08 GHz resonant frequency, the current flows from end of the SSRR to another to form a full wavelength path. For the resultant of 3.08 GHz, full length path is considered equal to the inductance which is a series combination of L_1 and L_2 , as shown in 4.6(a).

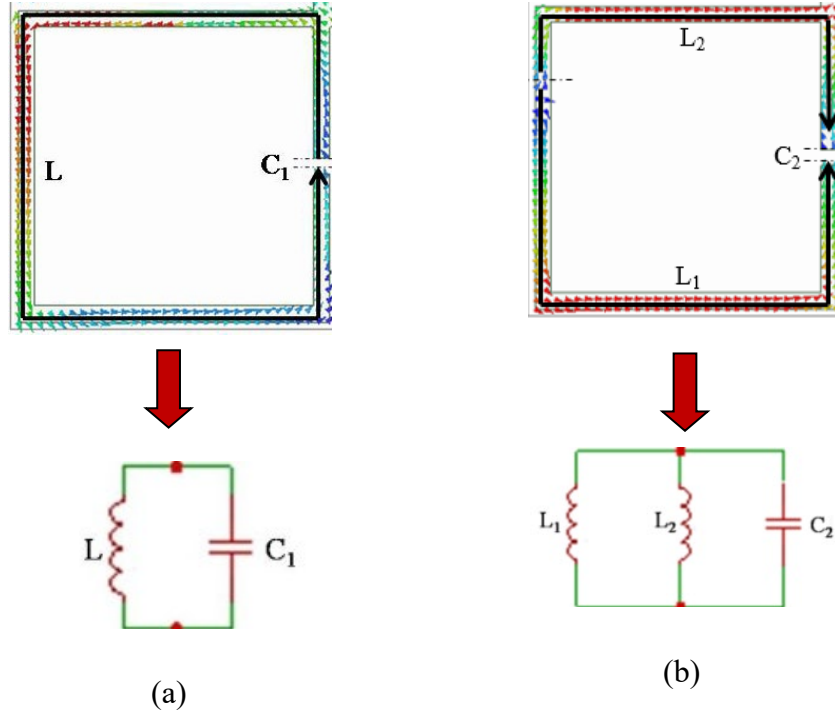


Figure 4-6 ECM with respect to surface current distribution for individual SSRR element at (a) 3.08 and (b) 10.2 GHz

Two wavelength paths get formed, when the surface current distribution is checked at 10.2 GHz. Hence the inductance here is equivalent to two inductances L_1 , L_2 and L_3 connected in parallel circuit, as shown in Figure 4.6(b). In the case of 10.2 GHz, the inductance of the structure is less than the former one, thus the structure resonates at higher frequency of the spectrum. The capacitance here is the addition of gap and surface capacitance.

The resonance frequency for SSRR at 3.08 GHz and 10.2 GHz is given as follows:

$$f_{3.08\text{GHz}}^{SSRR} = \frac{1}{2\pi\sqrt{L \times C_1}} \quad (4.1)$$

$$f_{10.2\text{GHz}}^{SSRR} = \frac{1}{2\pi\sqrt{(L_1 \parallel L_2) \times C_2}} \quad (4.2)$$

here C_1 and C_2 represents the capacitances and L_1 and L_2 represents the inductances of individual SSRR element. With the implementation of metallic patch, the surface current flows through it, as shown in Figure 4.5. Thus, the ECM is modified and the metallic

patch is represented as inductance L_M . As the current is moving in the same direction in both cases through the metallic patch and the SSRRs, both elements of SSRR are attached in series in the lumped circuit. C_c is the coupling capacitance. Thus, ECM of the dual notched FSS is presented in Figure 4.7 (a) and (b).

The overall transmission zero frequencies are as follows:

$$f_{3.08GHz} = \frac{1}{2\pi\sqrt{(2L + L_M) \times (2C_1 + C_{c1} / 2)}} \quad (4.3)$$

$$f_{10.2GHz} = \frac{1}{2\pi\sqrt{(2(L_1 \parallel L_2) + L_M) \times (2C_2 + C_{c2} / 2)}} \quad (4.4)$$

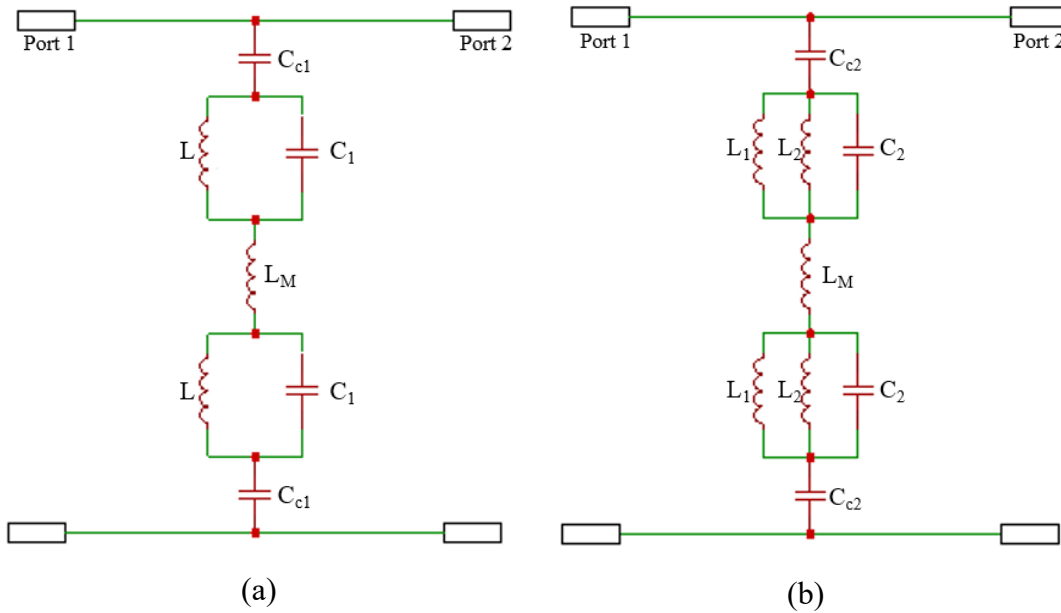


Figure 4-7 ECM with respect to surface current distribution for proposed FSS design at (a) 3.08 and (b) 10.2 GHz

All the values of modified SSRR at 3.08 and 10.2 GHz has been calculated similarly as that in Chapter 2. The calculation has been done at normal incidence under TE incident polarization. The calculated values are optimized in ADS and all the elements are listed as: $L = 9.45\text{nH}$, $L_1 = 6.63\text{nH}$, $L_2 = 2.75\text{nH}$, $L_3 = 2.6464\text{nH}$, $C_1 = 1.22\text{fF}$, $C_{c1} = 0.2746\text{ pF}$, $C_2 = 1.22\text{fF}$, $C_{c2} = 0.1223\text{ pF}$. Two of the above ECM models have been combined together in the ADS and the frequency response is extracted. Figure 4.8 shows the

comparison of the curve obtained by HFSS and ADS and almost similar response curves are obtained in both the simulator.

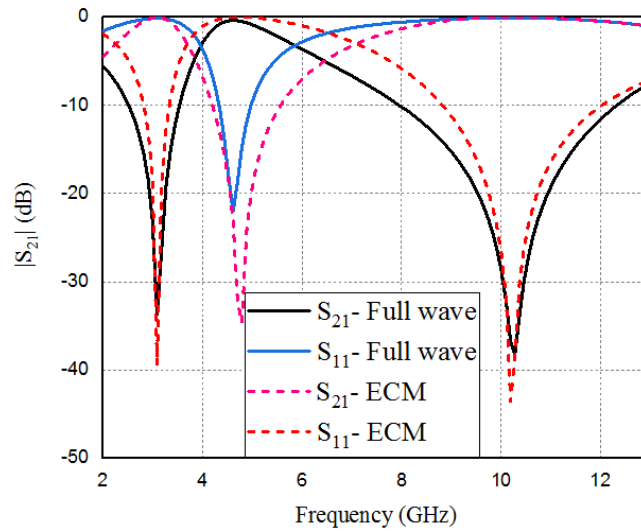


Figure 4-8 Comparison of frequency response curve for full wave and circuit simulator

4.3.4 Electromagnetic shielding

Shielding effectiveness with respect to the frequency is illustrated in Figure 4.9. Using the equation 1.14, under both the polarizations the attenuation of more than 10 dB is procured in the response curve. It is also observed that at normal incident wave maximum attenuation of 38 dB is attained.

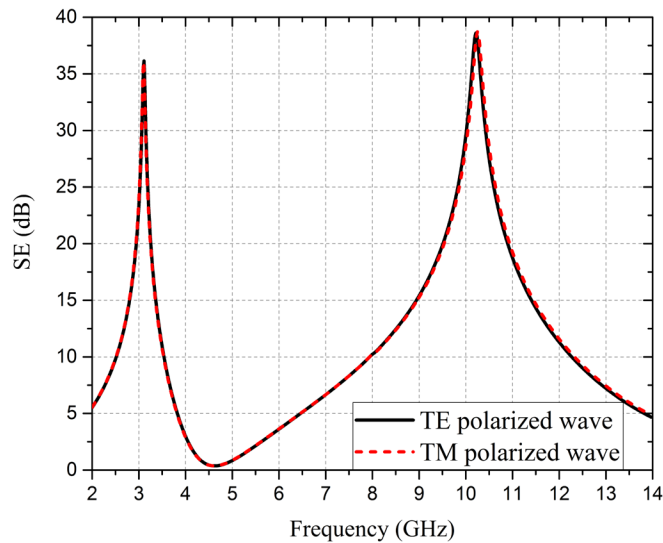
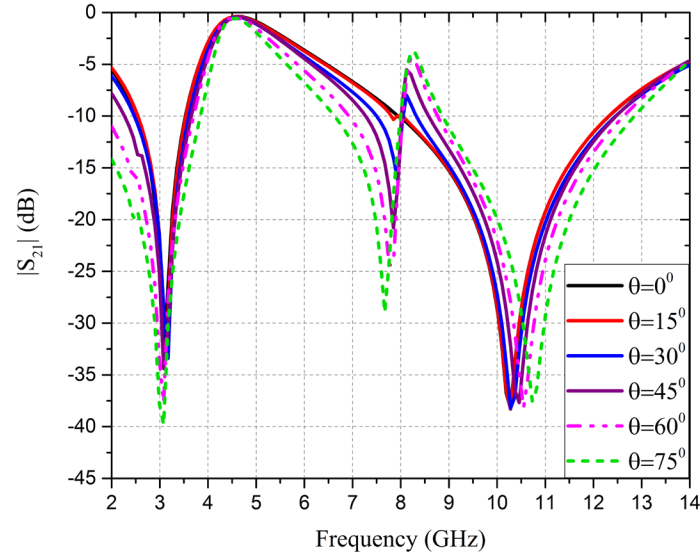


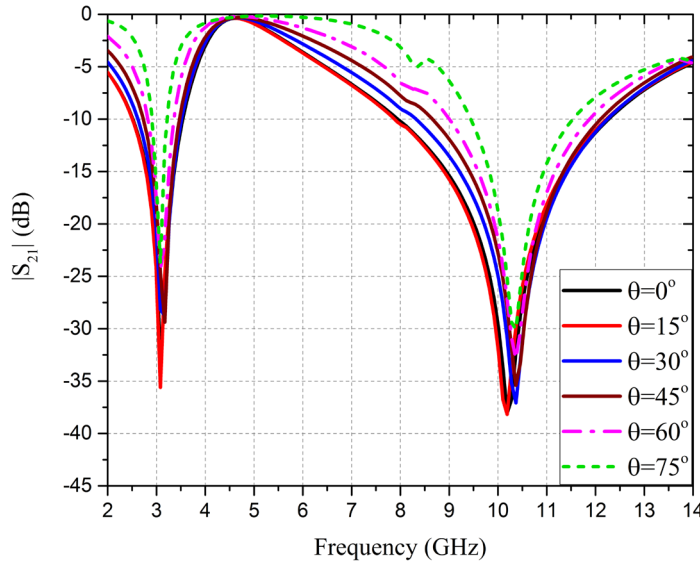
Figure 4-9 Shielding effectiveness at $\theta = 0^\circ$.

4.3.5 Frequency response curve at various incident and polarization angles

For FSS to be stable under varying environmental conditions, the frequency response should remain same even at different impinging incident angles as well as polarization angles. Transmission coefficient is studied at varying incident and polarization angle with respect to the frequency. Frequency response under wide incident angle (θ) at $\phi=0^\circ$ for both the TE and TM polarization is illustrated in Figure 4.10 (a) and (b).



(a)



(b)

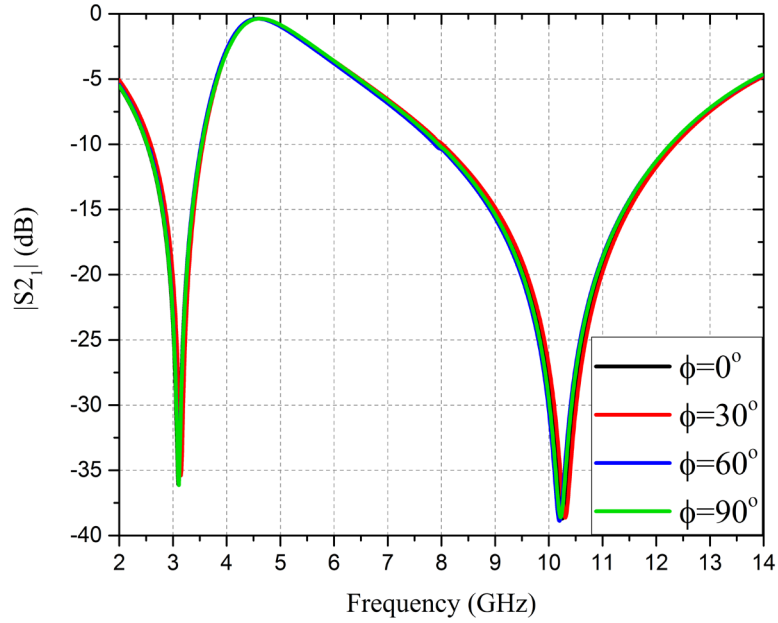
Figure 4-10 Frequency responses at varying angle of incidence at (a) TE and (b) TM mode

Up to 75° in both the wave polarization cases, the resonant notches are stable. In the case of TE polarized wave an additional resonance is obtained at 8 GHz after 30° angle of incidence. First resonance remains stable for all the incident angles but second resonant frequency shifts after 45° . Moreover, in case of TM polarized wave structure shows isotropic response for all the incident angles. Overall the structure shows a stable frequency response till 75° for all the resonant notches. It is observed that at $\theta = 75^\circ$, the maximum frequency deviation from the obtained transmission zero frequencies are 0.025 and 0.13 GHz under TM polarization, and 0.09 and 0.43 GHz under TE polarization. From equation 2.1, it is observed that the maximum relative deviation in between the dual resonant notches obtained at normal incidence and $\theta = 75^\circ$ incident TE polarized wave is 0.8% and 4.2%. The deviation at $\theta = 75^\circ$ incident TM polarized wave is 0.9% and 1.2%. Since the percentage deviation is very less, thus the dual notched FSS provides better steadiness towards wide incident angles. It is thus examined that the proposed FSS produces better angular stability under both the polarized waves. Under TM and TE polarization it is also evident that the bandwidth of the structure decreases and increases with wide angle of incidence, respectively. This occurs due to reduction of wave impedance under TM polarization and increment in the other. At $\theta=0^\circ$, the frequency response under wide polarization angle (ϕ) for both the polarizations is presented in Figure 4.11 (a) and (b).

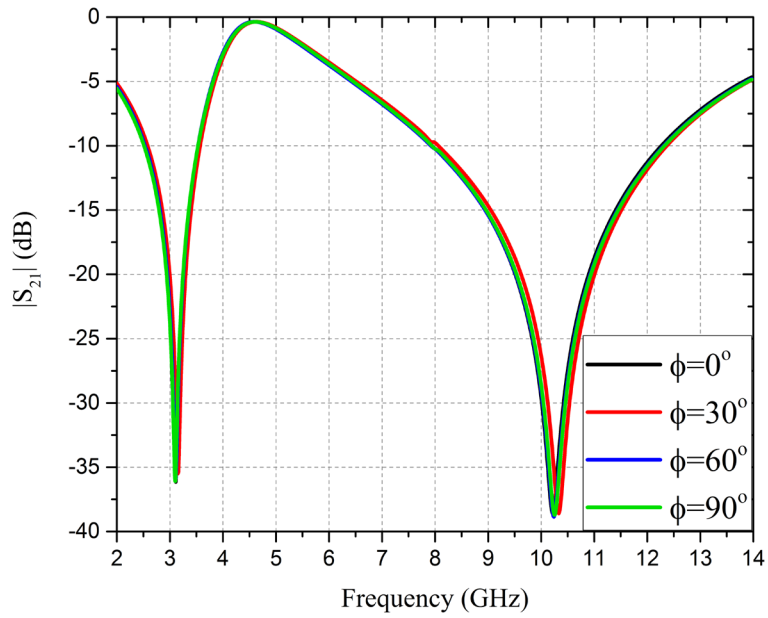
The frequency deviation under varying polarization angle is negligible in both the polarized waves. Due to symmetric nature of the given design, the structure assures approximately similar response curves regardless of the angle of polarization. Hence a steady response curve is attained. From equation 2.2, it is inferred that for both the notches, the highest tolerable limit of P is 49 mm and 14 mm, respectively. The given FSS has the value of P lower than the tolerable limit. Thus a good stability towards varying incident angle is observed till 75° .

4.3.6 Parametric analysis

At 3.08 and 10.2 GHz the given FSS design resonates. However, the resonance frequency of any given design depends upon the variation of its parameters. Here, the variation of width W_1 and gap G_1 is illustrated in Figure 4.12.



(a)

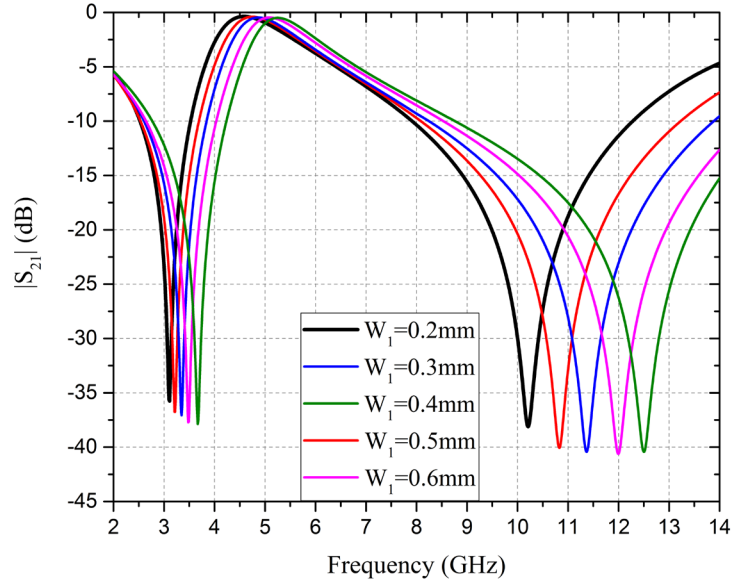


(b)

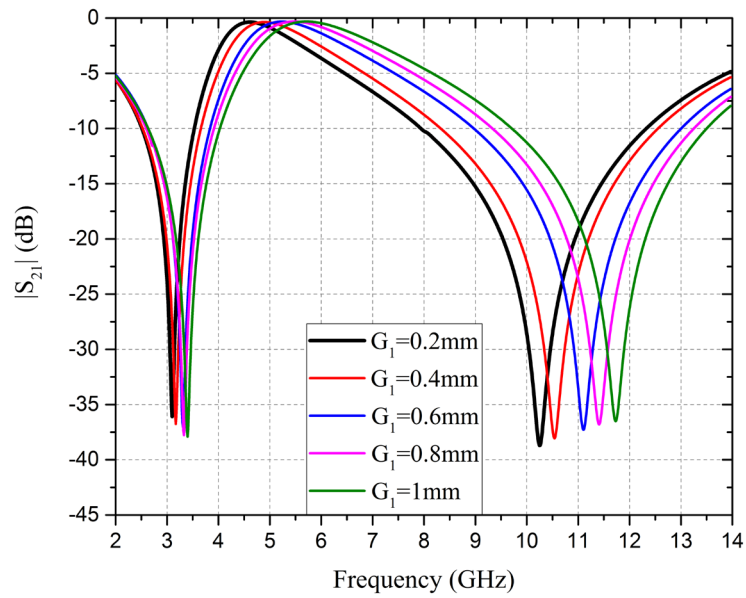
Figure 4-11 Frequency responses at varying polarization angles at (a) TE and (b) TM mode

With the enhancement of the width of the metallic arms, the resonant notch moves towards the higher end of the spectrum with enhanced bandwidth, as illustrated in Figure 4.12(a). With the variation of the gap G_1 , it is evident that as the gap in between the metallic loops of all the SSRRs increases equally, the overall capacitances decreases, thus

the resonant frequency increases. This is represented in Figure 4.12(b). The shift in both the resonant frequencies is obtained while the variation are shown for width W_1 and gap G_1 . However, the effect of variation is more visible in the second resonance.



(a)



(b)

Figure 4-12(a) Change in the width W_1 and (b) gap G_1

4.3.7 Verification of the simulated results experimentally

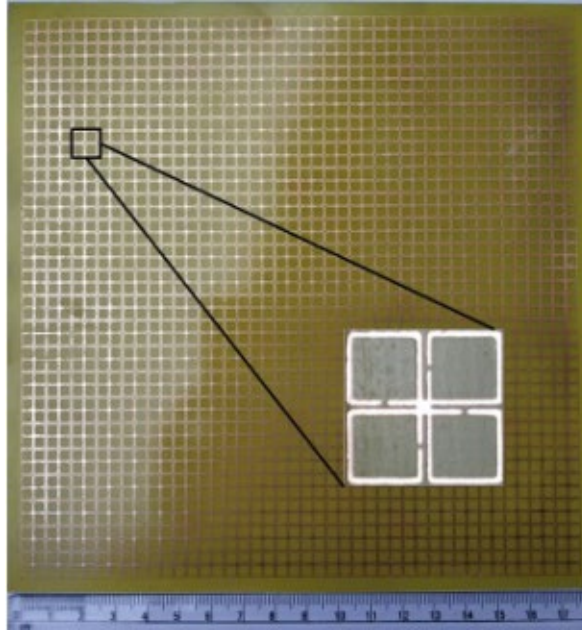
For the verification of the simulated results, the given design is implemented over FR-4

substrate of the height of 1.6 mm. A periodic array of 22×22 unit cells is implemented over a $176 \times 176 \text{ mm}^2$ dimensioned substrate. The manufactured FSS sheet is illustrated in Figure 4.13 (a). The measurement of response curves of frequency is accomplished inside the anechoic chamber. The image of the measurement setup is shown in Figure 4.13 (b). The measured result is obtained at normal as well as varying incident angle till 60° . On comparing the resultants obtained by simulation and measurement, a good match is procured which is presented in Figure 4.14 (a) and (b). It is observed that small variations are present in transmission curves of the measured results because of the limitation in measurement and fabrication error.

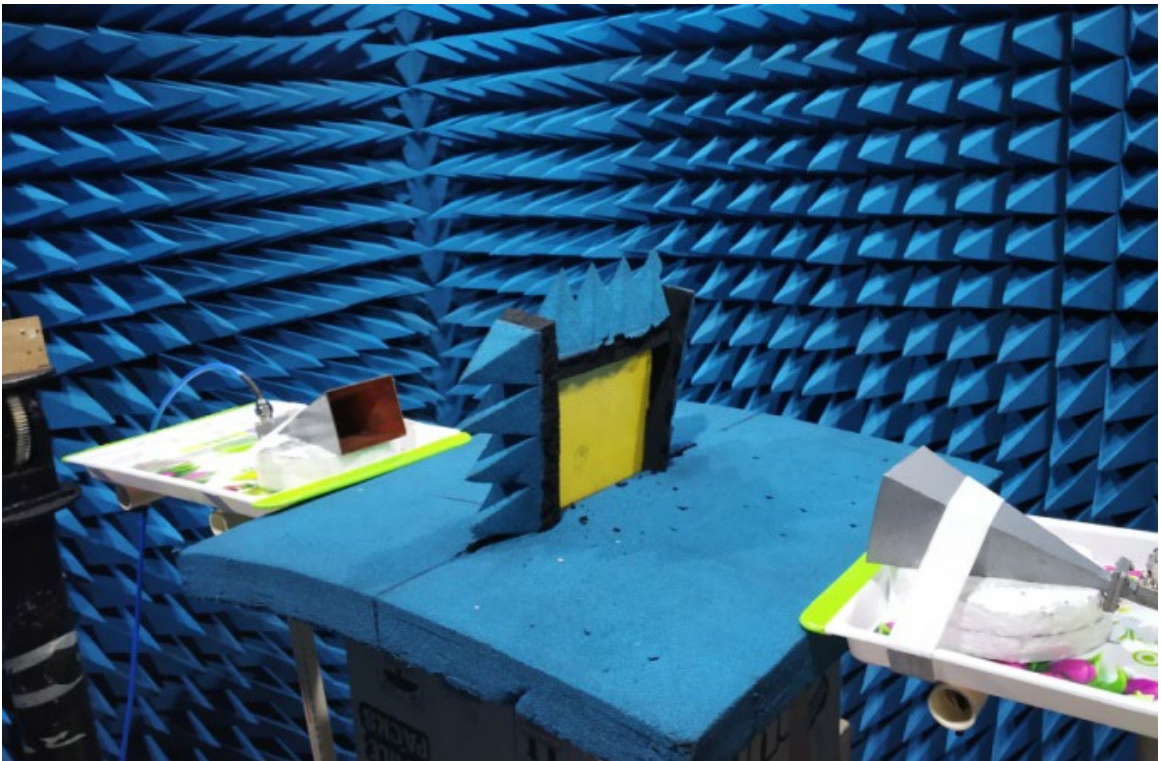
4.3.8 Comparison of various unit cell FSS

Table 4.2 contains the data of various FSS unit cell designs and is then compared with the given design. Dimensions of the unit cell, number of bands, number of resonating elements, resonant frequency, polarization stability and angular stability are the parameters on which the given FSS is compared with various FSS in the literature. It is clear from the table that the comparison is done for dual band stop designs with the designs present in [119], [174], [175] and [164]. Large unit cells such as that implemented in [119], [174] and [175] does not provide high angular stability. The design in [164] has used similar approach of using a rotational symmetric SRR structure but since the metallic loops are not interconnected, the design resonates at higher frequency. Moreover, the size of the structure is also quite large while comparing with the dual band notched FSS unit cell design.

While comparing design 1 and design 2 of chapter 3 and chapter 4, respectively, with FSS design 3 it is observed that the later provides better angular stability than the other two designs due to further miniaturization of the design. The maximum frequency deviation of design 3 is better than design 1 and design 2. Design 1 and design 2 uses three resonant elements to achieve triple band rejection, whereas, design 3 makes use of only single resonating element to provide dual band notched characteristics.



(a)



(b)

Figure 4-13 Fabrication prototype (a) top layer and (b) FSS sheet inside the anechoic chamber

Table 4-2 Comparison of dual band FSS with FSS design in literature

Ref.	Size of unit cell mm^3/λ	Band	No. of bands	f_r TE TM (GHz)	No. of elements	Operational bands	-10 dB Bandwidth (Freq. range)	MFD % TE TM (AS in Deg.)	PI
[119]	$20 \times 20 \times 2$ $0.16\lambda \times 0.16\lambda$	Stop	2	2.45, 5.5	1	Wi-Fi and WLAN	0.63, 1.43	< 2 < 2 (0°-45°)	Yes
		Pass		-			-		
[174]	$10 \times 10 \times 0.27$ $0.11\lambda \times 0.11\lambda$	Stop	2	3.46, 5.14	2	-	-	- - (0°-45°)	Yes
		Pass		-					
[175]	$10.4 \times 10.4 \times 1.6$ $0.088\lambda \times 0.088\lambda$	Stop	2	2.54, 3.54	2	S-band	0.315, 0.1785	- - (0°-60°)	Yes
		Pass	1	3.1					
[164]	$10 \times 10 \times 0.27$ $0.24\lambda \times 0.24\lambda$	Stop	2	7.23, 13.83	2	X and Ku band	-	- - (0°-75°)	Yes
		Pass	2	9, 14.5			-		
Design 1	$10 \times 10 \times 1.6$ $0.115\lambda \times 0.115\lambda$	Stop	3	3.45, 5.5, 8 -	3	WiMAX, WLAN and Satellite com., X-band	0.3 (3.3-3.6), 0.9 (5.1-6), 1.2 (7.2-8.4)	1.8, 5.3, 2.5 (0°-40°)	Yes
		Pass	1	-			0.3(3.9-4.2)		
Design 2	$10 \times 10 \times 1.6$ $0.13\lambda \times 0.13\lambda$	Stop	3	3.92, 5.68, 7.93	3	WiMAX/downlink satellite C band, WLAN, Satellite comm.	0.9 (3.3-4.2) 0.8(5.1-5.9) 1.2(7.2-8.4)	2, 0.5, 0.5, 0.5, 1.3 1.3 (0°-70°)	Yes
		Pass	2	4.37, 6.22		X-band	0.2(4.32-4.52), 0.22 (6.18-6.4)		
Design 3	$8 \times 8 \times 1.6$ $0.081\lambda \times 0.081\lambda$	Stop	2	3.08, 10.2	1	Mobile WiMAX and X-band	1.1 (2.5-3.6), 4.35(7.95-12.3)	0.8, 0.9, 4.2 1.2 (0°-75°)	Yes
		Pass	1	4.6			0.7 (4.3-5)		

* MFD –Maximum Frequency Deviation, AS – Angular Stability, PI – Polarization Insensitivity

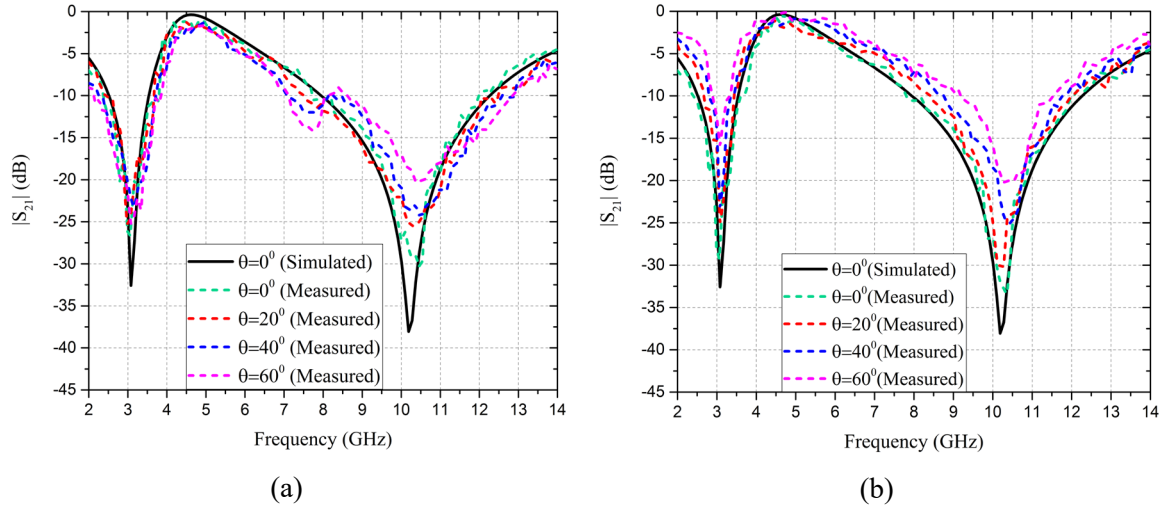


Figure 4-14 Measured frequency response curves under (a) TE and (b) mode, under normal and varying incident angles

4.4 Conclusion

A modified 90° clockwise rotational symmetric SSRR is implemented and studied in this chapter in which a metallic patch is implemented at the middle of FR-4 substrate to connect all the four SSRRs. The given unit cell is implemented upon $8 \times 8 \text{ mm}^2$ dielectric substrate which is effectively equivalent to $0.081\lambda \times 0.081\lambda$, where λ is the wavelength corresponding to the first resonant frequency. The proposed design resonates at 3.08 GHz (2.5-3.6 GHz) and 10.2GHz (8-12.3 GHz). Mobile WiMAX and X-band has been rejected using the presented design. At 4.6 GHz a -10 dB pass band resonant dip is also obtained and its impedance bandwidth is 0.7 GHz (4.3 - 5 GHz) which is observed using the reflection coefficient curve. For the first and second stop band, fractional bandwidth of 35.71% and 43% is attained, respectively. Moreover for the pass band, the fractional bandwidth of 15.21% is attained. At $\theta = 75^\circ$, the maximum relative deviation from the resonant frequency at normal incidence is reported to be of 1.2% for TM and 4.2% for TE mode. A good degree of similarity is obtained between the measured and simulated frequency response curves. Therefore, the proposed FSS design can become a suitable candidate in future communication systems for filtering applications.

CHAPTER 5

Design and Analysis of UWB FSS using Modified SL

5.1 Introduction

Adaptation to wireless technology is bliss as many of the systems are working in the microwave frequency range for commercial applications. UWB has been studied for ages and with the commercialization of this band, most of the work is carried out in this band, thus making the given frequency band more prone to saturate. To avoid the signal leakage or to shield a given system, the implementation of UWB FSS is a necessary. Therefore, for the shielding of 3.1 to 10.6 GHz UWB various methods have been implemented in the literature. A combination of offset modified cross dipoles and SL is imprinted over a substrate and is used to band reject 4 to 14 GHz frequency band [176]. In [177] modification on SL is performed with the implementation of metallic arm of cross shape to band reject 4.85 to 17.23 GHz frequency band. But with the implementation of largely sized FSS designs as the aforementioned ones, the angular stability of the structure reduces and it becomes difficult to cover the lower cut-off frequency of 3.1 GHz.

From previous chapters, as mentioned in chapter 2, 3 and 4, it is clear that to attain approximately similar EM characteristics in a practical scenario in a limited space as that of the ideal EM characteristics, the unit cell size should be made compact. The resonant frequency of any structure is dependent upon the inductance and capacitance of the given structure and the most common technique to reduce the size of the unit cell for any given FSS is by increasing the capacitance, inductance or both of the given FSS. This technique has been implemented in the literature a lot. On both the layers of the dielectric substrate a convoluted metallic element is implemented to band reject 3.1 to 13.3 GHz frequency range but has a stable frequency response up till 45° only [178]. A simple SL is modified such that the effective path length of the metallic element is increased to bandstop 2.72 – 13 GHz frequency range [179]. The designs mentioned above covers the whole UWB frequency range and are polarization insensitive but side band wastage is quite high. The other technique to obtain similar frequency response as that of the ideal one is to

implement multilayer FSS. Multilayer FSS designs have faster roll-off and much better frequency response than the planar FSS structures. With all the goodness, the main issue with stacking of the layers is bulky systems and the cost of the fabrication shoots up.

A recent approach to achieve size reduction with high angular stability is the implementation of 3D FSS design. In [180], a quasi-elliptical 3D FSS is implemented which provides an impedance bandwidth of more than 70%. Two identical vias are passed through the aperture at the middle of the ground with two dipoles cross tapered to implement a 3D FSS design. The above design band stops 3.1 to 10.6 GHz band [181]. The structure such as these attains way better frequency response with good level of compactness for a given design but designing and fabrication complexities are very high with high cost of production.

It has been observed in aforementioned designs that some fails to cover either the lower or higher cut-off frequency. While some structures do attain the desired frequency band but the designs are either bulky, difficult to design and fabrication or have high cost of production. It is a challenge to obtain the desired results using simple FSS structure. Therefore, in this chapter a simple and miniaturized SL is implemented to acquire an UWB FSS (3.1 – 10.8 GHz). The design is simple yet effective and provides high signal attenuation. The structure produces a steady response curve of frequency with respect to angle of incidence and polarization. The rest of the chapter is given as: in section 5.2 analysis and design of UWB FSS is included with its design principle. Section 5.3 contains the comparative study of resultant response curve corresponding to simulation and measurement. Moreover, UWB FSS is compared with various FSS in the literature. Conclusion of the chapter has been done in section 5.4.

5.2 Design analysis of UWB FSS unit cell

5.2.1 Unit cell model

Figure 5.1 illustrates the UWB FSS unit cell design. The brown color represents the metallic element placed over dielectric substrate. A modified SL is imprinted on the FR-4 substrate with the overall size of $6 \times 6 \text{ mm}^2$. The modification is performed in such a way that four similar metallic arm lengths are positioned at the corner of the traditional SL

and other four are implemented at the inner periphery of the aforementioned SL. The effective dimension of the proposed FSS is $0.062 \lambda \times 0.062 \lambda$. Here λ is the wavelength corresponding to the lower cut off frequency of UWB. The values of parameters of the UWB FSS design are presented in Table 5.1.

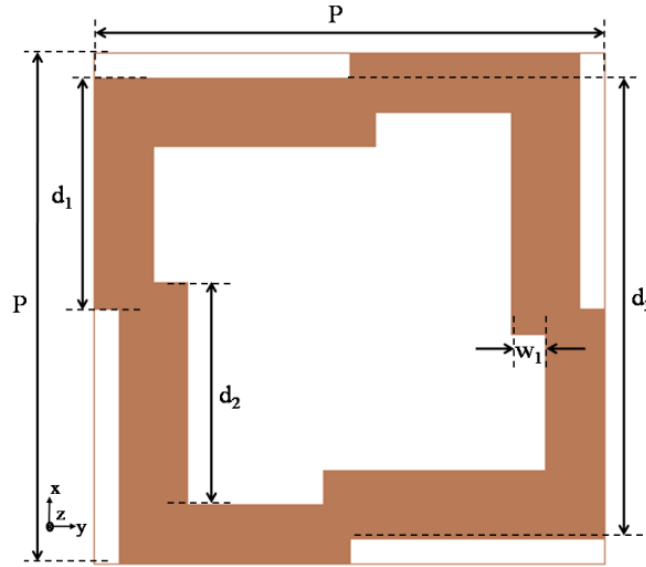


Figure 5-1 UWB FSS design

Table 5-1 Parameters' list

Parameter	P	d ₁	d ₂	d ₃	w ₁
Value (mm)	6	2.7	2.6	5.4	0.4

5.2.2 Principle of operation and stages in the making of UWB FSS

For a structure to remain refractive than diffractive and homogeneous, the periodicity for this structure is also taken to be less than $\lambda_g/4$. $P=\lambda_g/7.1$ is the average dimensions of UWB FSS unit cell, which is way smaller than mentioned limiting value of P. λ_g is equal to 6.95 GHz which is the centre frequency for 3.1 to 10.8 GHz frequency range. It is well known that a wide impedance bandwidth is obtained using conventional SL FSS design and overall perimeter of the given SL is equivalent to resonating wavelength. Despite being the simplest structure, the issue with SL is that it cannot attain the desired cut off frequency with the dimensions of the structure as small as $6 \times 6 \text{mm}^2$ under the tolerable limit of fabrication. Therefore the proposed structure is a modification of the

conventional SL structure. The resonating frequency of a closed loop structure is given by $f = 1/2\pi\sqrt{L_{eq}C_{eq}}$, where C_{eq} and L_{eq} are the equivalent capacitance and inductance, respectively. For the enhancement in inductance of the structure, the perimeter of the resonating element is increased to procure the lower cut off frequency. However, as the inductance increases the obtained bandwidth decreases ($BW \propto \sqrt{C_{eq}/L_{eq}}$). The decrement of the bandwidth is then adjusted by varying the width of SL, i.e., as the width of loop increases the bandwidth of the structure also increases. The structure is symmetrical thus provides similar frequency response for the incident wave at both the polarizations as well as under varying polarization angles. Therefore, the stages in the making of the UWB FSS are present in Figure 5.2.

As shown in Figure 5.2(a), initially a conventional SL is implemented having $d_1 = 5.4$ mm and 0.4 mm as width. 18.4 mm and 21.6 mm are the outer perimeter and inner perimeter of the design in stage 1, respectively. In stage 2, metallic arms which are four to count and of similar dimensions are implemented at the outer corner of this simple SL, as shown in Figure 5.2(b). While the inner perimeter remains the same, the outer perimeter becomes equal to 23.92 mm. Now overall width w_a becomes equal to 0.69 mm for the arm length where outer arm is connected. In stage 2 an intermediate step is also discussed for the evaluation of the given design completely. In this after the first stage of designing, four inner metallic arms are implemented having the width 0.4 mm and length $d_2 = 2.6$ mm, as illustrated in Figure 5.2(c). Here outer and inner perimeter remains same as stage 1. But SL width increases to $w_b = 0.8$ mm for the portion where inner loop is implemented. Finally, in stage 3, SL, inner arms and outer arms are implemented as illustrated in Figure 5.2(d). The overall width and perimeter of the UWB FSS enhances and thus the given structure rejects the entire UWB.

5.3 Simulated and experimental results

5.3.1 Frequency response of the UWB FSS

The reflection and transmission of the UWB FSS design is obtained under both the polarizations with respect to the frequency. Figure 5.3 illustrates the simulation of all the

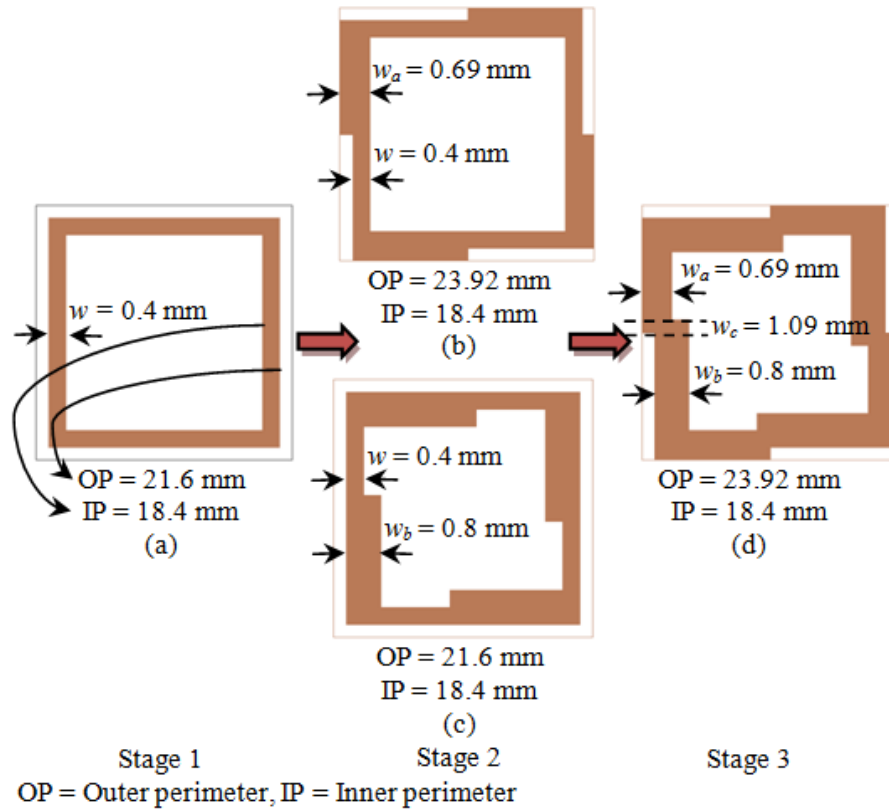


Figure 5-2 Stages in the making of UWB FSS design

stages implemented in the making of UWB FSS design. For stage 1, the simulation is performed in which only traditional SL is used. The structure at this point resonates at 9.9 GHz for 7 to 12.2 GHz frequency range. In the design of stage 2 case 1, the resonance is achieved at 5.35 GHz for 2.55 - 8.7 GHz frequency range. It can be seen that there is a drastic shift of the resonance downwards the spectrum which is the resultant of increased perimeter of the modified SL. The bandwidth of the structure has also been increased. This happens due to the increase in the modified SL width. Further, in case 2 of stage 2, the resonance is achieved at 10.8 GHz for 7.5 - 13.2 GHz frequency band. The perimeter of the structure does not change, however the width of the structure increases and therefore the bandwidth of the structure increases with increase in the resonant frequency. In the final stage, all the elements are implemented together which results in increased width and perimeter of the UWB FSS design. Thus, the structure resonates at 6.7 GHz and it ranges from 3.1 to 10.8 GHz, thus covering entire UWB frequency range.

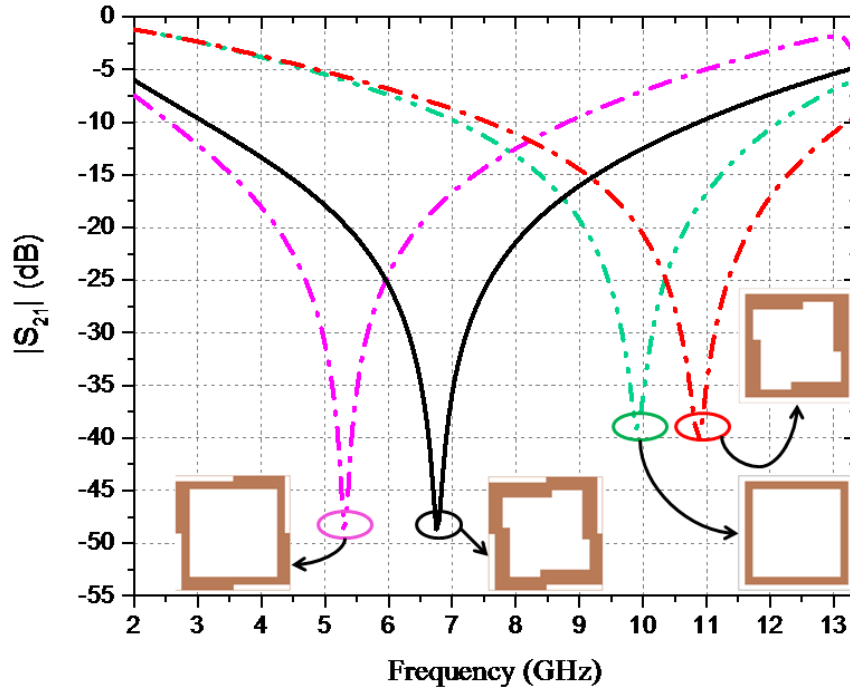


Figure 5-3 Simulation of various stages of UWB FSS

The response curves representing reflection and transmission characteristic of UWB is illustrated in Figure 5.4. It is evident from Figure 5.4 that the structure is polarization insensitive as the frequency response under both the polarizations is same. Under the TE polarized incident wave, UWB FSS produces resonance at 6.7 GHz for 3.1 to 10.8 GHz frequency bands. Approximately the same response curve is obtained for the TM polarized wave. The UWB FSS provides a resonance at 6.75 GHz for 3.1 to 10.8 GHz frequency bands. Therefore, given UWB FSS structure works upon the entire frequency band of UWB. For UWB stop band under both the polarizations, the fractional bandwidth of 110.79 % is achieved. It is also inferred that for both curves, the attenuation of more than 10 dB is procured. It is also observed that at normal incident wave maximum attenuation of 49 dB is attained.

5.3.2 Surface current distribution

For the analysis of the mechanism at which the UWB FSS design works, surface current distribution is showcased. The surface current distribution here is presented at 3.1 GHz (lower cut off frequency), 6.7 GHz (resonant frequency) and 10.8 GHz (upper cut off frequency) for TE polarized incident wave, as illustrated in Figure 5.5. At lower cut-off

frequency, i.e., at 3.1 GHz, the outer edges of the proposed design show the maximum current intensity, as illustrated in Figure 5.5(a). The current is equally distributed over the arms of resonant element of UWB FSS at 6.7 GHz. Moreover, at 10.8 GHz which is the upper cut off frequency, the maximum current intensity is examined at the inner side of the resonant element of UWB FSS. Therefore, it is evident that the upper and lower cut-off frequency is procured using inner and outer metallic arms of UWB FSS design, respectively.

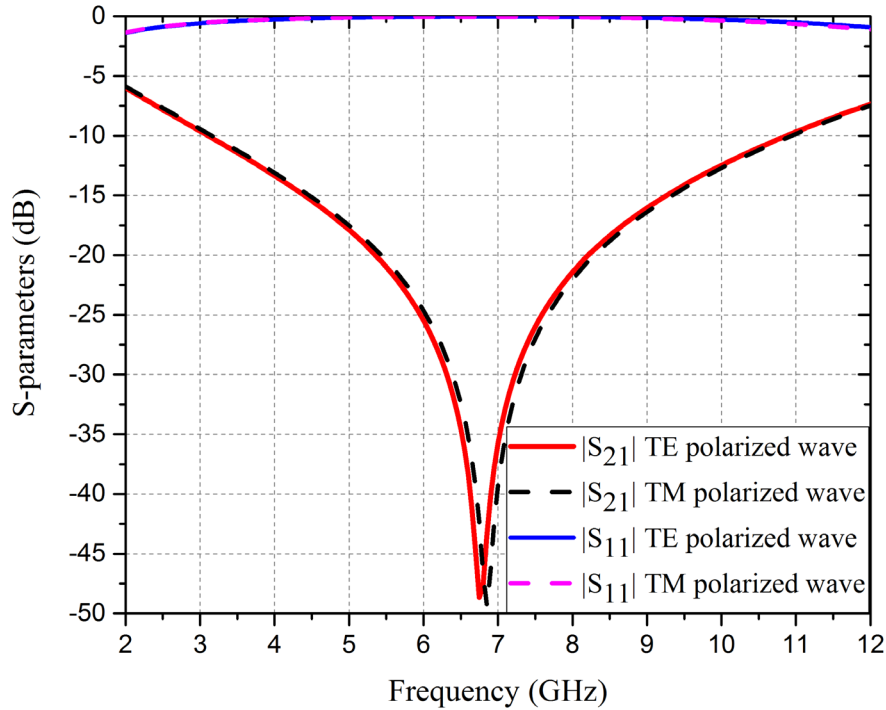


Figure 5-4 Transmission and reflection coefficient curve with respect to frequency

5.3.3 Equivalent circuit model (ECM)

Figure 5.6 presents the ECM of UWB FSS design which is developed with the help of vector surface current distribution. The two maximas are obtained between two minimas dividing the modified SL path length equally. Since the current is flowing in opposite direction, the current path is divided into two equal parts, as presented in Figure 5.6(a). Therefore, two parallel paths get formed. Each electrical length corresponding to current path represents the inductance of the loop. Thus, the equivalent inductance here is the parallel combination of two identical inductances in series LC circuit. The gap among adjoining unit cell is represented by C.

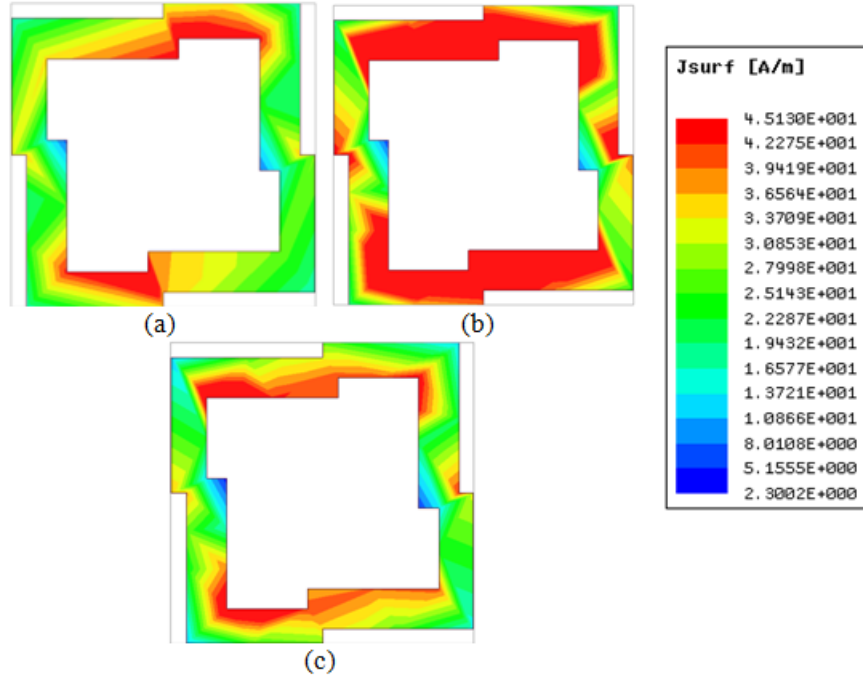


Figure 5-5 For the TE incident polarized wave the surface current distribution at (a) 3.1 GHz (b) 6.7 GHz and (c) 10.8 GHz

Therefore, the resonant frequency is formulated as:

$$f_z = \frac{1}{2\pi\sqrt{(L_1 \parallel L_1) \times C}} \quad (5.1)$$

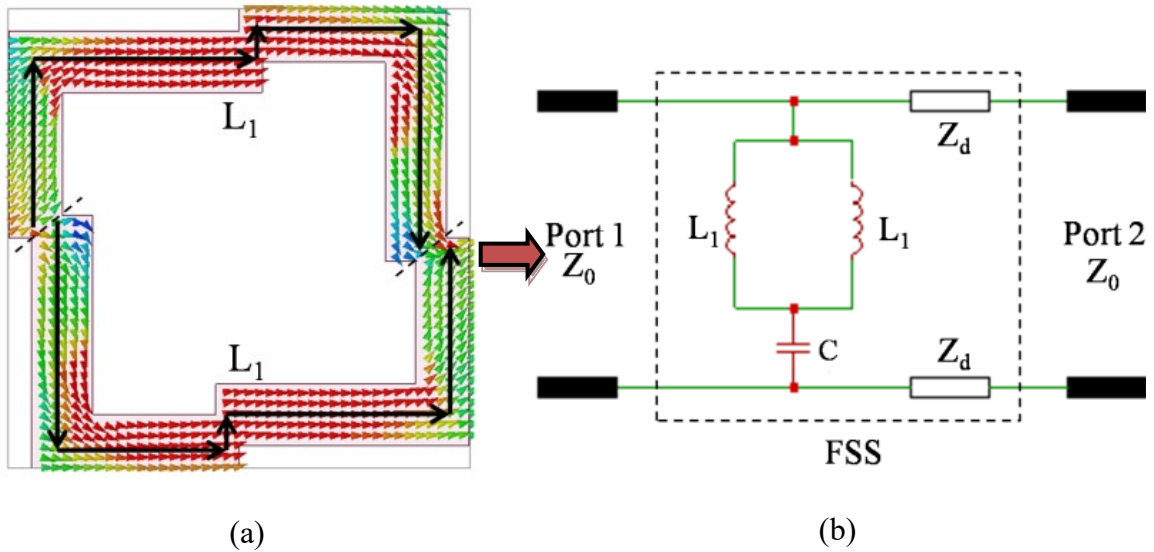


Figure 5-6 (a) Vector surface current distribution and (b) ECM

UWB FSS has varying lengths and widths all over the closed loop structure. Therefore, the length of every arm is divided into d_a , d_b and d_c which are having the width of w_a , w_b and w_c , respectively. The representation of all the variables is illustrated in Figure 5.7.

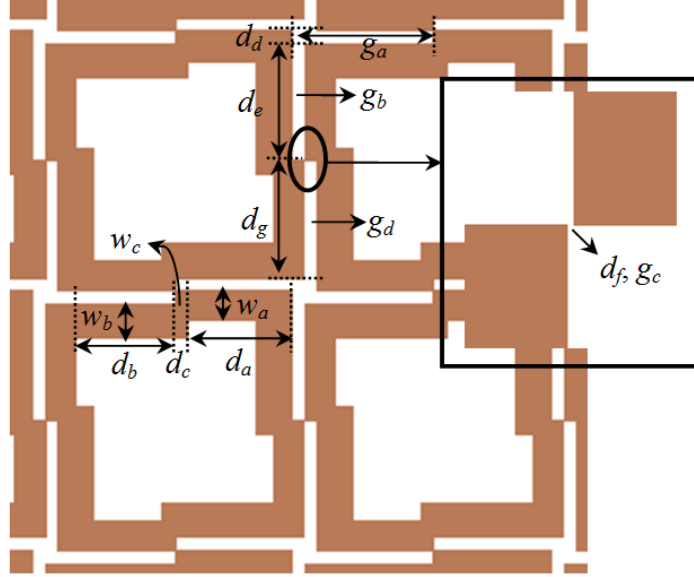


Figure 5-7 Representation of the unit cell of given FSS

Using the equations given by Marcuwitz [23], the inductance for every part is calculated. Each metallic part is considered as a strip and for an infinite array under TE polarization. The inductive reactance for strip grating is given by the equation (1.6) as:

$$\frac{X_L}{Z_0} = F(P, w, \lambda) = P \frac{\cos \theta}{\lambda} \left[\ln \left(\operatorname{cosec} \left(\frac{\pi w}{2P} \right) \right) + G(P, w, \lambda) \right] \quad (5.2)$$

where λ is wavelength of the resonating frequency, w is each strip width, P is period and θ is angle of incidence of impinging wave. The values of inductance is calculated at normal incidence angle ($\theta = 0^\circ$), therefore $\cos \theta = 1$. The inductance of each strip is calculated using the equation (1.10)

For each part the inductance is given by

$$\frac{wL_a}{Z_0} = \frac{d_a}{P} F(P, w_a, \lambda) \quad (5.3)$$

$$\frac{wL_b}{Z_o} = \frac{d_b}{P} F(P, w_b, \lambda) \quad (5.4)$$

$$\frac{wL_c}{Z_o} = \frac{d_c}{P} F(P, w_c, \lambda) \quad (5.5)$$

The values are $d_a = 2.4$ mm, $d_b = 2.3$ mm and $d_c = 0.3$ mm is 2.4 mm, and $w_a = 0.69$ mm, $w_b = 0.8$ mm and $w_c = 1.09$ mm. Therefore, L_I is formulated as:

$$L_1 = 2L_a + 2L_b + L_c + 2(0.5L_c) \quad (5.6)$$

Under TE polarization, the shunt susceptance is given by the equation (1.10). The susceptance of the given structure is reduced by d/p factor. Due to varying gap and arm length the capacitance will vary among the adjoining gaps of unit cells, as shown in Figure 5.7. Therefore, the capacitance is given by:

$$\frac{w_r C_a}{Y_o} = 4 \frac{d_d}{P} F(P, g_a, \lambda) \quad (5.7)$$

$$\frac{w_r C_b}{Y_o} = 4 \frac{d_e}{P} F(P, g_b, \lambda) \quad (5.8)$$

$$\frac{w_r C_c}{Y_o} = 4 \frac{d_f}{P} F(P, g_c, \lambda) \quad (5.9)$$

$$\frac{w_r C_d}{Y_o} = 4 \frac{d_g}{P} F(P, g_d, \lambda) \quad (5.10)$$

here $d_d = 0.29$ mm, $d_e = 2.7$ mm, $d_f = 0.001$ mm and $d_g = 2.7$ mm and gap is $g_a = 3.01$ mm,, $g_b = 0.31$ mm, $g_c = 0.02$ mm and $g_d = 0.31$ mm.

Therefore, C is formulated as:

$$C = C_a + C_b + C_c + C_d \quad (5.11)$$

Since the thickness of the dielectric substrate is of a very short electrical length, thus impedance of transmission line is given by $Z_d = Z_o / \sqrt{\epsilon_r} = 179.7\Omega$, where $Z_o = 120\pi \cdot$

The lumped circuit elements are then modeled in advanced design system (ADS) for the extraction of reflection and transmission characteristic response curves. Optimization of

the values has been done to produce the similar frequency response as that by the full wave simulator. The values are given by $C_a = 0.0292$ pF, $L_a = 0.9281$ nH, $C_b = 0.130$ pF, $L_b = 0.8733$ nH, $C_c = 0.0001$ pF, $L_c = 0.08751$ nH, $C_d = 0.130$ pF, $L_l = 3.7974$ nH $C = 0.2892$ pF and $L = 1.898$ nH. Figure 5.8 shows the comparison of the curve obtained by HFSS and ADS and almost similar response curves are obtained in both the simulator.

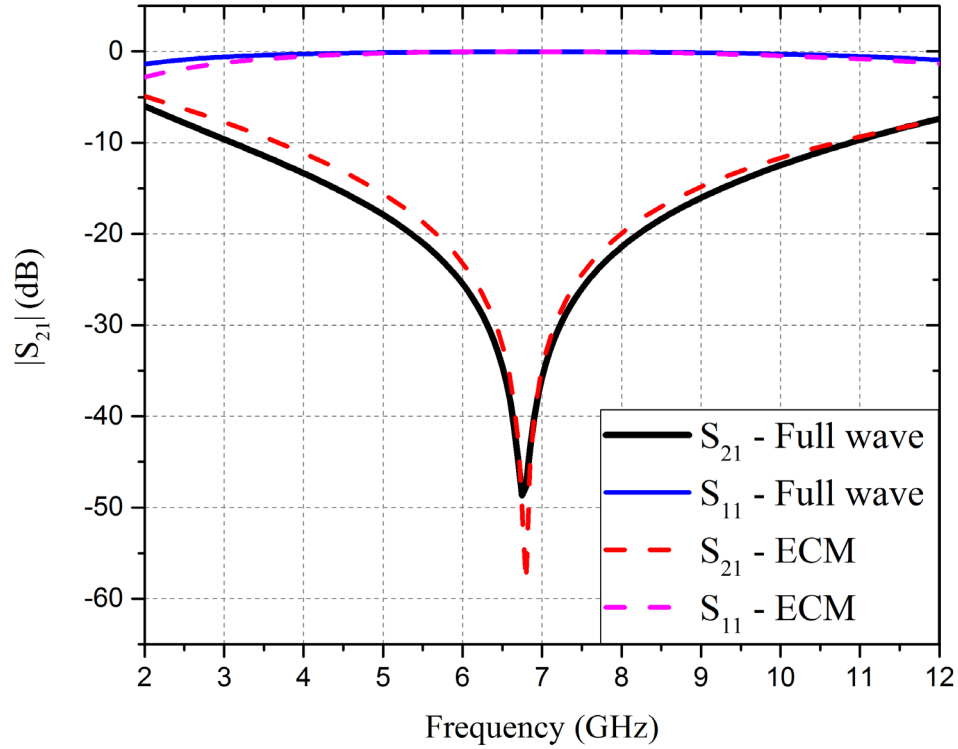
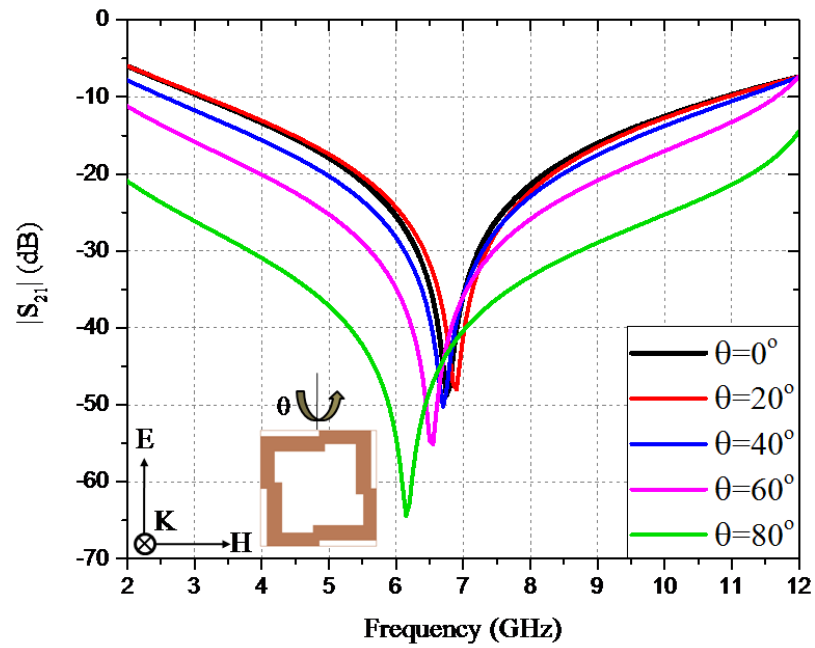


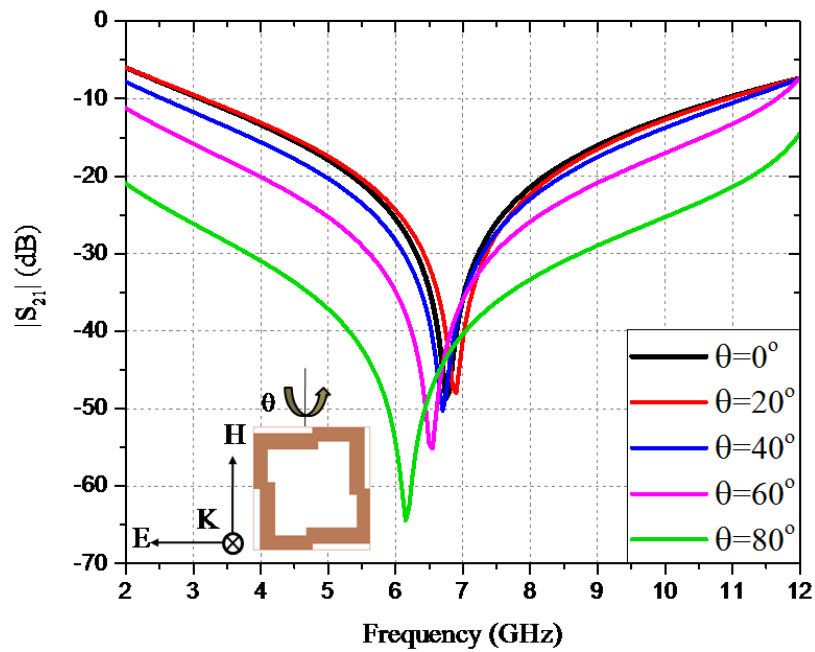
Figure 5-8 Comparison of frequency response of HFSS and ADS simulator

5.3.4 Frequency response curve at various incident and polarization angles

Transmission characteristic of UWB FSS is studied at varying incident (θ) as well as polarization angle (ϕ) as a function of frequency. Frequency response under wide incident angle (θ) at $\phi=0^\circ$ for both TE and TM polarization is illustrated in Figure 5.9(a) and (b). The structure appears to be stable up to 80° in both the polarized wave case and the resonance shifts slightly after 60° , but in both the polarization cases the structure rejects the entire UWB frequency range till 85° . The deviation of resonant notches at $\theta=0^\circ$ with $\theta=80^\circ$ is calculated using the equation 2.1 from chapter 2. The maximum relative deviation from resonant frequency for 0.4 GHz and 0.42 GHz of frequency deviation is 5.9 % and 6.2% for $\theta=80^\circ$ incident TE and TM polarized wave, respectively.



(a)



(b)

Figure 5-9 Frequency responses at varying incident angles under (a) TE and (b) TM polarization

Due to symmetric nature of the given design, the structure assures approximately similar response curve of frequency at wide polarization angles. The variation for polarization

angle with respect to frequency response is shown in Figure 5.10(a) and (b). From Figure 5.9 it is clear that structure provides polarization angle stability under both the polarizations, at $\theta=0^\circ$. From equation 2.1, the maximum relative deviation is calculated as 1.49 % for both $\theta=80^\circ$ TE and TM wave, which is very low. Thus, small structures provide steadiness in the response curves regardless of the angle of impinging wave and symmetrical structure provide steadiness in the response curves regardless of the polarization angles. Therefore, the given structure attains steady response curves of frequency for both the polarizations under varying incident and polarization angles. The frequency response of any given FSS structure also depends upon the periodicity of the structure. From equation 2.2, it is observed that the maximum tolerable limit of P is 0.5083λ which is equal to 22.5 mm at 80° incident angle. The given FSS has the value of P lower than the tolerable limit. Thus a good angular stability is obtained towards wide varying incident angles.

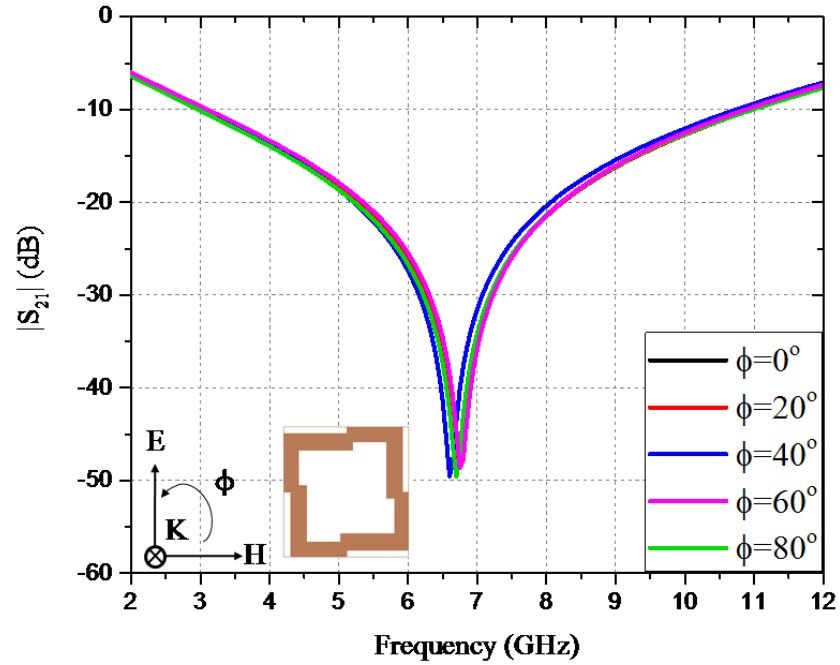
5.3.5 Parametric analysis

Figure 5.11, illustrates the change of d_1 , d_2 and w_1 . In the variation of all the outer arms d_1 as the length of the arm increases, the perimeter of the proposed FSS increases which further leads to increased inductance and therefore the lower cut-off and resonance decreases while the upper cut-off frequency remains same, as seen in Figure 5.11(a). Now when the length d_2 is increased, resonant frequency increases. This happens due to the enhancement of the width as the perimeter remains the same for the variation of inner arm length, as presented in Figure 5.11(b). Moreover, the variation is only observed in the upper cut-off frequency and resonant frequency whereas the lower cut-off frequency approximately remains the same. The bandwidth gets enhanced in both the aforementioned case, as width increases. Figure 5.11(c), shows the variation of the width w_1 . With the increment in the width of the modified SL, there is shift observed in the resonant frequency from lower end towards the higher end with enhanced bandwidth.

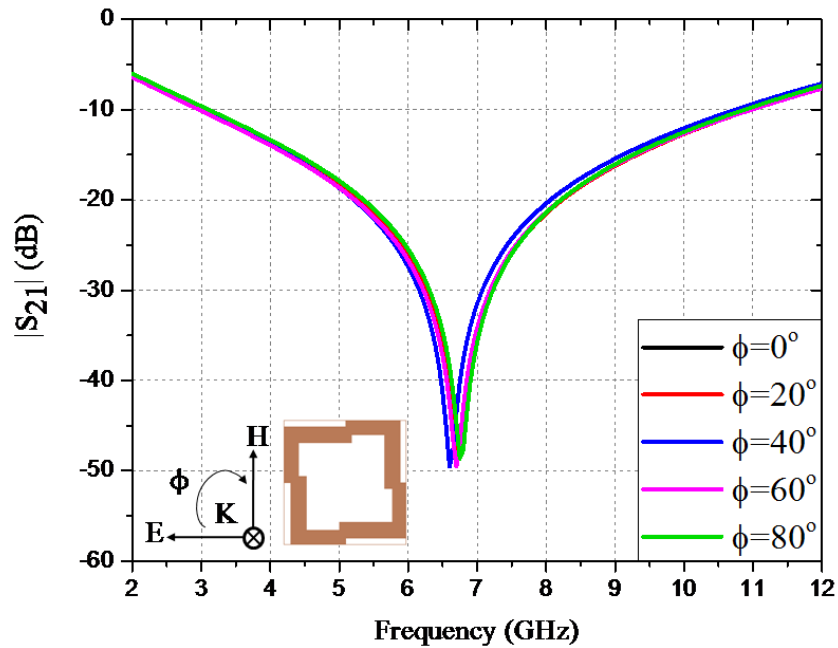
5.3.6 Verification of the simulated results experimentally

For the validation purpose, the UWB FSS is implemented over FR-4 substrate of 1.6 mm height. A periodic array of 30×30 unit cell is implemented over a $190 \times 190 \text{ mm}^2$ dimensioned substrate. The top view of the fabricated prototype is shown in Figure 5.12

(a). Here also the frequency response of the given structure is measured inside the anechoic chamber. Inside the measurement setup, FSS is placed in between a transmitter and receiver horn antenna. The photograph of the measurement setup is illustrated in Figure 5.12(b).



(a)



(b)

Figure 5-10 Frequency responses at varying polarization angles under (a) TE and (b) TM polarization

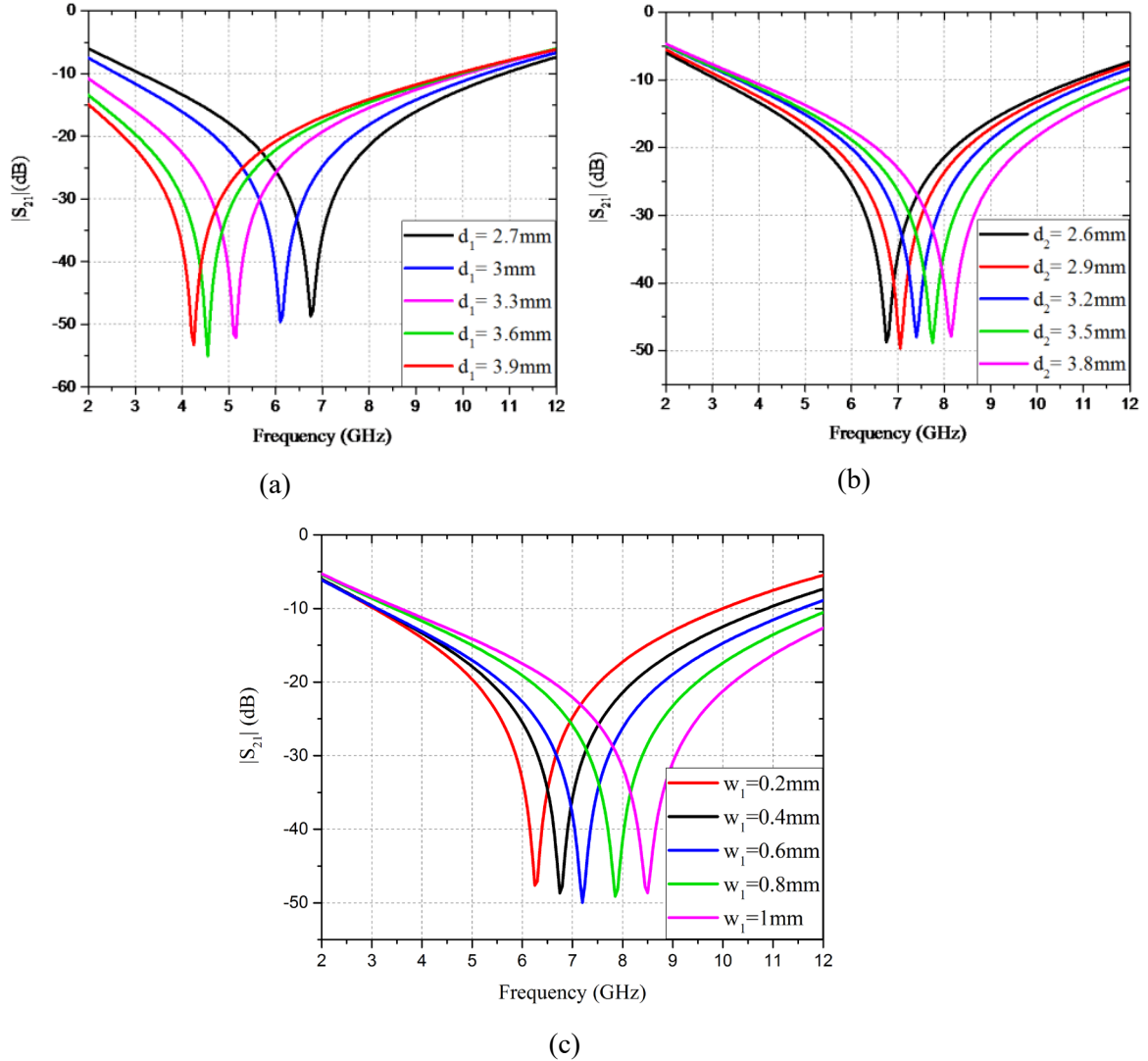
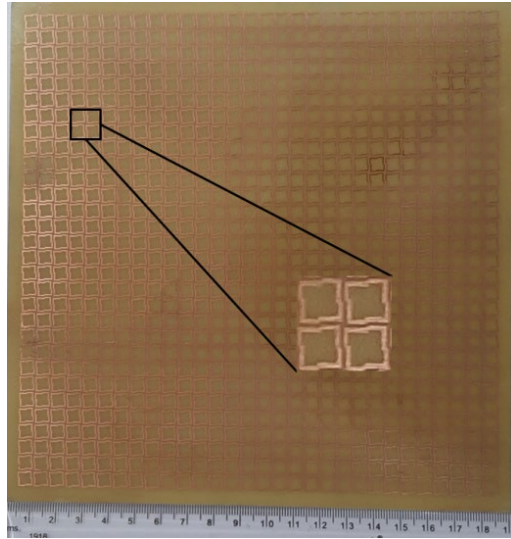
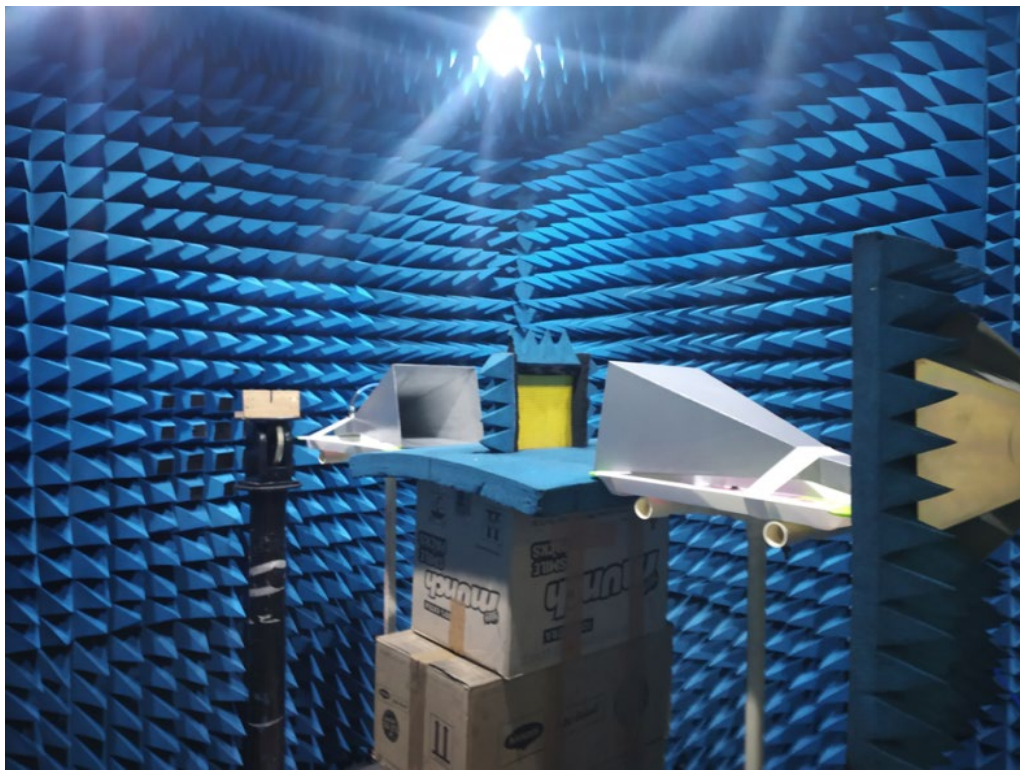


Figure 5-11 Change in the parameters (a) d_1 , (b) d_2 and (c) w_1

The measurement is performed similar to that shown in Chapter 2. The measured result is obtained at normal as well as varying incident angles and polarization angles till 80° . A good match has been confirmed in between the resultant response curve of simulation and measurement, as presented in Figure 5.13 and Figure 5.14. It is observed that small variations are present in transmission curves of the measured results. This occurs because of the limitation in measurement and fabrication error.

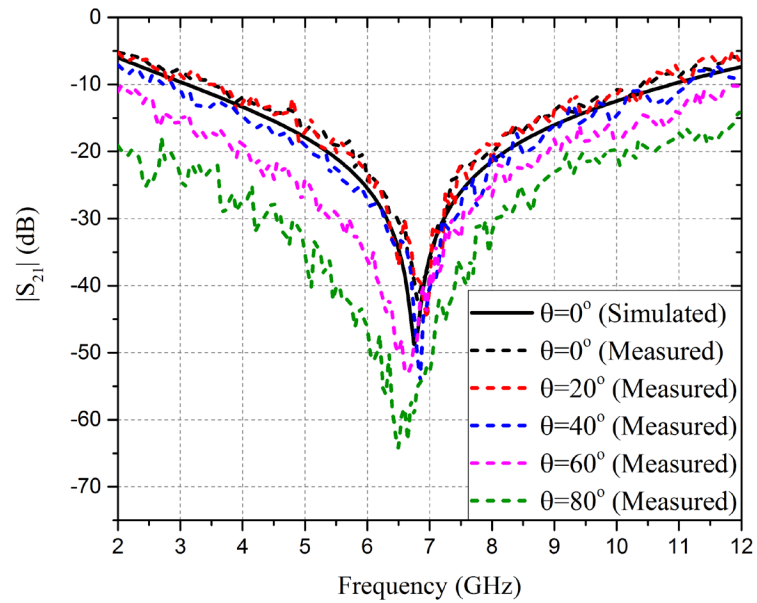


(a)

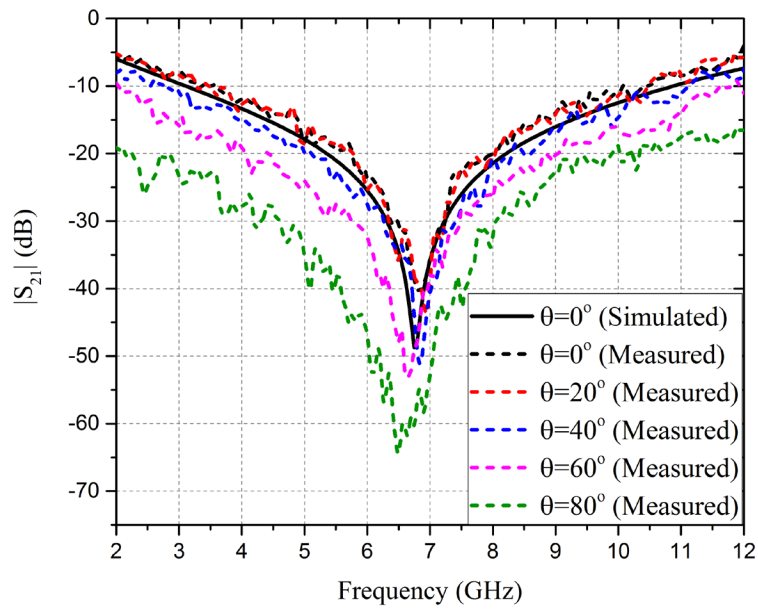


(b)

Figure 5-12 Fabrication prototype (a) top layer and (c) FSS sheet inside the anechoic chamber for the measurement of the frequency response

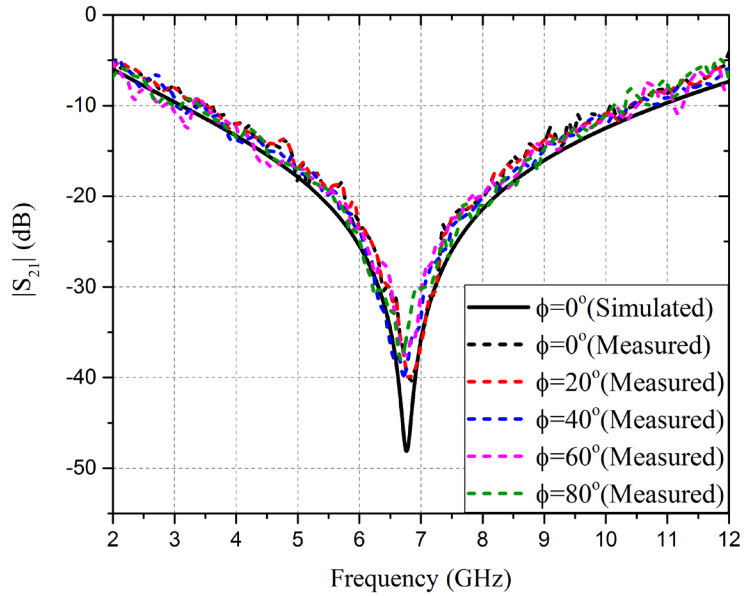


(a)

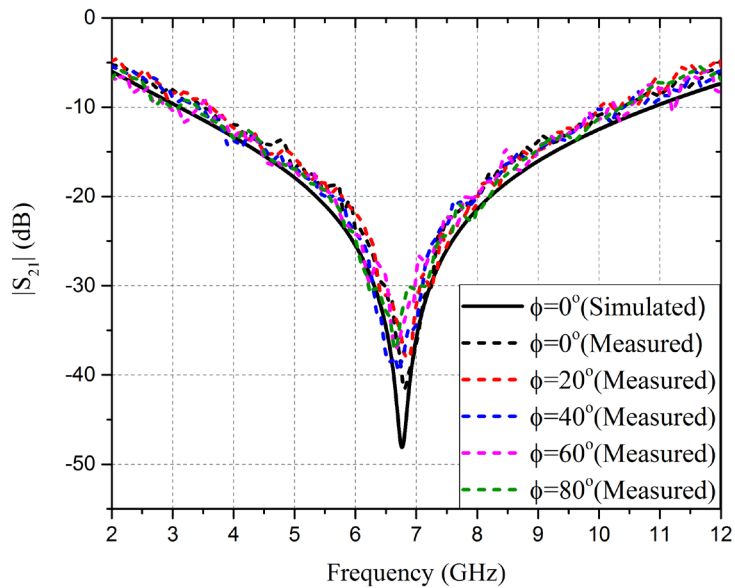


(b)

Figure 5-13 Measured frequency response curves under (a) TE and (b) TM polarized incident wave, under normal and varying incident angles



(a)



(b)

Figure 5-14 Measured frequency response curves under (a) TE and (b) TM polarized normal incident wave, under normal and varying polarization angles

5.3.7 Proposed FSS design compared with various other FSS design reported in literature

Table 5.2 contains the data of various FSS unit cell designs. Dimensions of the unit cell

Table 5-2 Various unit cell FSS compared with modified SL UWB FSS

Ref.	Size of unit cell (mm ³ λ)	Analysis of structure	f _z	-10 dB	10 dB	MFD		PI	
			TE TM (GHz)	Rejection BW (Freq. range)	FBW (%)	TE	TM		
						(AS in deg)			
[176]	14×14×1.6 0.18λ×0.18λ	On single side of substrate : SL with offset cross	-	10 (4-14)	111.1	-	-	Yes	(0°-45°)
[177]	9×9×0.8 0.14λ×0.14λ	On single side of substrate : SL and modified cross	10.1	12.38 (4.85-17.23)	112	-	-	Yes	(0°-30°)
[75]	9.6×11.1×0.7 0.063λ×0.072λ	One dual side of substrate : Hexagonal rings connected by vias	4.52	6.11 (1.97-8.08)	121.6	-	-	No	(0°-30°)
[182]	12×12×0.8 0.04λ×0.04λ	One dual side of substrate : SL and two split ring resonators	3.9	8.83 (1.01-9.84)	162.8	-	-	Yes	(0°-45°)
[52]	8×8×4 0.093λ×0.093λ	Triple layer dual substrate : Square patch and cross shaped metallic element	-	8.64 (3.49-12.13)	110	-	-	Yes	(0°-60°)
[183]	8×8×0.635 0.09λ×0.09λ	On single side of substrate : SL and circular ring inside it	-	7.1 (3.5-10.6)	100.7	-	-	No	-
[184]	11×11×13.3 0.11λ×0.11λ	Active p-i-n diodes with multilayer geometry	-	9.6 (3.18-12.78)	88	-	-	Yes	(0°-45°)
[185]	11×11×0.76 0.103λ×0.031λ	On single side of substrate : Aperture type metallic layer	-	17.12 (2.82-19.94)	150	-	-	No	-
[178]	10×10×1.6 0.13 λ×0.13λ	A dual sided convoluted structure	-	10.2 (3.1-13.3)	124	-	-	Yes	(0°-45°)
[179]	8×8×1.6 0.066λ×0.066λ	On single side of substrate : modified square ring	7.39	10.28 (2.72-13)	130.7	4	5.4	Yes	(0°-80°)
Design 4	6×6×1.6 0.062λ×0.062λ	On single side of substrate : modified metallic SL	6.7	7.7 (3.1-10.8)	110.79	5.9	6.2	Yes	(0°-80°)

* FBW - Fractional Bandwidth, MFD –Maximum Frequency Deviation, AS – Angular Stability, PI – Polarization Insensitivity

on the basis of effective dimension with respect to lower cut-off wavelength ‘λ’, number

of dielectric layer, number of bands, resonant frequency, polarization insensitivity (PI) and angular stability are the parameters on which the FSS is compared with various FSS implemented. For the desired UWB frequency range, the design [75] and [182] covers the lower cut-off frequency with both having lower angular stability in comparison to the given UWB FSS. For the desired UWB frequency range, structures of [176], [177], [52] and [183] attains upper cut-off frequency. These designs too provide low angular stability due to the large size of their unit cell. Moreover, the design in [183] is polarization sensitive and the frequency response for the varying incident angle is not observed. In the designs of [184], [185], [178] and [179], the side band wastage is high outside the desired frequency range of UWB. The design presented in [185] is polarization dependent and provides low angular stability. The given design provides a simple and compact structure. The design rejects the UWB frequency band exactly thus the side band wastage is reduced. Highly stable frequency response and polarization independence is obtained under varying polarization and incident angles. Thus, it is inferred that the proposed structure has the potential to work in UWB antenna system for the performance enhancement.

5.4 Conclusion

In this chapter a simplified SL based FSS is designed to work over frequency band of UWB. The design is modified by implementing the inner and outer arms at the corners of the conventional SL. The design is implemented over an FR-4 substrate and the size of this UWB FSS is $6 \times 6 \text{ mm}^2$. The effective size of the UWB FSS is $0.062 \lambda \times 0.062 \lambda$ and λ is the wavelength corresponding to the lower cut-off frequency, making it the smallest structure in the literature to attain the desired frequency range. The structure band rejects UWB from 3.1 to 10.8 GHz frequency band. At $\theta = 80^\circ$, the maximum relative deviation of 6.2 % and 5.9 % is obtained under both the polarizations, respectively. Moreover, at $\phi = 40^\circ$, the maximum relative deviation of 1.49 % is obtained under both the polarizations. A good degree of match is found among the resultant response curves of simulation and measurement, thus this UWB FSS is applicable in future wireless communication as well as in UWB antenna system.

CHAPTER 6

2.5D FSS for Sub 6 GHz 5G Communication System

6.1 Introduction

The need of the hour is to provide high data rate for the end users. 5th generation (5G) wireless communication is getting world widely renowned as it provides high data rate, better channel capacity, short delays and high spectral efficiency, than the immediate predecessors [186]–[191]. In various countries accordingly the frequency band is allocated for the 5G setup. The sub 6GHz frequency falls in the category of frequency range 1(FR-1) and C-band ranging from 3.4-3.6 GHz has been allocated by international telecommunication union (ITU) as 5G spectrum. With respect to the long term evolution bands (LTE), the band 42 (3.4-3.6 GHz) and 43 (3.6-3.8 GHz) are allocated to work for 5G frequency band [165]. The frequency ranging from 3.3 to 3.4 GHz and 3.6 to 3.7 GHz is also allocated by many countries. The new radio band range considered by 3GPP is N78 which ranges from 3.3 to 3.8 GHz [193], [194]. The main issue arises is the EMI on 5G communication band by the commercially available devices operating in the narrow bands which ranges from 3.3 to 3.8 GHz. This might result in the performance degradation of the system. These EMI have to be oppressed to avoid any unwanted radiation. Mostly 2 D FSS structure is implemented for filtering applications as it is easy to design and implement. Various techniques have been implemented in the size miniaturization of the FSS to attain approximately the same behaviour which is of an ideal FSS [195], [196]. However, 2D structure cannot reduce the size of the FSS after a certain limit, as the elements stagnate at either side of substrate. In many designs on both the sides of the substrate, single and multi-resonant elements are printed for obtaining the desired results[197]–[200]. But it is observed that the effective dimension of the 2D structure still remains large and frequency deviation is high at wide incident angles. Moreover due to this, it lacks in providing a better frequency response, which is a major setback. Therefore to improve the frequency response, multilayer and 3D FSS structures are studied in the literature widely [174], [175]. But the problem arises of high design complexity, bulky structure and manufacturing costs as discussed in previous chapters.

Therefore, for further reduction of size with highly stable frequency response and less bulky structure, recently 2.5 D FSS has come into enactment. The major space limitation of 2D FSS has been addressed by 2.5D FSS. In this the elements placed at the top and bottom layer of the substrate are interconnected using the metallic vias inserted in the substrate which results in increased electrical length. To enhance the bandwidth and angular stability, substrate-integrated waveguide technology is implemented in [76]. Tapered meander lines and convoluted rings when interconnected with metallic vias, obtains an ultra-miniaturized structure with highly stable frequency response [80], [81]. However, as the number of vias increases in a unit cell, the design becomes complex and the fabrication costs increases. Therefore, in [66] and [203] a closed loop FSS is developed which used only four vertical vias. Due to the loop structure, the overall perimeter of the structure is increased to a great extent and an ultra miniaturized structure is obtained with less hassles.

In relation with 2D and 3D FSS structures, closed loop 2.5 D FSS provides a fair trade-off. With respect to 2D structure it provides better frequency response using ultra miniaturized design and with respect to 3D structure it reduces the bulkiness and complexity of the designing and manufacturing. Therefore, here a closed loop 2.5 D FSS structure is implemented to protect sub 6 GHz 5G communication system from unwanted radiation or signal leakage. Four metallic vias are used to interconnect the metallic S-shaped and inverted S-shaped element placed at the upper and lower layer of the dielectric substrate. The proposed structure covers the 3.2 to 3.9 GHz range with resonant notch at 3.62 GHz, therefore covering the entire sub 6 GHz 5G frequency band. The reset of the chapter is shown below: in section 6.2 analysis and design of the proposed FSS is included with its design principle. Section 6.3 contains the simulated results as well as measured results. Comparison of various FSS design in the literature with the proposed FSS has been done. Conclusion of the chapter is written in section 6.4.

6.2 Design analysis of the FSS unit cell

6.2.1 Unit cell model

The proposed design works on the concept of increasing the length of the metallic element. Therefore, an S-shaped and inverted S-shaped metallic element is inserted at one

side of the dielectric substrate, meanwhile similar arrangement with 90° rotation is inserted at the other. These metallic elements are connected using four vias which are etched inside the substrate using plated through holes (PTH) technology and placed at the inner edges of the metallic element to form a closed loop. Figure 6.1 represents the configuration of the proposed designs.

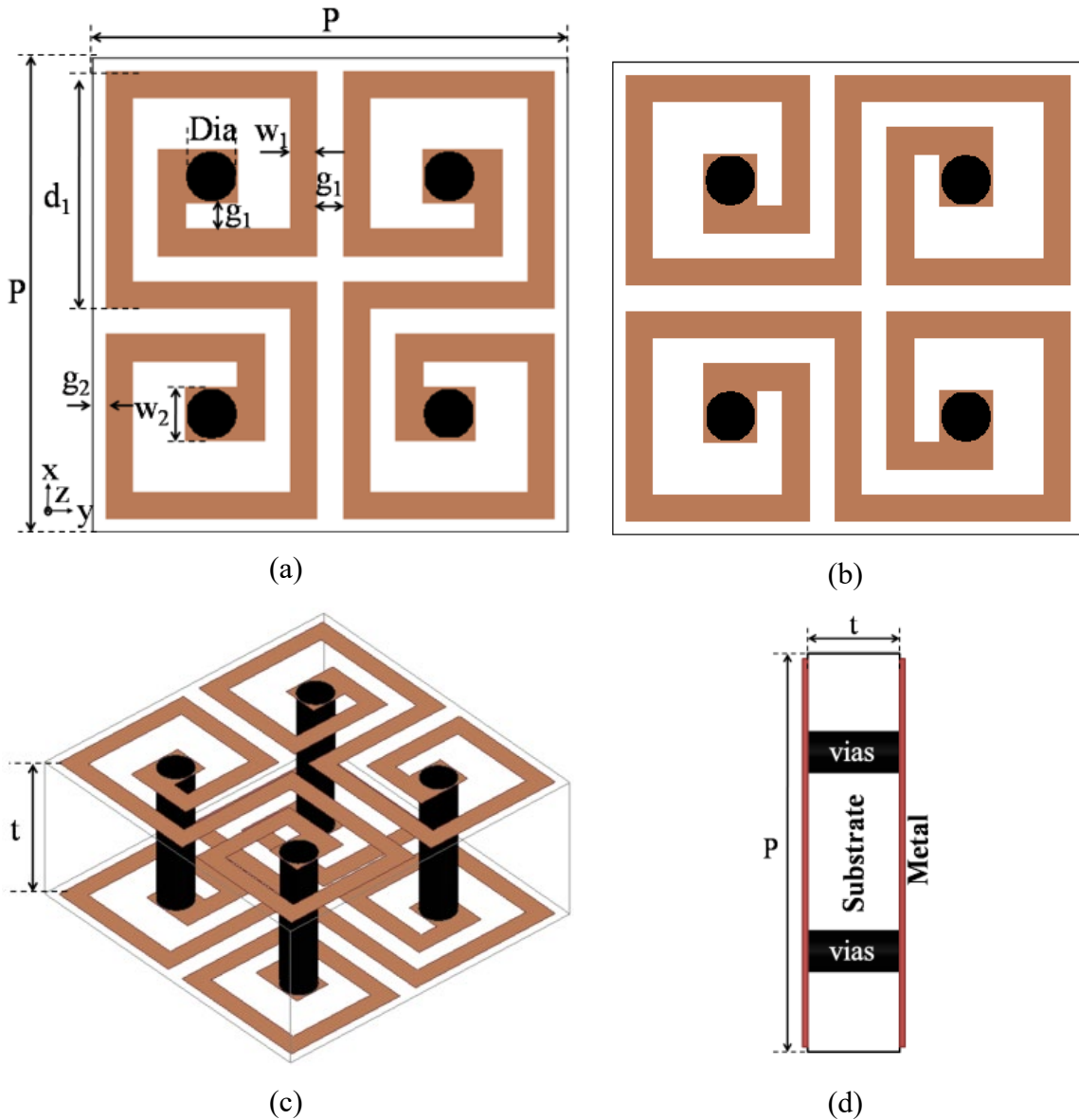


Figure 6-1 Sub 6 GHz 5G unit cell design (a) Top, (b) Bottom, (c) 3-D and (d) Side view

The proposed model is implemented over the FR-4 substrate of dimensions 3.6×3.6 mm². The effective dimension of the proposed FSS with respect to the wavelength ' λ ' of

the resonant frequency is $0.04 \lambda \times 0.04 \lambda$, which is an ultra miniaturized design size. The values of each parameter are presented in Table 6.1.

Table 6-1 Parameters' list

Parameter	P	d ₁	w ₁	w ₂	g ₁	g ₂	Dia
Value (mm)	3.6	1.8	0.2	0.4	0.2	0.1	0.4

6.2.2 Principle of operation and development of FSS element

The proposed FSS unit cell has an average size of $P=\lambda_g/23.48$. λ_g is equal to 3.55 GHz, which is the centre frequency of the operational band of 3.2 to 3.9 GHz. The structure designed here is the modification of the conventional SL. It has been studied before that the closed loop structures resonates at $f = 1/2\pi\sqrt{L_{eq}C_{eq}}$ and increase in the effective inductance and capacitance can help in lowering down the resonant frequency. With increase in the path length, the perimeter increases and so does the inductance. However, after a certain limit the path length cannot be increased in conventional 2D FSS designs, thus further downshift of resonant frequency and size miniaturization is not possible. Therefore in the proposed design metallic vias are inserted inside the substrate to interconnect the elements placed at both side of the substrate to create a modified SL structure. Moreover with increased inductance the bandwidth of the design decreases which is desired for this proposed FSS design. All the stages implemented in the development of the proposed design are illustrated in Figure 6.2. A single metallic S-shaped element is implemented over the top layer of the substrate of 17 mm perimeter as shown in stage 1. Then in stage 2, a metallic via is inserted at the inner edge of the top metallic element which is interconnecting the inner edge of the bottom inverted S-shaped metallic element to increase the perimeter to 35.6 mm. Stage 3 consists of another metallic via and an inverted S-shaped metallic element at top layer of the substrate which has 54.2 mm as overall perimeter. Stage 4 connects all the vias and metallic elements by implementing an S-shaped metallic element at the bottom layer and the overall perimeter becomes 74.4 mm.

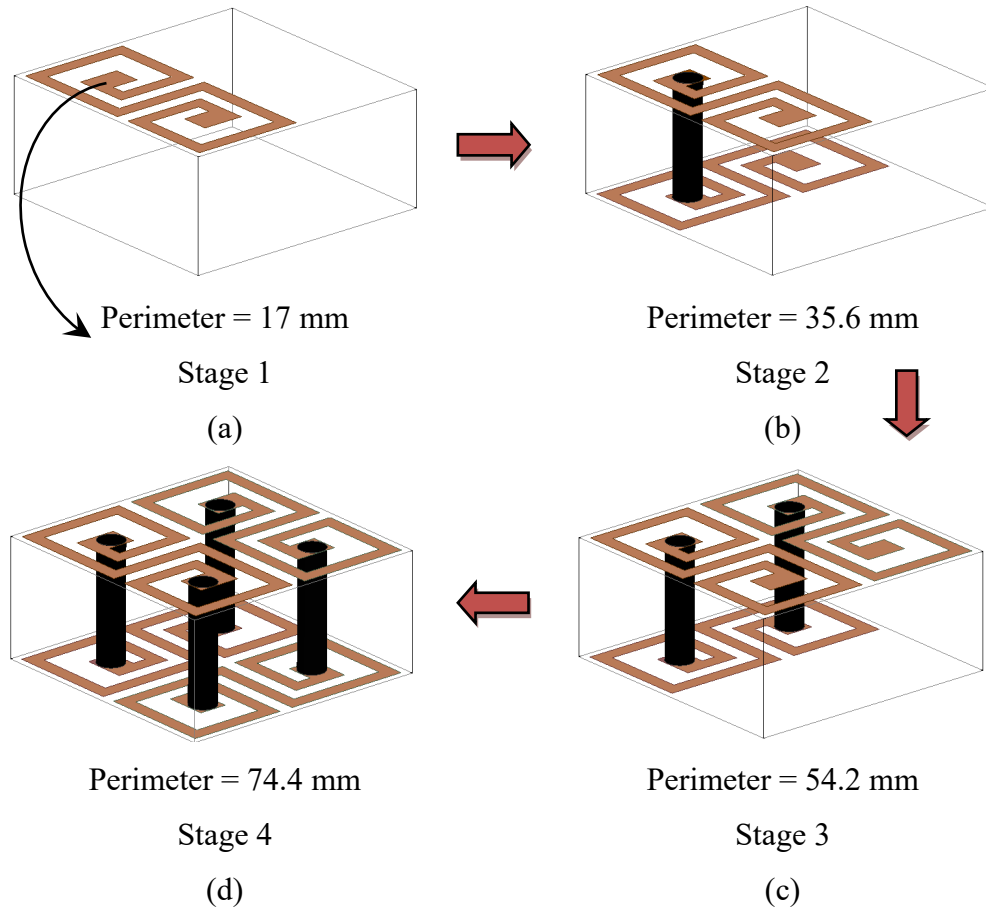


Figure 6-2 Stages in the making of main unit cell design

6.3 Simulated and experimental results

6.3.1 Frequency response of the proposed unit cell

Figure 6.3 represents the simulated response curve of transmission coefficient of the proposed FSS design at all the stages of design development. Normal TE incident wave is impinged for this purpose. In stage 1, with the implementation of an individual S-shaped metallic element the design provides a resonant notch at 7 GHz. 0.8 GHz is the impedance bandwidth obtained ranging from 6.5 to 7.3 GHz. Due to the potential mismatch between the port and FSS, no resonant notch is obtained for stage 2 design. In the design stage 3, the resonant frequency reduces due to the increased perimeter which results in increased inductance. At this point, the design resonates at 5.8 GHz and has an impedance bandwidth of 0.8 GHz ranging from 5.3 to 6.1 GHz. Finally in stage 4, with the development of modified SL 2.5D closed loop FSS structure a drastic shift of

resonance is obtained at 3.62 GHz with bandwidth reduced to 0.7 GHz ranging from 3.2 to 3.9 GHz.

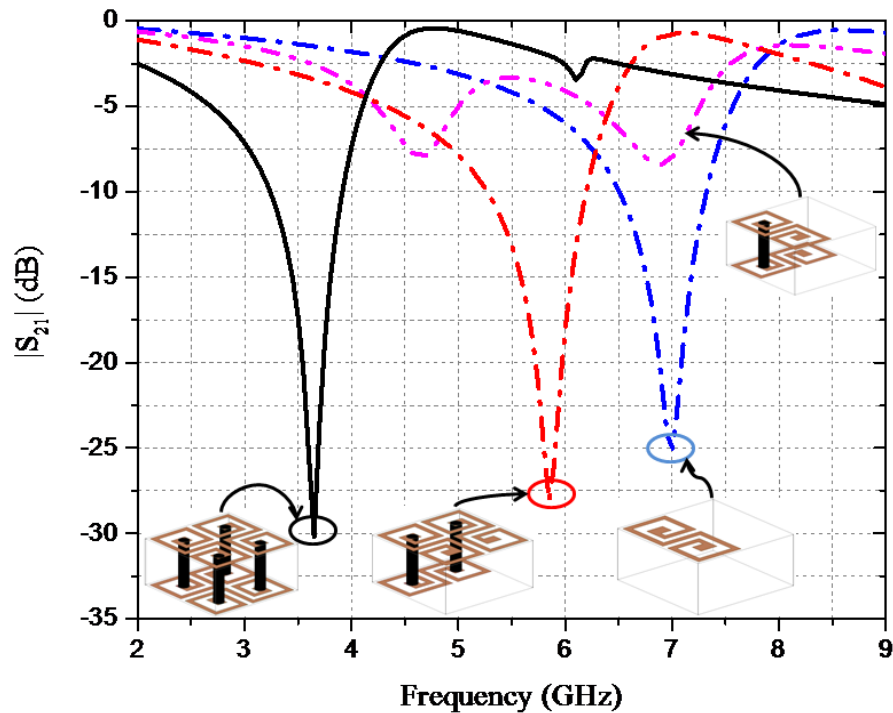


Figure 6-3 Simulation of all the stages implemented for a given unit cell of FSS.

The curves representing the transmission and reflection characteristics of the sub 6G 5G FSS under both the TE and TM polarization is shown in Figure 6.4. The design produces a polarization insensitive feature as the frequency response under both the polarizations is identical. The proposed structure covers the entire sub 6 GHz 5G communication frequency band. It is observed that for both curves obtained under TE and TM polarization, the attenuation of more than 10 dB is procured. It is also observed that at normal incident wave, maximum attenuation of 32 dB is attained. The fractional bandwidth of 19.7 % is extracted under both the polarized wave.

6.3.2 Surface current distribution with circuit modeling

Figure 6.5 illustrates the 3 D and planar view of surface current distribution of the proposed FSS design at the resonant frequency, 3.62 GHz. To simplify the understanding of current flow mechanism, black arrows are placed in the direction of current flow. The proposed structure thus forms two current paths at point a₁ and a₆, as the current starts to

flow in opposite direction. These are the two minimas which divides the current path equally and the two current paths associated with these points are $a_1-a_2-a_3-a_4-a_5-a_6$ and $a_1-a_7-a_8-a_9-a_{10}-a_6$. Therefore, the proposed loop behaves as a half wavelength path with the corresponding resonant notch. The ECM for the proposed FSS is extracted using the surface current. Here an assumption is made that the proposed design is planar as the height of the substrate is 0.04λ approximately. λ here is the wavelength corresponding to the resonant frequency, which is almost negligible.

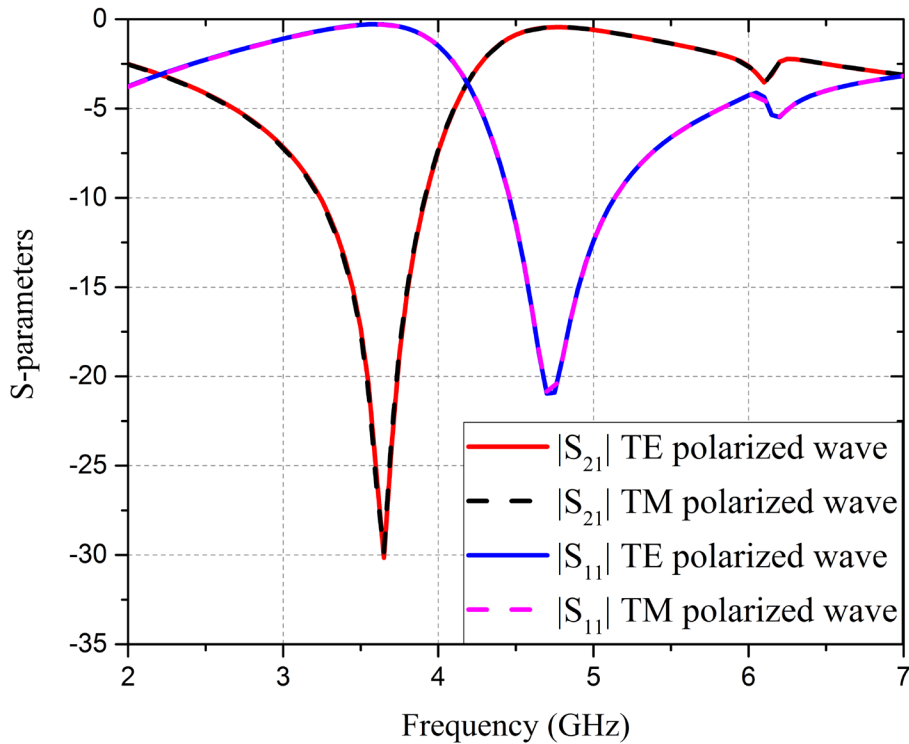


Figure 6-4 S-parameters with respect to frequency

The electric field is supposed to be along the y -axis of the substrate under TE polarization as illustrated in Figure 6.6 (a). The design acts as an equivalent LC series circuit, where L is the total inductance of the loop which is the parallel combination of two L_1 inductances and C is the gap capacitance among the adjacent unit cells which consists of the gap capacitance in between metallic elements (C_1) and metallic vias (C_v). Moreover, the inductance L_1 consists of metallic element inductance (L_L) and metallic via inductance (L_v). C_2 is the mutual coupling capacitance in between the proposed unit cell. At both the sides of the substrate free space is considered and is represented by the transmission line,

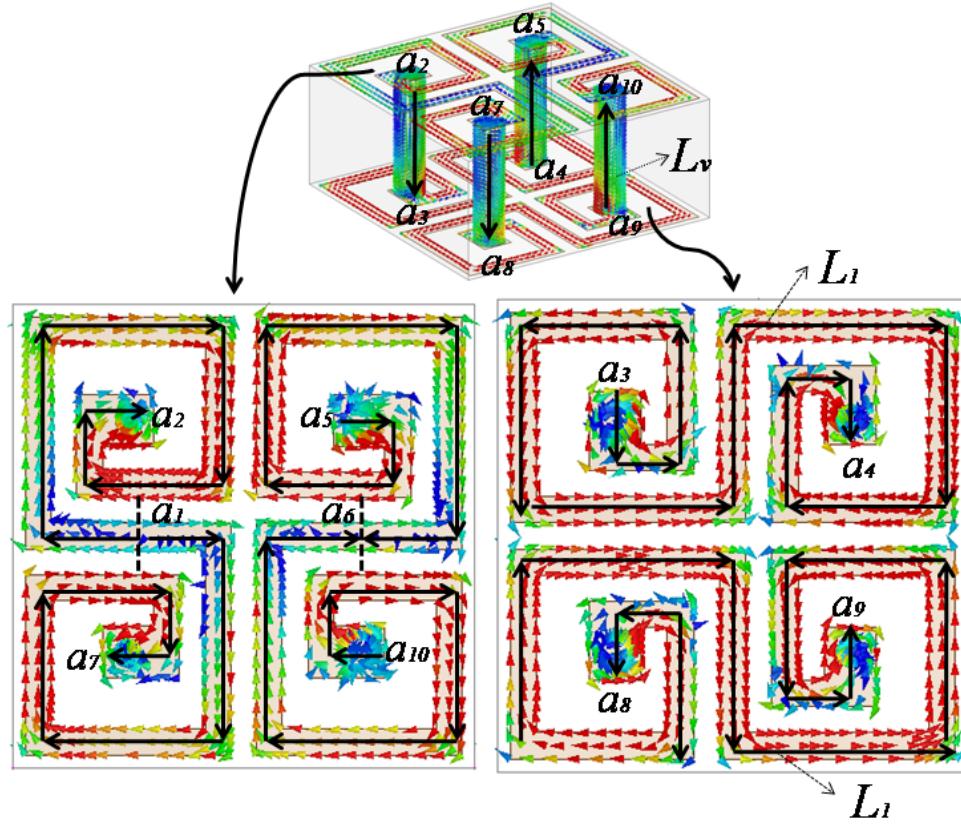


Figure 6-5 For the TE incident polarized wave the surface current distribution at 3.62 GHz

therefore the characteristic impedance is given by $Z_0 = 120\pi$. The characteristic impedance of the dielectric substrate as a transmission line is given by $Z_d = \frac{Z_0}{\sqrt{\epsilon_r}} = 179.7\Omega$. With the thickness of the substrate represented with respect to the resonant wavelength λ , the electrical length of the substrate is 7° . Therefore, an ECM is extracted and illustrated in Figure 6.6 (b).

The formula at 3.62 GHz resonant frequency is given below:

$$f_{3.62GHz} = \frac{1}{2\pi\sqrt{((L_1 \parallel L_1) \times (C_1 + C_v + C_2))}} \quad (6.1)$$

$$\text{where } L_1 = L_L + L_v \quad (6.2)$$

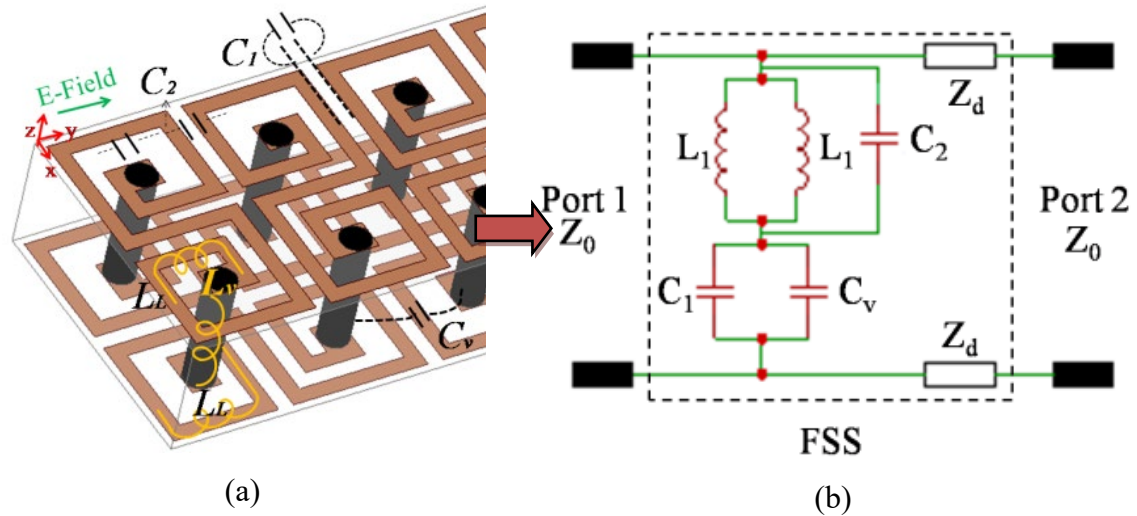


Figure 6-6 Lumped element representation and (b) ECM with respect to surface current distribution

The development of the reflection and transmission curve of ECM has been performed in advanced design system (ADS). The lumped element values are obtained using the close fitting curve method such that similar responses are obtained at both the circuit as well as full wave simulator. All the optimized values are as follows: $C_2 = 0.4608$ pF, $L_L = 4.524$ nH, $L = 2.419$ nH, $L_1 = 4.838$ nH, $C_v = 0.0749$ pF, $C_1 = 0.2525$ pF and $L_v = 0.314$ nH. It is inferred from Figure 6.7 that the curves simulated in both ADS and HFSS simulators have similar frequency response for transmission as well as reflection coefficient. However the nulls are deeper in the circuit simulation as there are no substrate and conductor losses.

6.3.3 Frequency response curve at various incident and polarization angles

Transmission coefficient curve as a function of frequency is studied under varying incident (θ) as well as polarization angle (ϕ). The striking incident wave on the surface of FSS is represented in Figure 6.8. For every oblique incident angle, polarization angle is changed and the variation is presented for $\phi = 0^\circ, 30^\circ, 60^\circ,$ and 90° . From Figure 6.9 (a) and (b), it is evident that the response curve of frequency remains steady up to 80° . The maximum relative deviation in between the resonant notch obtained at normal incidence and $\theta = 80^\circ$ incident TE and TM polarized wave is 0.5% and 0.2%, respectively. Thus the structure is highly stable regardless for variations of angle of incidence and polarization.

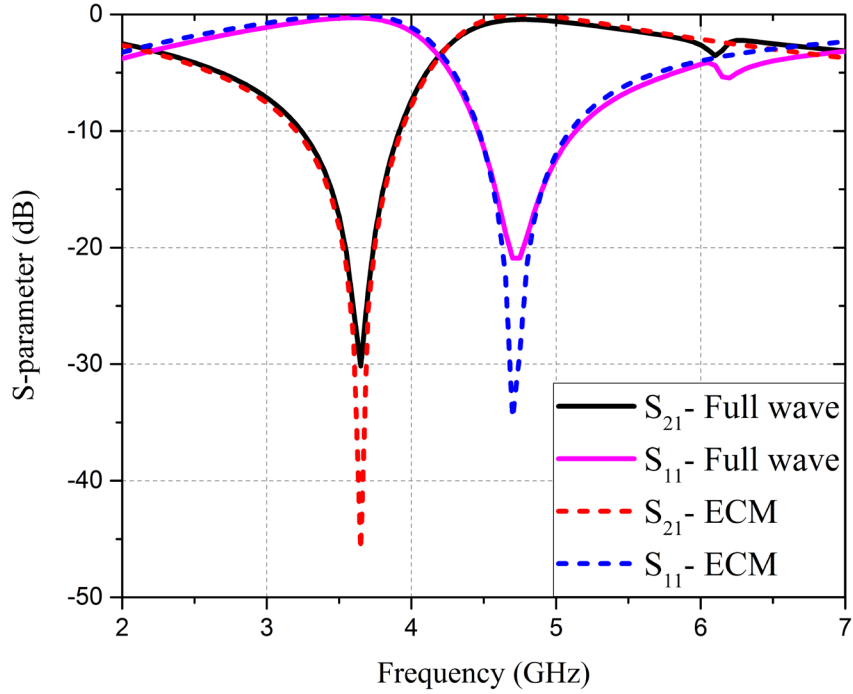


Figure 6-7 Comparison of frequency response of HFSS and ADS simulator

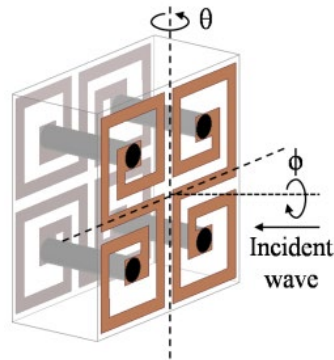


Figure 6-8 Representation of impinging incident wave on the surface of FSS

It is examined that the bandwidth gets enhanced for TE and reduced for TM. The resultant is because of increased wave impedance in TE and reduced in TM. Due to the compactness in size and symmetry in the structure, the frequency response remains stable under the influence of varying incident angles and polarization angles, respectively. With respect to the periodicity of the FSS, from equation 2.2, it is observed that the maximum tolerable limit of P is 0.503λ which is equal to 41.68 mm at 80° incident angle. The

given FSS has the value of P lower than the tolerable limit. Thus a good angular stability is obtained towards wide varying incident angles.

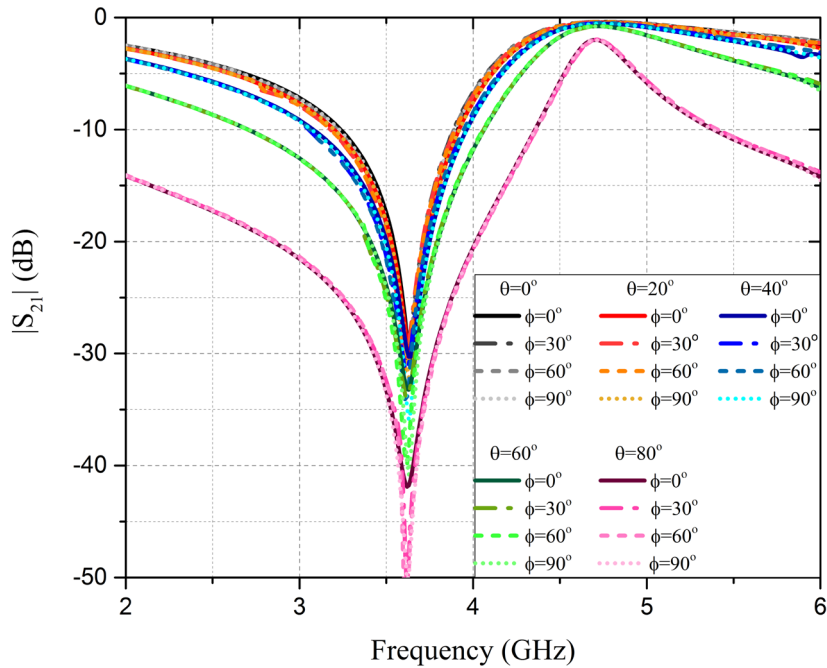
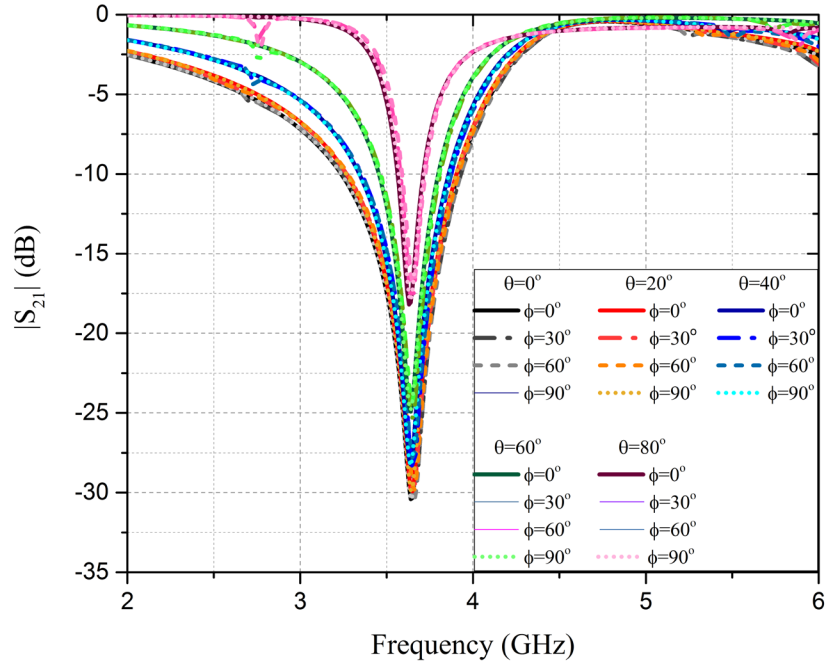


Figure 6-9 Frequency response for varying angles of incidence under (a) TE and (b) TM polarized wave

6.3.4 Parametric analysis

Figure 6.10 illustrates the variation of the parameters such as metallic vias' diameter, substrate height and elements length.

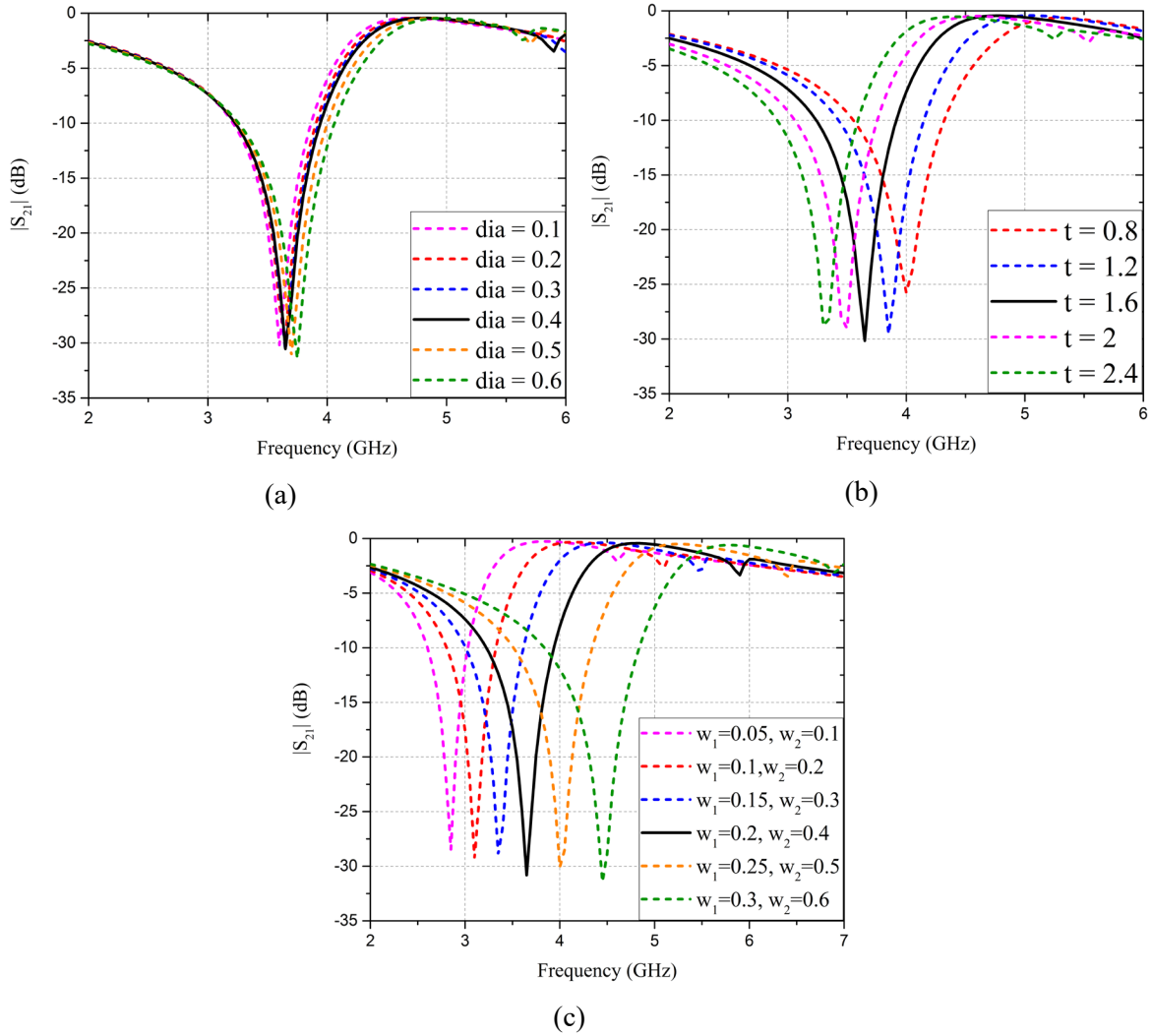


Figure 6-10 Change in the parameters (a) *dia*, (b) *t* and (c) w_1 & w_2

With the change in the diameter, the resonant frequency increases, as illustrated in Figure 6.10 (a). This occurs due to the increase in the volume of the metallic vias, which also results in the bandwidth enhancement. Further the height of the vias and the substrate thickness is changed to see the outcome on the frequency response, as shown in Figure 6.10 (b). With the increment in the thickness, the perimeter of the structure increases thus the inductance increases and the resonant frequency decreases. Figure 6.10 (c) illustrates the variation of transmission coefficient curve with respect to the change in metallic

elements' width w_1 and w_2 . As the width gets enhanced, towards the inner portion of the structure, the resonant frequency up shifts with enhanced bandwidth, meanwhile the perimeter of the structure remains the same.

6.3.6 Verification of the simulated results

For the validation purpose, the sub 6 GHz 5G FSS is implemented over FR-4 substrate of 1.6 mm height. A periodic array of 40×40 unit cell is implemented over a $144 \times 144 \text{ mm}^2$ dimensioned substrate. The top and bottom view of the fabricated prototype is shown in Figure 6.11. Here also the frequency response of the given structure is measured inside the anechoic chamber. Inside the measurement setup, FSS is placed in between a transmitter and receiver horn antenna. The photograph of the measurement setup is illustrated in Figure 6.12. A good match has been confirmed in between the resultant response curve of simulation and measurement, as presented in Figure 5.13 and Figure 5.14. It is observed that small variations are present in transmission curves of the measured results. This occurs because of the limitation in measurement and fabrication error.

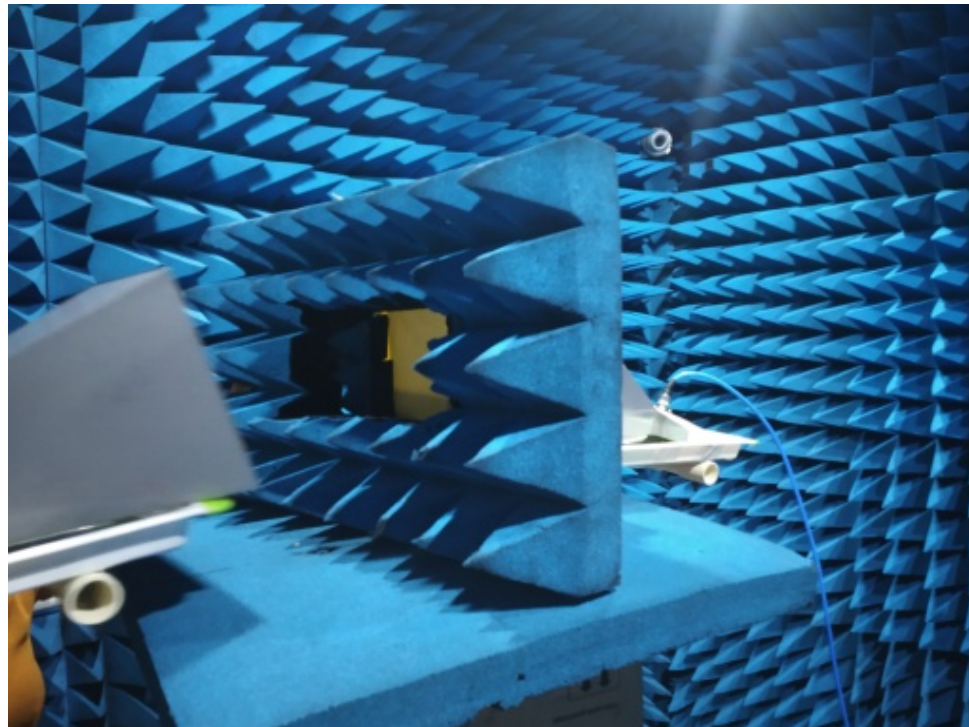


Figure 6-11 Measurement setup inside anechoic chamber

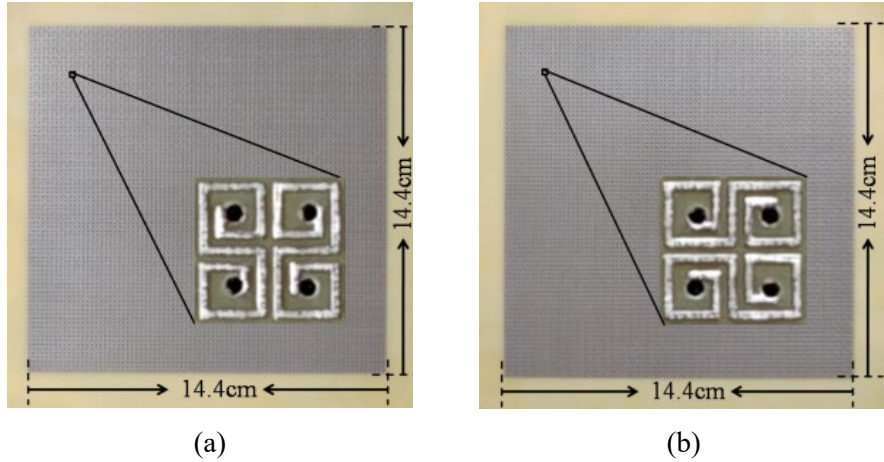
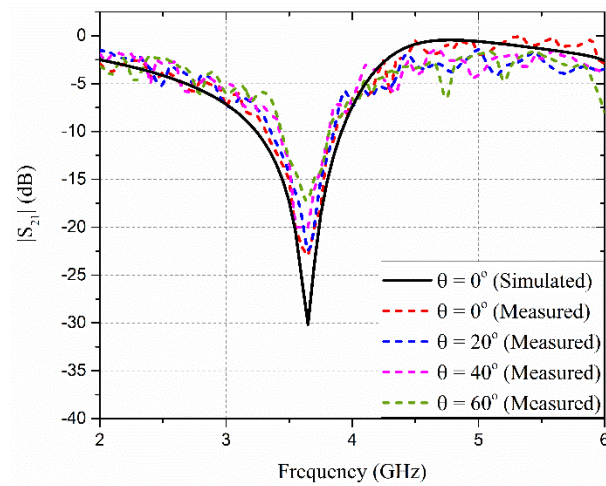
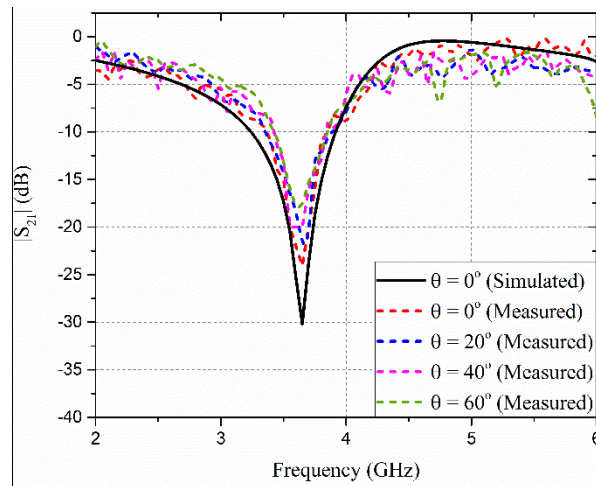


Figure 6-12 (a) Top View and (b) Bottom view of the fabricated prototype



(a)



(b)

Figure 6-13 Measured response curves w.r.t. frequency under (a) TE polarized incident wave and (b) TM polarized incident wave, for normal and oblique incident angles

6.3.5 Comparison of proposed 2.5D FSS with FSSs in literature

The proposed design is compared with the designs present in the literature which is done in Table 6.2.

Table 6-2 various unit cell FSS compared with the proposed FSS

Ref.	Size of unit cell (mm ³ λ)	Band	f _r TE TM (GHz)	Type of FSS	Operating band	-10 dB Bandwidth (Freq. range)	MFD		PI
							TE	TM (AS in Deg.)	
[149]	4.8×4.8×1.6 0.061λ×0.061λ	Stop Pass	- 3.82	2D	-	- -	0.25	2.1 (0-60°)	Yes
[204]	6.12×6.12×1.6 0.069 λ×0.069λ	Stop Pass	3.4, 4.9 4.2	2D	5G bands	0.95 (2.8-3.75) 0.85 (4.55-5.4) 0.15 (4.1-4.25)	2	2 (0-60°)	Yes
[205]	9.45×9.45×1.6 0.08λ×0.08λ	Stop Pass	3.25 2.6	2D	5G band	6.65 (3.35-10) 0.3 (2.4-2.7)	-	- (0-60°)	Yes
[72]	6×6×1.6 0.076λ×0.076λ	Stop Pass	3.8	2D	-	0.3 (3.6-3.9)	2.6	2.6 (0-60°)	Yes
[56]	5×5×1.6 0.058λ×0.058λ	Stop Pass	3.5 -	2.5D	-	- -	-	- (0-60°)	Yes
[206]	3.5×3.5×1 0.038 λ×0.038 λ	Stop Pass	3.3 -	2.5D	5G band	1.2 (2.6-3.8) -	0.3	0.3 (0-60°)	Yes
Design 5	3.6×3.6×1.6 0.04λ×0.04λ	Stop Pass	3.62 4.7	2.5D	5G LTE 42/43 band	0.7 (3.2-3.9) 0.65(4.5-5.15)	0.5	0.25 (0-80°)	Yes

*AS- Angular stability, MFD-maximum frequency deviation, PI-polarization insensitive

Size of the unit cell, angular stability, resonant frequency, number of vias and polarization insensitivity (PI) are some of the parameters at which the proposed design is

compared. All the designs illustrated in Table 6.2 operate in the similar frequency band as that of the proposed design. It is observed that the dimension of the designs in [149], [204], [205], [72], [56] with respect to their corresponding wavelength and physical size are larger than the proposed one. The maximum relative deviation w.r.t resonant frequency is quite high at $\theta = 60^\circ$ in the structures presented in [149], [204], [205] and [72]. The structure of [206] has dimension which is a little lesser than the proposed design. However, the aforementioned design makes use forty one metallic vias in a single unit cell, which makes this design very complex in fabrication and is not cost effective. The idea of making the proposed design is to make a simple design which has very impressive results with a desire to cover the trending sub 6 GHz 5G communication frequency band. The proposed design only uses four metallic vias which provides a highly stable frequency response at $\theta = 80^\circ$ and is effective in reducing the interference created by other sources. Therefore, for the 5G communication application the given design is practically applicable.

Table 6.3 compares all the FSS listed in this thesis. All the designs have been implemented over an FR-4 substrate of ϵ_r of 4.4 and thickness of 1.6 mm. It is observed that as the structure is miniaturized, the angular stability of the given structure increases. Design 1 provides triple band rejection at WiMAX, WLAN and X-band satellite communication band with angular stability of about 40° and maximum frequency deviation of 2.9, 5.3 and 2.5% at each resonant notch. Moreover, a -10 dB pass band is obtained at 4.02 GHz ranging from 3.9 to 4.2 GHz. However, due to the asymmetric structure the design is polarization sensitive. Design 2 further make use of asymmetrical SSRRs and make rotational symmetric SSRR to obtain polarization insensitive behavior. With the help of rotational symmetric SSRRs and SL triple band rejection is obtained at WiMAX/downlink satellite C band, WLAN, Satellite communication X-band. The dimensions of design 2 is similar as that of Design 1. However, Design 2 due the symmetric behavior provides better angular stability of 70° under both the polarizations. Moreover, a -10 dB pass band is obtained at 4.37 and 6.22 GHz ranging from 4.32 to 4.52 GHz and 6.18 to 6.4 GHz, respectively. The above two designs make use of multiple resonant elements to band reject triple. To reduce the use of multiple number of resonant element, another structure is implemented in design 3.

Table 6-3 Comparison of all the FSS covered in the thesis

Ref.	Size of unit cell $\text{mm}^3 \lambda$	Band	No. of bands	No. of RE	f_r TE TM	Operating bands	Freq. Ratio (f_h/f_l)	-10 dB Bandwidth (Freq range)	Type of FSS	MFD of TE (AS in Deg)	TM	PI
Design 1	$10 \times 10 \times 1.6$ $0.113\lambda \times 0.1$ 13λ	Stop	3	3	3.45, 5.5, 7.9	WiMAX, WLAN, X-band Satellite comm.	1.64, 1.41	0.3 (3.3-3.6), 0.9 (5.1-6), 1.2 (7.2-8.4)	2 D	1.8, 5.3, 2.5 (0-40°)	-	No
		Pass	1		4.02			0.3 (3.9-4.2)				
Design 2	$10 \times 10 \times 1.6$ $0.13\lambda \times 0.13$ λ	Stop	3	3	3.92, 5.68, 7.93	WiMAX/downlink satellite C band, WLAN, Satellite comm. X-band	1.44, 1.39	0.9 (3.3-4.2), 0.8 (5.1-5.9), 1.2 (7.2-8.4)	2 D	2, 0.5, 0.5, 1.3 (0-70°)	0.5, 0.08	Yes
		Pass	2		4.37, 6.22		1.42	0.2(4.32-4.52), 0.22(6.18-6.4)				
Design 3	$8 \times 8 \times 1.6$ $0.081\lambda \times$ 0.081λ	Stop	2	1	3.08, 10.2	Mobile WiMAX and X-band	3.34	1.1 (2.5-3.6), 4.35(7.95- 12.3)	2 D	0.8, 4.2 (0-75°)	0.9, 1.2	Yes
		Pass	1		4.6		-	0.7 (4.3-5)				
Design 4	$6 \times 6 \times 1.6$ $0.061\lambda \times$ 0.061λ	Stop	1	1	6.7	UWB frequency range	-	7.7 (3.1-10.8)	2 D	5.9 (0-80°)	6.2	Yes
		Pass	-		-			-				
Design 5	$3.6 \times 3.6 \times 1.6$ $0.04\lambda \times$ 0.04λ	Stop	1	1	3.62	5G LTE 42/LTE 43 band	-	0.7 (3.2-3.9)	2.5 D	0.5 (0-80°)	0.25	Yes
		Pass	1		4.7		-	0.65(4.5-5.15)				

* RE- Resonating elements, MFD- maximum frequency deviation, AS- angular stability, PI – polarization insensitive

A single modified rotational symmetric SSRR has been implemented for the ease of designing and fabrication. As the dimension of the structure is reduced further to $8 \times 8 \text{ mm}^2$, the angular stability of the structure increases. It is observed that the angular stability of 75° is obtained with better frequency deviation from oblique angles under both the polarizations. A pass band is obtained at 4.6 GHz, ranging from 4.6 to 5 GHz. These aforementioned designs are the narrow band designs made for the certain

frequency ranges in which they can be used. Design 4 has been designed to work on the entire UWB frequency as a whole. Simple modified SL FSS structure has been designed with by far the smallest dimensions in the category. The structure provides a high angular stability in both the TE and TM incident polarized wave upto 80° , with MFD of 5.9 and 6.2 % at TE and TM incident polarized wave, respectively. The designs from 1 to 4 are 2 dimensional designs, therefore further miniaturization of the structures are difficult. Therefore, it is observed that the MFD is little high in all the above mentioned designs with respect to the oblique incidence angle. This has been overcome with the help of 2.5D FSS which is represented by design 5. The dimensions of the structure reduces further with the help of metallic vias to $3.6 \times 3.6 \text{ mm}^2$, therefore the angular stability increases. With respect to the angular stability of Design 4, it is observed that the MFD in design 5 at widest incident angle is 0.4 and 0.25 for TE and TM incident polarized wave, respectively, which is very less. Moreover, on comparing the first resonant notch of Design 1 and Design 2, it is clearly evident that with the use of 2.5 D FSS better angular stability is obtained for Design 5 with negligible frequency deviation percentage.

6.4 Conclusion

In this chapter a 2.5 D based FSS is presented to protect entire sub 6 GHz 5G frequency band. The metallic elements implanted at either side of the substrate are interconnected using four metallic vias forming a closed loop structure. The proposed structure resonates at 3.62 GHz covering -10 dB impedance bandwidth ranging from 3.2 to 3.9 GHz and the fractional bandwidth is 19.7 %. The effective dimensions of the proposed FSS with respect to the wavelength at resonant wavelength ' λ ' is $0.04 \lambda \times 0.04 \lambda$, making it an ultra-miniaturized unit cell. At $\theta = 80^\circ$, the maximum relative deviation of 0.25 % and 0.4 % is obtained under TM and TE incident polarized wave, respectively. Thus, the structure shows highly stable frequency response curves regardless of the angle of incidence and polarization of the wave. A good degree of match is found in between the measured and simulated results, thus proposed FSS is applicable in sub 6 GHz 5G frequency band for wireless communication.

CHAPTER 7

Conclusion and Future Scope

7.1 Conclusion

To control the influence of interference among the devices being operated in the closely separated narrow bands and in the entire UWB frequency range, some kind of filters must hold the necessity in antenna system which bestow strong band stop or band pass filtering behaviour. The need of the hour is to isolate the devices to avoid any leakage from within the system or unwanted inference from outside the given system. Potentially, FSS has the major advantage in doing so and is the most suitable option in spatial filtering. The study of current state of art in the designing of the FSS, filtering behaviour particularly with the scattering parameters such as impedance bandwidth, frequency response, polarization as well as angular stability is likely required.

This thesis covers various techniques to achieve bandstop characteristics to electromagnetically shield the operating devices. The method to yield the parameters of SL and SSRR and their modified versions has been explored, which is consequently useful in the designing and analysis of all the FSS developed in the course of this work. At every frequency of interest, the designs presented are simulated in full wave Ansoft HFSS simulator and further supported by fabrication and then experimental verified. In numerical analysis, the mathematical expressions for ECM is computed in the advanced design system (ADS) circuit simulator and results are validated by comparing the results of both the simulators. The proposed techniques have been used to bandstop the mostly used narrow bands such as WiMAX (3.3-3.6 GHz), Satellite communication X-band (7.2-8.4 GHz), WLAN (5-6 GHz), Sub 6 GHz 5G communication band (3.3-3.8 GHz), Satellite communication C-band (3.8-4.2 GHz), X-band (8-12 GHz) and the UWB (3.1-10.6 GHz). Multiple-bands as well as single bands using single design have been band stopped in this work.

First and foremost, the structure is dealt with the use of multi-resonant elements such as conventional SL and SSRR structure. The structure band stops WiMAX, WLAN and

Satellite communication X-band with resonant frequencies at 3.4 (3.3-3.6 GHz), 5.6 (5.1-6 GHz) and 7.9 GHz (7.2-8.4 GHz). The structure provides a decent angular stability towards varying incident angles till 40° . The maximum relative deviation in between the response curves obtained at normal incidence and $\theta = 40^\circ$ incident TE polarized wave is 2.9%, 5.3% and 2.5%. Thus, with respect to the research gap 1 the design has effectively shielded or band stopped triple bands at UWB frequency range.

Many applications demands highly stable frequency response regardless of the widest angle polarization angle and angle of incidence. Therefore, various techniques for the improvement of scattering parameters have been investigated as well. A significant change in asymmetric SSRR design into four identical 90° rotational SSRR yields a novel symmetric SSRR structure which when implemented with SL forms a miniaturized structure. The proposed design is simple, low profile, light-weight and offers multi-resonant characteristics. Additionally, it provides better angular stability and due to symmetric behaviour polarization insensitivity is also achieved. Using triple resonant rotational symmetric SSRR₁, SSRR₂ and SL, WiMAX/ C-band Satellite communication downlink (3.3-4.2 GHz), WLAN (5.1-5.9 GHz) and Satellite communication X-band (7.2-8.4 GHz) are band stopped, respectively. The resonant notched frequencies are obtained at 3.92, 5.68 and 7.92 GHz. The structure also works as a band pass at 4.37 and 6.22 GHz. The maximum relative deviation in between the triple resonant notches obtained at normal incidence and $\theta = 70^\circ$ incident TE polarized wave is 2%, 0.5% and 1.3%. The deviation at $\theta = 70^\circ$ incident TM polarized wave is 1.5%, 0.5% and 0.08%. Thus an angularly stable and polarization insensitive frequency response has been achieved in this design, which fulfil the requirements mentioned in research gap 2.

In this way, another novel FSS structure has been developed which makes use two different approaches. Rotational symmetric SSRR are implemented with metallic patch inserted in the middle to controls the direct flow of current in the rotational arms of SSRR to further reduce the size of the structure with more frequency stabilization at varying impinging wave. The given structure band rejects dual frequency bands using a single resonant structure, i.e., mobile WiMAX band ranging from 2.5 to 2.7/3.3 to 3.6 GHz and X-band ranging from 8 to 12 GHz. A resonant dip is obtained at 4.6 GHz ranging from

4.3 to 5 GHz. The structure shows a stable frequency response till 75° . The maximum relative deviation in between the dual resonant notches obtained at normal incidence and $\theta = 75^\circ$ incident TE polarized wave is 0.5% and 4.2%. The deviation at $\theta = 75^\circ$ incident TM polarized wave is 0.2% and 1.2%. Therefore, with this the miniaturization is further achieved and using single metallic element dual stop bands have been achieved as mentioned in the research gap 3.

SL finds a potential application in controlling the bandwidth of the electromagnetic spectrum. A substantial change in SL width shows a tremendous effect in the bandwidth of the structure. SL inserted with metallic arms to increase the perimeter and width, backed on the dielectric substrate yields a novel modified SL structure to bandstop entire UWB frequency band. The structure resonates at 6.7 GHz (3.1 to 10.8 GHz). The structure shows high angular stability till 80° . The maximum relative deviation in between the resonant notch obtained at normal incidence and $\theta = 80^\circ$ incident TE and TM polarized wave is 5.9% and 6.2%, respectively. Therefore, for the performance enhancement of UWB antennas this design is implemented and fulfills the requirement of research gap 4.

Further, the length of SL also contributes a noteworthy control over the bandwidth and resonant frequency of a given structure. The increment in the perimeter results in down shift of the resonant frequency with decrease in the bandwidth. The currently trending 5G wireless communication system requires a narrow band characteristic with extremely stable frequency response. The increment in the length of loop is bestowed by interconnecting the metallic elements positioned at either side of the substrate using metallic vias which are inserted inside the substrate to yield a modified 2.5D FSS closed loop structure. The structure resonates at 3.62 GHz (3.2 - 3.9 GHz), therefore covering the entire sub 6 GHz frequency range. The maximum relative deviation in between the resonant notch obtained at normal incidence and $\theta = 80^\circ$ incident TE and TM polarized wave is 0.5% and 0.2%, respectively. A ultra miniaturized and extremely high angularly stable frequency response has been obtained using this design which is the requirement of the research gap 5.

Therefore, it is observed that all the designs have been implemented with the latest techniques to overcome EMI related to various narrow band and ultra-wide band applications. All the designs are novel and can be used in the respective applications to which they belong.

7.2 Future work

FSS can be used in wide variety of work due to its multifunctional behaviour. However, the work present in this thesis is limited to the implementation of passive FSS in which metallic elements are imprinted over the dielectric substrate. The implementation of the FSS with any practical antenna for performance enhancement is yet to be performed. Further, in the futurist communication various aspects are required to be covered, some of them are listed as follows:

1. Reconfigurable FSS shall be implemented for an easy switch between various commercially available communication systems. Reconfigurable FSS requires the use of active elements such as PIN diodes to toggle between the different systems.
2. Another aspect for 5G beyond communication is opting adaptive beamsteering than mechanical beamsteering using smart surfaces.
3. Implementation of conformal FSS is another great aspect of future communication system. Conformal FSS can be used for the radar cross section reduction.
4. Implementation of FSS on textile surface.
5. Dual polarized multi band FSS is also an important topic which is required to be addressed for the enhancement of communication system.

REFERENCES

- [1] B. A. Munk, *Frequency Selective Surfaces: Theory and Design*, Wiley Online Library: Hoboken, NJ, USA, vol. 29, 2000.
- [2] L. Li *et al.*, “Frequency Selective Reflectarray Using Crossed-Dipole Elements With Square Loops for Wireless Communication Applications,” *IEEE Transactions on Antennas and Propagation*, vol. 59, no. 1, pp. 89–99, Jan. 2011..
- [3] D. Singh, A. Kumar, S. Meena, and V. Agarwala, “Analysis of Frequency Selective Surfaces for Radar Absorbing Materials,” *Progress In Electromagnetics Research B*, vol. 38, pp. 297–314, 2012.
- [4] S. Keyrouz, G. Perotto, and H. J. Visser, “Frequency selective surface for radio frequency energy harvesting applications,” *IET Microwaves, Antennas & Propagation*, vol. 8, no. 7, pp. 523–531, Jan. 2014.
- [5] Y. Ranga, L. Matekovits, A. R. Weily, and K. P. Esselle, “A low-profile dual-layer ultra-wideband frequency selective surface reflector,” *Microwave and Optical Technology Letters*, vol. 55, no. 6, pp. 1223–1227, 2013,.
- [6] F. C. G. da S. Segundo and A. L. P. S. Campos, “Compact frequency selective surface with dual band response for WLAN applications,” *Microwave and Optical Technology Letters*, vol. 57, no. 2, pp. 265–268, 2015.
- [7] A. Fallahi, M. Mishrikey, C. Hafner, and R. Vahldieck, “Efficient Procedures for the Optimization of Frequency Selective Surfaces,” *IEEE Transactions on Antennas and Propagation*, vol. 56, no. 5, pp. 1340–1349, May 2008.
- [8] O. Necibi, D. Hamzaoui, T. P. Vuong, and A. Gharsallah, “A novel RFID-HIS-PRS reader antenna for the millimeter wave band 30 GHz,” *Microwave and Optical Technology Letters*, vol. 57, no. 8, pp. 1835–1842, 2015.
- [9] H.-T. Liu, H.-F. Cheng, Z.-Y. Chu, and D.-Y. Zhang, “Absorbing properties of frequency selective surface absorbers with cross-shaped resistive patches,” *Materials & Design*, vol. 28, no. 7, pp. 2166–2171, Jan. 2007.
- [10] T. Hassan, M. U. Khan, H. Attia, and M. S. Sharawi, “An FSS Based Correlation Reduction Technique for MIMO Antennas,” *IEEE Transactions on Antennas and Propagation*, vol. 66, no. 9, pp. 4900–4905, Sep. 2018.

- [11] P. Mahouti, F. Güneş, M. A. Belen, A. Çalışkan, S. Demirel, and Z. Sharipov, “Horn antennas with enhanced functionalities through the use of frequency selective surfaces,” *International Journal of RF and Microwave Computer-Aided Engineering*, vol. 26, no. 4, pp. 287–293, 2016.
- [12] H. Chen, Q. Cao, and Y. Wang, “A Wideband Switchable Absorber/Reflector Based on Active Frequency Selective Surface,” in *2020 IEEE Asia-Pacific Microwave Conference (APMC)*, Dec. 2020, pp. 902–904.
- [13] H. Li, F. Costa, J. Fang, Y. Wang, Q. Cao, and A. Monorchio, “Dual-functional active frequency selective surface using parallel feeding configuration and its equivalent circuit model,” *International Journal of RF and Microwave Computer-Aided Engineering*, vol. 28, no. 7, p. e21450, 2018
- [14] F. Costa, S. Genovesi, and A. Monorchio, “On the Bandwidth of High-Impedance Frequency Selective Surfaces,” *IEEE Antennas and Wireless Propagation Letters*, vol. 8, pp. 1341–1344, 2009.
- [15] S. Islam *et al.*, “Effect of inter-element spacings variation on the performance of linear grounded frequency selective surface arrays in W-band,” *Microwave and Optical Technology Letters*, vol. 52, no. 1, pp. 155–160, 2010.
- [16] H.-H. Sung, *Frequency Selective Wallpaper for Mitigating Indoor Wireless Interference*. University of Auckland, 2006.
- [17] Z. L. Wang, K. Hashimoto, N. Shinohara, and H. Matsumoto, “Frequency-selective surface for microwave power transmission,” *IEEE Transactions on Microwave Theory and Techniques*, vol. 47, no. 10, pp. 2039–2042, Oct. 1999.
- [18] T. Larsen, “A Survey of the Theory of Wire Grids,” *IRE Transactions on Microwave Theory and Techniques*, vol. 10, no. 3, pp. 191–201, May 1962.
- [19] R. J. Langley and A. J. Drinkwater, “Improved empirical model for the Jerusalem cross,” *IEE Proceedings H (Microwaves, Optics and Antennas)*, vol. 129, no. 1, pp. 1–6, Feb. 1982.
- [20] F. Costa, A. Monorchio, and G. Manara, “Efficient Analysis of Frequency-Selective Surfaces by a Simple Equivalent-Circuit Model,” *IEEE Antennas and Propagation Magazine*, vol. 54, no. 4, pp. 35–48, Aug. 2012.

- [21] B. Mandal, A. Chatterjee, and S. K. Parui, "Acrylic substrate based low profile wearable button antenna with FSS layer for WLAN and Wi-Fi applications," *Microwave and Optical Technology Letters*, vol. 57, no. 5, pp. 1033–1038, 2015.
- [22] M. Sesay, X. Jin, and Z. Ouyang, "Frequency Selective Surface with Arbitrary Shapes and its Application to Filter Design," *Progress In Electromagnetics Research B*, vol. 57, pp. 75–85, 2014.
- [23] N. Marcuvitz, *Waveguide Handbook*. IET Digital Library, 1986.
- [24] R. J. Langley and E. A. Parker, "Equivalent circuit model for arrays of square loops," *Electronics Letters*, vol. 18, no. 7, pp. 294–296, Apr. 1982.
- [25] S. N. Zabri, R. Cahill, and A. Schuchinsky, "Polarisation independent split ring frequency selective surface," *Electronics Letters*, vol. 49, no. 4, pp. 245–246, Feb. 2013.
- [26] S. Vegesna, Y. Zhu, Y. Zhao, Z. Fan, A. Bernussi, and M. Saed, "Terahertz frequency selective surface with reconfigurable polarization characteristics using vanadium dioxide," *Journal of Electromagnetic Waves and Applications*, vol. 28, no. 1, pp. 83–90, Jan. 2014.
- [27] R. Cahill and E. A. Parker, "Frequency selective surface design for submillimetric demultiplexing," *Microwave and Optical Technology Letters*, vol. 7, no. 13, pp. 595–597, 1994.
- [28] S. Islam, J. Stiens, I. Jaeger, G. Poesen, and R. Vounckx, "Implementation of dynamic Hadamard diffuser as a frequency selective surface for W-band active millimeter wave imaging," *Microwave and Optical Technology Letters*, vol. 51, no. 6, pp. 1440–1445, 2009.
- [29] S. Monni, A. Neto, G. Gerini, F. Nennie, and A. Tijhuis, "Frequency-Selective Surface to Prevent Interference Between Radar and SATCOM Antennas," *IEEE Antennas and Wireless Propagation Letters*, vol. 8, pp. 220–223, 2009.
- [30] B. Li, Y.-S. Zeng, B.-J. Chen, and C. H. Chan, "Terahertz Frequency-Selective Surface With Polarization Selection and Conversion Characteristics," *IEEE Transactions on Terahertz Science and Technology*, vol. 9, no. 5, pp. 510–519, Sep. 2019.

- [31] J. Poojali, S. Ray, B. Pesala, K. C. Venkata, and K. Arunachalam, "Quad-Band Polarization-Insensitive Millimeter-Wave Frequency Selective Surface for Remote Sensing," *IEEE Antennas and Wireless Propagation Letters*, vol. 16, pp. 1796–1799, 2017.
- [32] X. Sheng, J. Ge, K. Han, and X.-C. Zhu, "Transmissive/Reflective Frequency Selective Surface for Satellite Applications," *IEEE Antennas and Wireless Propagation Letters*, vol. 17, no. 7, pp. 1136–1140, Jul. 2018.
- [33] K. Katoch, N. Jaglan, S. D. Gupta, and M. S. Sharawi, "Design of a triple band notched polarization independent compact FSS at UWB frequency range," *International Journal of RF and Microwave Computer-Aided Engineering*, vol. 31, no. 6, p. e22631, 2021.
- [34] M. S. Durschlag and T. A. DeTemple, "Far-IR optical properties of freestanding and dielectrically backed metal meshes," *Appl. Opt., AO*, vol. 20, no. 7, pp. 1245–1253, Apr. 1981.
- [35] R. Ulrich, "Far-infrared properties of metallic mesh and its complementary structure," *Infrared Physics*, vol. 7, no. 1, pp. 37–55, Mar. 1967.
- [36] K. Katoch, N. Jaglan, and S. D. Gupta, "Design and Analysis of Single Sided Modified Square Loop UWB Frequency Selective Surface," *IEEE Transactions on Electromagnetic Compatibility*, pp. 1–10, 2021.
- [37] B. Sanz-Izquierdo, E. A. Parker, J.-B. Robertson, and J. C. Batchelor, "Singly and Dual Polarized Convolutional Frequency Selective Structures," *IEEE Transactions on Antennas and Propagation*, vol. 58, no. 3, pp. 690–696, Mar. 2010.
- [38] W. Y. Yong *et al.*, "Flexible Convolutional Ring Shaped FSS for X-Band Screening Application," *IEEE Access*, vol. 6, pp. 11657–11665, 2018.
- [39] W. T. S. Ramos, R. C. Mesquita, and E. J. Silva, "Frequency selective surface using meander line inclusions," *Journal of Electromagnetic Waves and Applications*, vol. 32, no. 11, pp. 1440–1447, Jul. 2018.
- [40] S. Habib, G. I. Kiani, and M. F. U. Butt, "A Convolutional Frequency Selective Surface for Wideband Communication Applications," *IEEE Access*, vol. 7, pp. 65075–65082, 2019.

- [41] S. Bilvam, R. Sivasamy, M. Kanagasabai, G. N. A. M, and S. Baisakhiya, “Miniaturized Band Stop FSS Using Convoluted Swastika Structure,” *Frequenz*, vol. 71, no. 1–2, pp. 51–56, Jan. 2017.
- [42] F. Huang, J. C. Batchelor, and E. A. Parker, “Interwoven convoluted element frequency selective surfaces with wide bandwidths,” *Electronics Letters*, vol. 42, no. 14, pp. 788–790, Jul. 2006.
- [43] P.-C. Zhao, Z.-Y. Zong, W. Wu, and D.-G. Fang, “A Convoluted Structure for Miniaturized Frequency Selective Surface and Its Equivalent Circuit for Optimization Design,” *IEEE Transactions on Antennas and Propagation*, vol. 64, no. 7, pp. 2963–2970, Jul. 2016.
- [44] N. Liu, X. Sheng, C. Zhang, J. Fan, and D. Guo, “A Miniaturized Triband Frequency Selective Surface Based on Convoluted Design,” *IEEE Antennas and Wireless Propagation Letters*, vol. 16, pp. 2384–2387, 2017.
- [45] A. B. Varuna, S. Ghosh, and K. V. Srivastava, “A miniaturized-element bandpass frequency selective surface using meander line geometry,” *Microwave and Optical Technology Letters*, vol. 59, no. 10, pp. 2484–2489, 2017.
- [46] F. Bayatpur and K. Sarabandi, “Multipole Spatial Filters Using Metamaterial-Based Miniaturized-Element Frequency-Selective Surfaces,” *IEEE Transactions on Microwave Theory and Techniques*, vol. 56, no. 12, pp. 2742–2747, Dec. 2008.
- [47] S. Narayan, G. Gulati, B. Sangeetha, and R. U. Nair, “Novel Metamaterial-Element-Based FSS for Airborne Radome Applications,” *IEEE Transactions on Antennas and Propagation*, vol. 66, no. 9, pp. 4695–4707, Sep. 2018.
- [48] M. Majidzadeh, “2.4/5.8 GHz WLAN Filtering in Secure Electromagnetic Applications: A Single Layer Frequency Selective Surface,” *Smart Science*, vol. 5, no. 4, pp. 199–205, Oct. 2017.
- [49] M. Karahan and E. Aksoy, “Design and analysis of angular stable antipodal F-type frequency selective surface with multi-band characteristics,” *International Journal of RF and Microwave Computer-Aided Engineering*, vol. 30, no. 12, p. e22466, 2020.

- [50] M. R. Chaharmir and J. Shaker, "Design of a Multilayer X-/Ka-Band Frequency-Selective Surface-Backed Reflectarray for Satellite Applications," *IEEE Transactions on Antennas and Propagation*, vol. 63, no. 4, pp. 1255–1262, Apr. 2015.
- [51] H. Zhou *et al.*, "Ultra-wideband frequency selective surface," *Electronics Letters*, vol. 48, no. 1, pp. 11–13, Jan. 2012.
- [52] B. Hua, X. Liu, X. He, and Y. Yang, "Wide-Angle Frequency Selective Surface with Ultra-Wideband Response for Aircraft Stealth Designs," *Progress In Electromagnetics Research C*, vol. 77, pp. 167–173, 2017.
- [53] A. Chatterjee and S. K. Parui, "A triple-layer dual-bandpass frequency selective surface of third order response with equivalent circuit analysis," *International Journal of RF and Microwave Computer-Aided Engineering*, vol. 30, no. 2, p. e22047, 2020.
- [54] T. Hong, M. Wang, K. Peng, Q. Zhao, and S. Gong, "Compact Ultra-Wide Band Frequency Selective Surface With High Selectivity," *IEEE Transactions on Antennas and Propagation*, vol. 68, no. 7, pp. 5724–5729, Jul. 2020.
- [55] M. N. Hussein, J. Zhou, Y. Huang, M. Kod, and A. P. Sohrab, "A Miniaturized Low-Profile Multilayer Frequency-Selective Surface Insensitive to Surrounding Dielectric Materials," *IEEE Transactions on Microwave Theory and Techniques*, vol. 65, no. 12, pp. 4851–4860, Dec. 2017.
- [56] M. Hussein, J. Zhou, Y. Huang, and B. Al-Juboori, "A Low-Profile Miniaturized Second-Order Bandpass Frequency Selective Surface," *IEEE Antennas and Wireless Propagation Letters*, vol. 16, pp. 2791–2794, 2017.
- [57] K. Tao, B. Li, Y. Tang, M. Zhang, and Y. Bo, "Analysis and implementation of 3D bandpass frequency selective structure with high frequency selectivity," *Electronics Letters*, vol. 53, no. 5, pp. 324–326, Jan. 2017.
- [58] M. Bouslama, M. Traii, A. Gharsallah, and T. A. Denidni, "Reconfigurable dual-band 3D Frequency Selective Surface unit-cell," in *2015 IEEE International Symposium on Antennas and Propagation USNC/URSI National Radio Science Meeting*, Jul. 2015, pp. 1264–1265.

- [59] L. Li *et al.*, “All-Dielectric Frequency Selective Surface Based on 3D Printing Materials,” *physica status solidi (a)*, vol. 215, no. 14, p. 1700840, 2018.
- [60] W. S. T. Rowe, A. R. As-Saber, S. N. Azemi, and K. Ghorbani, “3D frequency selective surfaces with highly selective responses,” in *2015 Loughborough Antennas Propagation Conference (LAPC)*, Nov. 2015, pp. 1–4.
- [61] I. G. Lee and I. P. Hong, “3D frequency selective surface for stable angle of incidence,” *Electronics Letters*, vol. 50, no. 6, pp. 423–424, Mar. 2014.
- [62] R. Sivasamy and M. Kanagasabai, “Novel Reconfigurable 3-D Frequency Selective Surface,” *IEEE Transactions on Components, Packaging and Manufacturing Technology*, vol. 7, no. 10, pp. 1678–1682, Oct. 2017.
- [63] S. Can, E. Karakaya, F. Bagci, A. E. Yilmaz, and B. Akaoglu, “Dual-Band Double-Cylindrical-Ring 3D Frequency Selective Surface,” *ETRI Journal*, vol. 39, no. 1, pp. 69–75, 2017.
- [64] J. Zhu, Z. Hao, C. Wang, Z. Yu, C. Huang, and W. Tang, “Dual-Band 3-D Frequency Selective Surface With Multiple Transmission Zeros,” *IEEE Antennas and Wireless Propagation Letters*, vol. 18, no. 4, pp. 596–600, Apr. 2019.
- [65] M. Harnois, M. Himdi, W. Y. Yong, S. K. A. Rahim, K. Tekkouk, and N. Cheval, “An Improved Fabrication Technique for the 3-D Frequency Selective Surface based on Water Transfer Printing Technology,” *Sci Rep*, vol. 10, no. 1, Art. no. 1, Feb. 2020.
- [66] Y. Shi, W. Zhuang, W. Tang, C. Wang, and S. Liu, “Modeling and Analysis of Miniaturized Frequency-Selective Surface Based on 2.5-Dimensional Closed Loop With Additional Transmission Pole,” *IEEE Transactions on Antennas and Propagation*, vol. 64, no. 1, pp. 346–351, Jan. 2016.
- [67] Z. Yang, W. Jiang, Q. Huang, and T. Hong, “2.5D Miniaturized Frequency Selective Resorber with A Wide High-Transmission Passband,” *IEEE Antennas and Wireless Propagation Letters*, pp. 1–1, 2021.
- [68] K. K. Varikuntla and R. Singaravelu, “Design of a Novel 2.5D Frequency Selective Surface Element Using Fibonacci Spiral for Radome Application,” in *2018 Asia-Pacific Microwave Conference (APMC)*, Nov. 2018, pp. 1289–1291.

- [69] P. Wang and W. Jiang, “Miniaturised Bandstop Frequency Selective Surface Based on Multilayer 2.5-Dimensional Structure,” in *2019 International Symposium on Antennas and Propagation (ISAP)*, Oct. 2019, pp. 1–3.
- [70] Z.-Z. Zhao, X.-M. Chen, A. A. Kishk, and A.-X. Zhang, “2.5D frequency selective surface with quasi-elliptical bandpass response,” *Microwave and Optical Technology Letters*, vol. 63, no. 6, pp. 1693–1698, 2021.
- [71] M. Jia, X. He, Y. Yang, B. Hua, W. Hu, and X. Qian, “Wideband Ultraminiaturised-Element Frequency Selective Surface Based on Interlocked 2.5-Dimensional Structures,” *Progress In Electromagnetics Research Letters*, vol. 88, pp. 37–42, 2020.
- [72] Y. Shi, W. Tang, W. Zhuang, and C. Wang, “Miniaturised frequency selective surface based on 2.5-dimensional closed loop,” *Electronics Letters*, vol. 50, no. 23, pp. 1656–1658, Oct. 2014.
- [73] W. Yin, H. Zhang, T. Zhong, and X. Min, “A Novel Compact Dual-Band Frequency Selective Surface for GSM Shielding by Utilizing a 2.5-Dimensional Structure,” *IEEE Transactions on Electromagnetic Compatibility*, vol. 60, no. 6, pp. 2057–2060, Dec. 2018.
- [74] H. Li *et al.*, “2.5-D Miniaturized Multifunctional Active Frequency-Selective Surface,” *IEEE Transactions on Antennas and Propagation*, vol. 67, no. 7, pp. 4659–4667, Jul. 2019.
- [75] B. Hua, X. He, and Y. Yang, “Polarisation-independent UWB frequency selective surface based on 2.5D miniaturised hexagonal ring,” *Electronics Letters*, vol. 53, no. 23, pp. 1502–1504, 2017.
- [76] K. K. Varikuntla and R. Singaravelu, “Design and implementation of 2.5D frequency-selective surface based on substrate-integrated waveguide technology,” *International Journal of Microwave and Wireless Technologies*, vol. 11, no. 3, pp. 255–267, Apr. 2019.
- [77] D. Li, T. Li, and E. Li, “Implementation of ultra-miniaturised frequency-selective structures based on 2.5D convoluted segments,” *Electronics Letters*, vol. 54, no. 8, pp. 476–478, Mar. 2018.

- [78] T. Hussain, Q. Cao, J. K. Kayani, and I. Majid, "Miniaturization of Frequency Selective Surfaces Using 2.5-D Knitted Structures: Design and Synthesis," *IEEE Transactions on Antennas and Propagation*, vol. 65, no. 5, pp. 2405–2412, May 2017.
- [79] S. Ghosh, "Miniaturized-Element Frequency Selective Surface based on 2.5-Dimensional Meander Lines," in *2019 IEEE Asia-Pacific Microwave Conference (APMC)*, Dec. 2019, pp. 850–852..
- [80] M. W. Niaz, Y. Yin, and J. Chen, "Synthesis of Ultraminiaturized Frequency-Selective Surfaces Utilizing 2.5-D Tapered Meandering Lines," *IEEE Antennas and Wireless Propagation Letters*, vol. 19, no. 1, pp. 163–167, Jan. 2020.
- [81] M. W. Niaz, Y. Yin, S. Zheng, L. Zhao, and J. Chen, "Design and Analysis of an Ultraminiaturized FSS Using 2.5-D Convolute Square Spirals," *IEEE Transactions on Antennas and Propagation*, vol. 68, no. 4, pp. 2919–2925, Apr. 2020.
- [82] R. S. Anwar, L. Mao, and H. Ning, "Frequency Selective Surfaces: A Review," *Applied Sciences*, vol. 8, no. 9, Art. no. 9, Sep. 2018.
- [83] R. Natarajan, M. Kanagasabai, S. Baisakhiya, R. Sivasamy, S. Palaniswamy, and J. K. Pakkathillam, "A Compact Frequency Selective Surface With Stable Response for WLAN Applications," *IEEE Antennas and Wireless Propagation Letters*, vol. 12, pp. 718–720, 2013.
- [84] S. Ünalđı, S. Çimen, G. Çakır, and U. E. Ayten, "A Novel Dual-Band Ultrathin FSS With Closely Settled Frequency Response," *IEEE Antennas and Wireless Propagation Letters*, vol. 16, pp. 1381–1384, 2017.
- [85] M. Bashiri, C. Ghobadi, J. Nourinia, and M. Majidzadeh, "WiMAX, WLAN, and X-Band Filtering Mechanism: Simple-Structured Triple-Band Frequency Selective Surface," *IEEE Antennas and Wireless Propagation Letters*, vol. 16, pp. 3245–3248, 2017.
- [86] A. Ghosh, M. Kumar, S. N. Islam, and S. Das, "Design and Analysis of a Compact Penta-Band Polarization-Insensitive Bandstop Frequency Selective Surface," *IEEE Antennas and Wireless Propagation Letters*, vol. 19, no. 1, pp. 59–63, Jan. 2020.

- [87] K. R. Jha, G. Singh, and R. Jyoti, "A Simple Synthesis Technique of Single-Square-Loop Frequency Selective Surface," *Progress In Electromagnetics Research B*, vol. 45, pp. 165–185, 2012.
- [88] J. Costantine, Y. Tawk, S. E. Barbin, and C. G. Christodoulou, "Reconfigurable Antennas: Design and Applications," *Proceedings of the IEEE*, vol. 103, no. 3, pp. 424–437, Mar. 2015.
- [89] S. C. Bakshi, D. Mitra, and S. Ghosh, "A Frequency Selective Surface Based Reconfigurable Resorber With Switchable Transmission/Reflection Band," *IEEE Antennas and Wireless Propagation Letters*, vol. 18, no. 1, pp. 29–33, Jan. 2019.
- [90] M. Niroo-Jazi and T. A. Denidni, "Electronically Sweeping-Beam Antenna Using a New Cylindrical Frequency-Selective Surface," *IEEE Transactions on Antennas and Propagation*, vol. 61, no. 2, pp. 666–676, Feb. 2013.
- [91] H. L. Zhu, X. H. Liu, S. W. Cheung, and T. I. Yuk, "Frequency-Reconfigurable Antenna Using Metasurface," *IEEE Transactions on Antennas and Propagation*, vol. 62, no. 1, pp. 80–85, Jan. 2014.
- [92] X. Yan *et al.*, "Water-Based Reconfigurable Frequency Selective Resorber With Thermally Tunable Absorption Band," *IEEE Transactions on Antennas and Propagation*, vol. 68, no. 8, pp. 6162–6171, Aug. 2020.
- [93] N. C. Karmakar and M. E. Bialkowski, "A beam-forming network for a circular switched-beam phased array antenna," *IEEE Microwave and Wireless Components Letters*, vol. 11, no. 1, pp. 7–9, Jan. 2001.
- [94] L. Ge and K. M. Luk, "Band-Reconfigurable Unidirectional Antenna: A simple, efficient magneto-electric antenna for cognitive radio applications.," *IEEE Antennas and Propagation Magazine*, vol. 58, no. 2, pp. 18–27, Apr. 2016.
- [95] L. Zou and C. Fumeaux, "A Cross-Shaped Dielectric Resonator Antenna for Multifunction and Polarization Diversity Applications," *IEEE Antennas and Wireless Propagation Letters*, vol. 10, pp. 742–745, 2011.
- [96] M. K. Saleem, M. A. S. Alkanhal, and A. F. Sheta, "Dual Strip-Excited Dielectric Resonator Antenna with Parasitic Strips for Radiation Pattern Reconfigurability," *International Journal of Antennas and Propagation*, vol. 2014, p. e865620, Jan. 2014.

- [97] A. Edalati and T. A. Denidni, "Reconfigurable Beamwidth Antenna Based on Active Partially Reflective Surfaces," *IEEE Antennas and Wireless Propagation Letters*, vol. 8, pp. 1087–1090, 2009.
- [98] L.-Y. Ji, Z.-Y. Zhang, and N.-W. Liu, "A Two-Dimensional Beam-Steering Partially Reflective Surface (PRS) Antenna Using a Reconfigurable FSS Structure," *IEEE Antennas and Wireless Propagation Letters*, vol. 18, no. 6, pp. 1076–1080, Jun. 2019.
- [99] S. M. Mahmood and T. A. Denidni, "Pattern-Reconfigurable Antenna Using a Switchable Frequency Selective Surface With Improved Bandwidth," *IEEE Antennas and Wireless Propagation Letters*, vol. 15, pp. 1148–1151, 2016.
- [100] M. N. Jazi and T. A. Denidni, "Agile Radiation-Pattern Antenna Based on Active Cylindrical Frequency Selective Surfaces," *IEEE Antennas and Wireless Propagation Letters*, vol. 9, pp. 387–388, 2010.
- [101] M. Bouslama, M. Traii, T. A. Denidni, and A. Gharsallah, "Beam-Switching Antenna With a New Reconfigurable Frequency Selective Surface," *IEEE Antennas and Wireless Propagation Letters*, vol. 15, pp. 1159–1162, 2016.
- [102] M. Bouslama, M. Traii, T. A. Denidni, and A. Gharsallah, "Reconfigurable frequency selective surface for beam-switching applications," *IET Microwaves, Antennas & Propagation*, vol. 11, no. 1, pp. 69–74, Jan. 2017.
- [103] C. Gu *et al.*, "Dual-Band Electronically Beam-Switched Antenna Using Slot Active Frequency Selective Surface," *IEEE Transactions on Antennas and Propagation*, vol. 65, no. 3, pp. 1393–1398, Mar. 2017.
- [104] A. Kesavan, M. Mantash, J. Zaid, and T. A. Denidni, "A Dual-Plane Beam-Sweeping Millimeter-Wave Antenna Using Reconfigurable Frequency Selective Surfaces," *IEEE Antennas and Wireless Propagation Letters*, vol. 17, no. 10, pp. 1832–1836, Oct. 2018.
- [105] S. Ghosh and S. Lim, "Fluidically Reconfigurable Multifunctional Frequency-Selective Surface With Miniaturization Characteristic," *IEEE Transactions on Microwave Theory and Techniques*, vol. 66, no. 8, pp. 3857–3865, Aug. 2018.
- [106] A. Goldsmith, *Wireless Communications*. Cambridge: Cambridge University Press, 2005.

- [107] R. Karimian and H. Tadayon, "Multiband MIMO Antenna System with Parasitic Elements for WLAN and WiMAX Application," *International Journal of Antennas and Propagation*, vol. 2013, p. e365719, Nov. 2013.
- [108] S. H. Chae, S. Oh, and S.-O. Park, "Analysis of Mutual Coupling, Correlations, and TARC in WiBro MIMO Array Antenna," *IEEE Antennas and Wireless Propagation Letters*, vol. 6, pp. 122–125, 2007.
- [109] M. S. Sharawi, *Printed MIMO Antenna Engineering*, Artech House, USA, 2014
- [110] R. Mitra, *Developments in Antenna Analysis and Design: Volume 1*. IET Digital Library, 2018.
- [111] Z. Liu, S. Jie, H. Ma, X.-Y. Zhang, and B. Xing, "A Novel Dual-Passband Net-Shaped FSS Structure Used for MIMO Antennas," *Progress In Electromagnetics Research C*, vol. 90, pp. 29–39, 2019.
- [112] X. Zhu, X. Yang, Q. Song, and B. Lui, "Compact UWB-MIMO antenna with metamaterial FSS decoupling structure," *EURASIP Journal on Wireless Communications and Networking*, vol. 2017, no. 1, p. 115, Jun. 2017.
- [113] B. Zhang, J. M. Jornet, I. F. Akyildiz, and Z. P. Wu, "Mutual Coupling Reduction for Ultra-Dense Multi-Band Plasmonic Nano-Antenna Arrays Using Graphene-Based Frequency Selective Surface," *IEEE Access*, vol. 7, pp. 33214–33225, 2019.
- [114] A. P. Feresidis and J. C. Vardaxoglou, "High gain planar antenna using optimised partially reflective surfaces," *IEE Proceedings - Microwaves, Antennas and Propagation*, vol. 148, no. 6, pp. 345–350, Dec. 2001.
- [115] A. Kesavan, R. Karimian, and T. A. Denidni, "A Novel Wideband Frequency Selective Surface for Millimeter-Wave Applications," *IEEE Antennas and Wireless Propagation Letters*, vol. 15, pp. 1711–1714, 2016.
- [116] R. Karimian, A. Kesavan, M. Nedil, and T. A. Denidni, "Low-Mutual-Coupling 60-GHz MIMO Antenna System With Frequency Selective Surface Wall," *IEEE Antennas and Wireless Propagation Letters*, vol. 16, pp. 373–376, 2017.
- [117] M. Bilal, R. Saleem, Hammad. H. Abbasi, M. F. Shafique, and A. K. Brown, "An FSS-Based Nonplanar Quad-Element UWB-MIMO Antenna System," *IEEE Antennas and Wireless Propagation Letters*, vol. 16, pp. 987–990, 2017.

- [118] G. Das, N. K. Sahu, A. Sharma, R. K. Gangwar, and M. S. Sharawi, "FSS-Based Spatially Decoupled Back-to-Back Four-Port MIMO DRA With Multidirectional Pattern Diversity," *IEEE Antennas and Wireless Propagation Letters*, vol. 18, no. 8, pp. 1552–1556, Aug. 2019.
- [119] U. Farooq, M. F. Shafique, and M. J. Mughal, "Polarization Insensitive Dual Band Frequency Selective Surface for RF Shielding Through Glass Windows," *IEEE Transactions on Electromagnetic Compatibility*, vol. 62, no. 1, pp. 93–100, Feb. 2020.
- [120] R. Sivasamy, L. Murugasamy, M. Kanagasabai, E. F. Sundarsingh, and M. Gulam Nabi Alsath, "A Low-Profile Paper Substrate-Based Dual-Band FSS for GSM Shielding," *IEEE Transactions on Electromagnetic Compatibility*, vol. 58, no. 2, pp. 611–614, Apr. 2016.
- [121] M. Nauman, R. Saleem, A. K. Rashid, and M. F. Shafique, "A Miniaturized Flexible Frequency Selective Surface for X-Band Applications," *IEEE Transactions on Electromagnetic Compatibility*, vol. 58, no. 2, pp. 419–428, Apr. 2016.
- [122] I. S. Syed, Y. Ranga, L. Matekovits, K. P. Esselle, and S. G. Hay, "A Single-Layer Frequency-Selective Surface for Ultrawideband Electromagnetic Shielding," *IEEE Transactions on Electromagnetic Compatibility*, vol. 56, no. 6, pp. 1404–1411, Dec. 2014.
- [123] A. Foroozesh and L. Shafai, "Investigation Into the Effects of the Patch-Type FSS Superstrate on the High-Gain Cavity Resonance Antenna Design," *IEEE Transactions on Antennas and Propagation*, vol. 58, no. 2, pp. 258–270, Feb. 2010.
- [124] K. Mondal, D. C. Sarkar, and P. P. Sarkar, " 5×5 Matrix Patch Type Frequency Selective Surface Based Miniaturized Enhanced Gain Broadband Microstrip Antenna for WLAN/WiMAX /ISM Band Applications," *Progress In Electromagnetics Research C*, vol. 89, pp. 207–219, 2019.
- [125] D. Gangwar, S. Das, R. L. Yadava, and B. K. Kanaujia, "Frequency Selective Surface as Superstrate on Wideband Dielectric Resonator Antenna for Circular

- Polarization and Gain Enhancement,” *Wireless Pers Commun*, vol. 97, no. 2, pp. 3149–3163, Nov. 2017.
- [126] A. Pirhadi, H. Bahrami, and J. Nasri, “Wideband High Directive Aperture Coupled Microstrip Antenna Design by Using a FSS Superstrate Layer,” *IEEE Transactions on Antennas and Propagation*, vol. 60, no. 4, pp. 2101–2106, Apr. 2012.
- [127] M. Akbari, S. Gupta, M. Farahani, A. R. Sebak, and T. A. Denidni, “Gain Enhancement of Circularly Polarized Dielectric Resonator Antenna Based on FSS Superstrate for MMW Applications,” *IEEE Transactions on Antennas and Propagation*, vol. 64, no. 12, pp. 5542–5546, Dec. 2016.
- [128] L. Moustafa and B. Jecko, “Design of a Wideband Highly Directive EBG Antenna Using Double-Layer Frequency Selective Surfaces and Multifield Technique for Application in the Ku-Band,” *IEEE Antennas and Wireless Propagation Letters*, vol. 9, pp. 342–346, 2010.
- [129] R. Yahya, A. Nakamura, M. Itami, and T. A. Denidni, “A Novel UWB FSS-Based Polarization Diversity Antenna,” *IEEE Antennas and Wireless Propagation Letters*, vol. 16, pp. 2525–2528, 2017.
- [130] Y. Ranga, L. Matekovits, K. P. Esselle, and A. R. Weily, “Multioctave Frequency Selective Surface Reflector for Ultrawideband Antennas,” *IEEE Antennas and Wireless Propagation Letters*, vol. 10, pp. 219–222, 2011.
- [131] Y. Ranga, L. Matekovits, A. R. Weily, and K. P. Esselle, “A Constant Gain Ultra-Wideband Antenna with a Multi-Layer Frequency Selective Surface,” *Progress In Electromagnetics Research Letters*, vol. 38, pp. 119–125, 2013.
- [132] A. Chatterjee and S. K. Parui, “Beamwidth Control of Omnidirectional Antenna Using Conformal Frequency Selective Surface of Different Curvatures,” *IEEE Transactions on Antennas and Propagation*, vol. 66, no. 6, pp. 3225–3230, Jun. 2018.
- [133] A. Chatterjee and S. K. Parui, “Frequency-Dependent Directive Radiation of Monopole-Dielectric Resonator Antenna Using a Conformal Frequency Selective Surface,” *IEEE Transactions on Antennas and Propagation*, vol. 65, no. 5, pp. 2233–2239, May 2017.

- [134] C. Lee, R. Sainati, and R. R. Franklin, "Frequency Selective Surface Effects on a Coplanar Waveguide Feedline in Fabry–Perot Cavity Antenna Systems," *IEEE Antennas and Wireless Propagation Letters*, vol. 17, no. 5, pp. 768–771, May 2018, .
- [135] Z. Duan, G. Abomakhleb, and G. Lu, "Perforated Medium Applied in Frequency Selective Surfaces and Curved Antenna Radome," *Applied Sciences*, vol. 9, no. 6, Art. no. 6, Jan. 2019
- [136] H. Chen, X. Hou, and L. Deng, "Design of Frequency-Selective Surfaces Radome for a Planar Slotted Waveguide Antenna," *IEEE Antennas and Wireless Propagation Letters*, vol. 8, pp. 1231–1233, 2009.
- [137] H. Zhou *et al.*, "Filter-Antenna Consisting of Conical FSS Radome and Monopole Antenna," *IEEE Transactions on Antennas and Propagation*, vol. 60, no. 6, pp. 3040–3045, Jun. 2012.
- [138] B.-Q. Lin, F. Li, Q.-R. Zheng, and Y.-S. Zen, "Design and Simulation of a Miniature Thick-Screen Frequency Selective Surface Radome," *IEEE Antennas and Wireless Propagation Letters*, vol. 8, pp. 1065–1068, 2009.
- [139] A. A. Omar and Z. Shen, "Thin 3-D Bandpass Frequency-Selective Structure Based on Folded Substrate for Conformal Radome Applications," *IEEE Transactions on Antennas and Propagation*, vol. 67, no. 1, pp. 282–290, Jan. 2019.
- [140] J. Huang, T.-K. Wu, and S.-W. Lee, "Tri-band frequency selective surface with circular ring elements," *IEEE Transactions on Antennas and Propagation*, vol. 42, no. 2, pp. 166–175, Feb. 1994.
- [141] S. Abbasi, J. Nourinia, C. Ghobadi, M. Karamirad, and B. Mohammadi, "A sub-wavelength polarization sensitive band-stop FSS with wide angular response for X- and Ku-bands," *AEU - International Journal of Electronics and Communications*, vol. 89, pp. 85–91, May 2018.
- [142] Q. Zhou, P. Liu, K. Wang, H. Liu, and D. Yu, "Absorptive frequency selective surface with switchable passband," *AEU - International Journal of Electronics and Communications*, vol. 89, pp. 160–166, May 2018.

- [143] F. Wang, K. Li, Y. Ren, and Y. Zhang, "A novel reconfigurable FSS applied to the antenna radar cross section reduction," *International Journal of RF and Microwave Computer-Aided Engineering*, vol. 29, no. 7, p. e21729, 2019.
- [144] N. Jaglan, S. D. Gupta, B. Kanaujia, S. Srivastava, and E. Thakur, "Triple Band Notched DG-CEBG Structure Based UWB MIMO/Diversity Antenna," *Progress In Electromagnetics Research C*, vol. 80, pp. 21–37, 2018.
- [145] J. Prasanth Kumar and G. Karunakar, "Compact UWB-MIMO Triple Notched Antenna for Isolation Reduction," *Wireless Pers Commun*, vol. 115, no. 3, pp. 2113–2125, Dec. 2020.
- [146] E. Thakur, N. Jaglan, and S. D. Gupta, "Design of compact triple band-notched UWB MIMO antenna with TVC-EBG structure," *Journal of Electromagnetic Waves and Applications*, vol. 34, no. 11, pp. 1601–1615, Jul. 2020.
- [147] Z.-X. Yang, H.-C. Yang, J.-S. Hong, and Y. Li, "A miniaturized triple band-notched MIMO antenna for UWB application," *Microwave and Optical Technology Letters*, vol. 58, no. 3, pp. 642–647, 2016.
- [148] Z. Tang, X. Wu, J. Zhan, S. Hu, Z. Xi, and Y. Liu, "Compact UWB-MIMO Antenna With High Isolation and Triple Band-Notched Characteristics," *IEEE Access*, vol. 7, pp. 19856–19865, 2019.
- [149] G. Yang, T. Zhang, W. Li, and Q. Wu, "A Novel Stable Miniaturized Frequency Selective Surface," *IEEE Antennas and Wireless Propagation Letters*, vol. 9, pp. 1018–1021, 2010.
- [150] C.-N. Chiu and K.-P. Chang, "A Novel Miniaturized-Element Frequency Selective Surface Having a Stable Resonance," *IEEE Antennas and Wireless Propagation Letters*, vol. 8, pp. 1175–1177, 2009.
- [151] W. Jiang, T. Hong, S. Gong, and C. Li, "Miniaturized frequency selective surface with a bionical structure," *Microwave and Optical Technology Letters*, vol. 55, no. 2, pp. 335–337, 2013.
- [152] R. Sivasamy, B. Moorthy, M. Kanagasabai, V. R. Samsingh, and M. G. N. Alsath, "A Wideband Frequency Tunable FSS for Electromagnetic Shielding Applications," *IEEE Transactions on Electromagnetic Compatibility*, vol. 60, no. 1, pp. 280–283, Feb. 2018.

- [153] S. Garg and S. Yadav, "A Triple Band-Reject Frequency Selective Surface for Broadband Applications" *Optical and Wireless Technology*, vol. 472 pp. 437–446, 2018.
- [154] C. Caloz and T. Itoh, "Electromagnetic Metamaterials: Transmission Line Theory and Microwave Applications", Hoboken, NJ, USA: Wiley, 2005
- [155] F. Wang, "A Tri-band Angularly Stable Frequency Selective Surface with Controllable Resonances for EM Shielding," *Frequenz*, vol. 74, no. 1–2, pp. 25–31, Jan. 2020.
- [156] R. A. Hill and B. A. Munk, "The effect of perturbing a frequency-selective surface and its relation to the design of a dual-band surface," *IEEE Transactions on Antennas and Propagation*, vol. 44, no. 3, pp. 368–374, Mar. 1996.
- [157] J. P. Gianvittorio, J. Romeu, S. Blanch, and Y. Rahmat-Samii, "Self-similar prefractal frequency selective surfaces for multiband and dual-polarized applications," *IEEE Transactions on Antennas and Propagation*, vol. 51, no. 11, pp. 3088–3096, Nov. 2003.
- [158] C.-N. Chiu and W.-Y. Wang, "A Dual-Frequency Miniaturized-Element FSS With Closely Located Resonances," *IEEE Antennas and Wireless Propagation Letters*, vol. 12, pp. 163–165, 2013.
- [159] R. Qi, H. Zhai, D. Yang, and K. Xue, "An angular-stable multi-layer reconfigurable frequency selective surface based on varactor with wide tuning range," *International Journal of RF and Microwave Computer-Aided Engineering*, vol. 30, no. 2, p. e22049, 2020.
- [160] M. Abdollahvand, K. Forooghi, J. A. Encinar, Z. Atlasbaf, and E. Martinez-de-Rioja, "Design and demonstration of a tri-band frequency selective surface for space applications in X, K, and Ka bands," *Microwave and Optical Technology Letters*, vol. 62, no. 4, pp. 1742–1751, 2020.
- [161] C. Gao, H. Pu, S. Gao, C. Chen, and Y. Yang, "Design and analysis of a tri-band frequency selective surface with a second-order response," *International Journal of Microwave and Wireless Technologies*, vol. 12, no. 3, pp. 205–211, Apr. 2020.

- [162] A. G. Neto, J. C. e Silva, I. B. G. Coutinho, M. de O. Alencar, and D. M. de Andrade, "Triple Band Reject Frequency Selective Surface with Application to 2.4 GHz Band," *Journal of Communication and Information Systems*, vol. 35, no. 1, Art. no. 1, Apr. 2020.
- [163] A. G. Neto, J. C. e Silva, J. N. de Carvalho, A. P. da Costa, and L. C. M. de Moura, "Bandpass frequency selective surface using asymmetrical slot four arms star geometry," *Microwave and Optical Technology Letters*, vol. 58, no. 5, pp. 1105–1109, 2016.
- [164] S. Khan and T. F. Eibert, "A Multifunctional Metamaterial-Based Dual-Band Isotropic Frequency-Selective Surface," *IEEE Transactions on Antennas and Propagation*, vol. 66, no. 8, pp. 4042–4051, Aug. 2018.
- [165] M. Kartal, J. J. Golezani, and B. Doken, "A Triple Band Frequency Selective Surface Design for GSM Systems by Utilizing a Novel Synthetic Resonator," *IEEE Transactions on Antennas and Propagation*, vol. 65, no. 5, pp. 2724–2727, May 2017.
- [166] A. Vallecchi, E. Shamonina, and C. J. Stevens, "Analytical model of the fundamental mode of 3D square split ring resonators," *Journal of Applied Physics*, vol. 125, no. 1, p. 014901, Jan. 2019.
- [167] A. A. Omar and Z. Shen, "Thin Bandstop Frequency-Selective Structures Based on Loop Resonator," *IEEE Transactions on Microwave Theory and Techniques*, vol. 65, no. 7, pp. 2298–2309, Jul. 2017.
- [168] A. Yelizarov and A. Kukharenko, "Metamaterial-based frequency selective surface with a band gap electronic adjustment," in *2016 German Microwave Conference (GeMiC)*, Mar. 2016, pp. 271–273.
- [169] L. Li *et al.*, "Reconfigurable all-dielectric metamaterial frequency selective surface based on high-permittivity ceramics," *Sci Rep*, vol. 6, no. 1, Art. no. 1, Apr. 2016.
- [170] K. Patchala, Y. R. Rao, and A. M. Prasad, "Meta Material based MIMO Antenna with Frequency Selective Surface for Gain Enhancement," *International Journal of Advanced Science and Technology*, vol. 29, no. 7, Art. no. 7, May 2020.

- [171] J. P. Turpin, J. A. Bossard, K. L. Morgan, D. H. Werner, and P. L. Werner, "Reconfigurable and Tunable Metamaterials: A Review of the Theory and Applications," *International Journal of Antennas and Propagation*, vol. 2014, p. e429837, May 2014.
- [172] I. B. Vendik and O. G. Vendik, "Metamaterials and their application in microwaves: A review," *Tech. Phys.*, vol. 58, no. 1, pp. 1–24, Jan. 2013.
- [173] V. Bhope and A. R. Harish, "A Novel Bandstop Frequency Selective Surface Using Coupled Split Ring Resonators," in *2019 IEEE Asia-Pacific Microwave Conference (APMC)*, Dec. 2019, pp. 1745–1747.
- [174] S. Khajevandi, H. Oraizi, and M. Poordaraee, "Design of Planar Dual-Bandstop FSS Using Square-Loop-Enclosing Superformula Curves," *IEEE Antennas and Wireless Propagation Letters*, vol. 17, no. 5, pp. 731–734, May 2018.
- [175] R. Sivasamy and M. Kanagasabai, "A Novel Dual-Band Angular Independent FSS With Closely Spaced Frequency Response," *IEEE Microwave and Wireless Components Letters*, vol. 25, no. 5, pp. 298–300, May 2015.
- [176] R. Sivasamy, B. Moorthy, M. Kanagasabai, J. V. George, L. Lawrance, and D. B. Rajendran, "Polarization-independent single-layer ultra-wideband frequency-selective surface," *International Journal of Microwave and Wireless Technologies*, vol. 9, no. 1, pp. 93–97, Feb. 2017.
- [177] D. Kanchana, S. Radha, B. S. Sreeja, and E. Manikandan, "A Single Layer UWB Frequency Selective Surface for Shielding Application," *Journal of Elec Materi*, vol. 49, no. 8, pp. 4794–4800, Aug. 2020.
- [178] S. S. Sampath and R. Sivasamy, "A Single-Layer UWB Frequency-Selective Surface With Band-Stop Response," *IEEE Transactions on Electromagnetic Compatibility*, vol. 62, no. 1, pp. 276–279, Feb. 2020.
- [179] G. S. Paul and K. Mandal, "Polarization-Insensitive and Angularly Stable Compact Ultrawide Stop-Band Frequency Selective Surface," *IEEE Antennas and Wireless Propagation Letters*, vol. 18, no. 9, pp. 1917–1921, Sep. 2019.
- [180] C. Pelletti, G. Bianconi, R. Mittra, and Z. Shen, "Frequency selective surface with wideband quasi-elliptic bandpass response," *Electronics Letters*, vol. 49, no. 17, pp. 1052–1053, Aug. 2013.

- [181] R. Yahya, A. Nakamura, and M. Itami, "3D UWB band-pass frequency selective surface," in *2016 IEEE International Symposium on Antennas and Propagation (APSURSI)*, Jun. 2016, pp. 959–960.
- [182] R. Adeline Mellita, D. S. Chandu, S. S. Karthikeyan, and P. Damodharan, "A miniaturized wideband frequency selective surface with interconnected cell structure," *AEU - International Journal of Electronics and Communica.*, doi: 10.1016/j.aeue.2020.153196.
- [183] R. Yahya, A. Nakamura, and M. Itami, "[Paper] Low Profile UWB Frequency Selective Surface based Antenna," *ITE Transactions on Media Technology and Applications*, vol. 4, no. 4, pp. 369–374, 2016.
- [184] S. Ghosh and K. V. Srivastava, "A Polarization-Independent Broadband Multilayer Switchable Absorber Using Active Frequency Selective Surface," *IEEE Antennas and Wireless Propagation Letters*, vol. 16, pp. 3147–3150, 2017.
- [185] S. Kundu, "A compact uniplanar ultra-wideband frequency selective surface for antenna gain improvement and ground penetrating radar application," *International Journal of RF and Microwave Computer-Aided Engineering*, vol. 30, no. 10, p. e22363, 2020.
- [186] J. Tao, M. Umair, M. Ali, and J. Zhou, "The impact of Internet of Things supported by emerging 5G in power systems: A review," *CSEE Journal of Power and Energy Systems*, vol. 6, no. 2, pp. 344–352, Jun. 2020.
- [187] A. Gohil, H. Modi, and S. K. Patel, "5G technology of mobile communication: A survey," in *2013 International Conference on Intelligent Systems and Signal Processing (ISSP)*, Mar. 2013, pp. 288–292.
- [188] K. Kour and K. Ali, "A Review Paper on 5G Wireless Networks", *International Journal of Engineering Research & Technology*, vol. 4, no. 32, pp. 793-797, Jul. 2018.
- [189] B. T. Jijo *et al.*, "A Comprehensive Survey of 5G mm-Wave Technology Design Challenges," *Asian Journal of Research in Computer Science*, pp. 1–20, Apr. 2021.

- [190] W. Hong *et al.*, “The Role of Millimeter-Wave Technologies in 5G/6G Wireless Communications,” *IEEE Journal of Microwaves*, vol. 1, no. 1, pp. 101–122, winter 2021.
- [191] P. K. Choudhury and M. A. El-Nasr, “Massive MIMO toward 5G,” *Journal of Electromagnetic Waves and Applications*, vol. 34, no. 9, pp. 1091–1094, Jun. 2020.
- [192] N. Jaglan, S. D. Gupta, and M. S. Sharawi, “18 Element Massive MIMO/Diversity 5G Smartphones Antenna Design for Sub-6 GHz LTE Bands 42/43 Applications,” *IEEE Open Journal of Antennas and Propagation*, vol. 2, pp. 533–545, 2021.
- [193] H. Wang, R. Zhang, Y. Luo, and G. Yang, “Compact Eight-Element Antenna Array for Triple-Band MIMO Operation in 5G Mobile Terminals,” *IEEE Access*, vol. 8, pp. 19433–19449, 2020.
- [194] J. Dong, S. Wang, and J. Mo, “Design of a Twelve-Port MIMO Antenna System for Multi-Mode 4G/5G Smartphone Applications Based on Characteristic Mode Analysis,” *IEEE Access*, vol. 8, pp. 90751–90759, 2020.
- [195] D. Hu, H. Zhai, L. Liu, J. Shi, and Z. Nie, “A new miniaturized frequency selective surface designed for Ku-band absorption and low-frequency bandpass,” *Microwave and Optical Technology Letters*, vol. 62, no. 1, pp. 315–321, 2020.
- [196] N. Liu, X.-J. Sheng, and J.-J. Fan, “A Compact Miniaturized Frequency Selective Surface with Stable Resonant Frequency,” *Progress In Electromagnetics Research Letters*, vol. 62, pp. 17–22, 2016.
- [197] A. G. Neto, A. G. DAssunção Junior, J. Costa e Silva, J. Do Nascimento Cruz, J. B. de Oliveira Silva, and N. J. Pereira de Lyra Ramos, “Multiband frequency selective surface with open matryoshka elements,” in *2015 9th European Conference on Antennas and Propagation (EuCAP)*, Apr. 2015, pp. 1–5.
- [198] C. de L. Nóbrega, M. R. da Silva, P. H. da F. Silva, A. G. D’Assunção, and G. L. Siqueira, “Simple, Compact, and Multiband Frequency Selective Surfaces Using Dissimilar Sierpinski Fractal Elements,” *International Journal of Antennas and Propagation*, vol. 2015, p. e614780, Nov. 2015.

- [199] G. Bharti, K. R. Jha, G. Singh, and R. Jyoti, "Planar tri-band frequency selective surface with transmission in S-band and reflection in Ka/Ku-band," *Radioelectron.Commun.Syst.*, vol. 58, no. 11, pp. 479–486, Nov. 2015.
- [200] E. Moharamzadeh and A. M. Javan, "Triple-Band Frequency-Selective Surfaces to Enhance Gain of X-Band Triangle Slot Antenna," *IEEE Antennas and Wireless Propagation Letters*, vol. 12, pp. 1145–1148, 2013.
- [201] Y. Xu and M. He, "Design of Multilayer Frequency-Selective Surfaces by Equivalent Circuit Method and Basic Building Blocks," *International Journal of Antennas and Propagation*, vol. 2019, p. e9582564, Aug. 2019.
- [202] K. Tao, B. Li, Y. Tang, and Q. Wu, "Multi-layer tri-band frequency selective surface using stepped- and uniform-impedance resonators," *Electronics Letters*, vol. 52, no. 8, pp. 583–585, Mar. 2016.
- [203] M. Chaluvadi, V. K. Kanth, and K. G. Thomas, "Design of a Miniaturized 2.5-D Frequency Selective Surface With Angular Incidence and Polarization Stability," *IEEE Transactions on Electromagnetic Compatibility*, vol. 62, no. 4, pp. 1068–1075, Aug. 2020.
- [204] H. Wang, S. Qu, J. Wang, M. Yan, and L. Zheng, "Dual-band miniaturised FSS with stable resonance frequencies of 3.4/4.9 GHz for 5G communication systems applications," *IET Microwaves, Antennas & Propagation*, vol. 14, no. 1, pp. 1–6, 2020.
- [205] M. Qu, Y. Feng, J. Su, and S. M. A. Shah, "Design of a Single-Layer Frequency Selective Surface for 5G Shielding," *IEEE Microwave and Wireless Components Letters*, vol. 31, no. 3, pp. 249–252, Mar. 2021.
- [206] P. Zhao, Y. Zhang, R. Sun, W.-S. Zhao, Y. Hu, and G. Wang, "Design of a Novel Miniaturized Frequency Selective Surface Based on 2.5-Dimensional Jerusalem Cross for 5G Applications," *Wireless Communications and Mobile Computing*, vol. 2018, p. e3485208, Apr. 2018.

APPENDIX

Frequency Selective Surface Fabrication

The accuracy of the FSS dimensions is very critical in microwave frequencies. Therefore EP 2006 PCB PROTOTYPE MACHINE is used to fabricate the FSS sheet. EP2006 series PCB Prototype Machine brings us the most simple, quick and precise way to make our own PCB prototype. The fabrication prototype machine is shown in Figure A.1.



Figure A.1 Fabrication prototype machine

Anechoic Chamber

The measurement setup inside an anechoic chamber is shown in Figure A.2. The anechoic chamber provides a non-reflective and echo-free quiet zone. It is designed to completely absorb reflections of EM waves and isolate the system inside from any wave entering from the surroundings. Therefore, it is used to measure the FSS characteristics accurately. All the FSS characterizations are done inside an anechoic chamber to avoid reflections from nearby objects. The absorbers fixed on the walls are highly lossy at microwave frequencies, as shown in Figure A.3. They have tapered shapes to achieve good impedance matching for the microwave power impinging upon it. The chamber is made free from the surrounding EM interferences by covering all the walls and the roof with aluminum sheet.

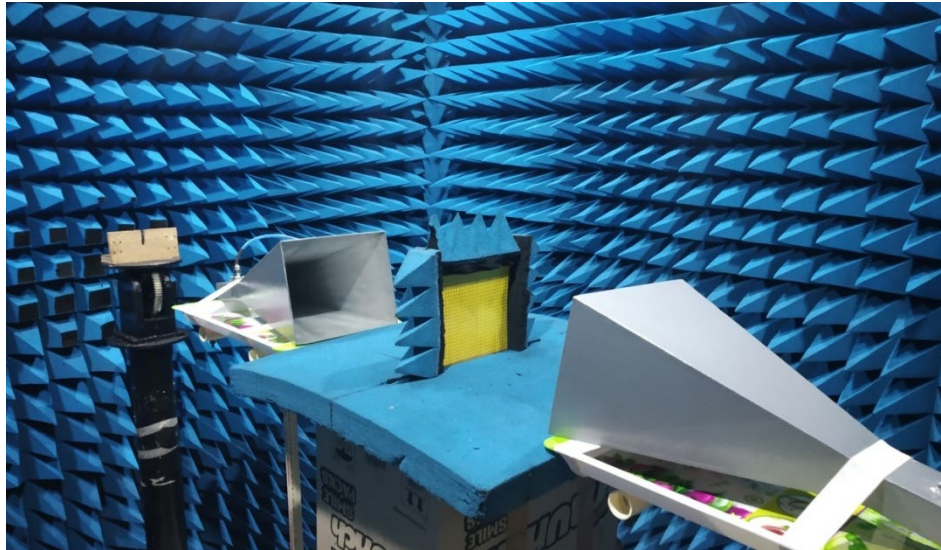


Figure A.2 Anechoic chamber

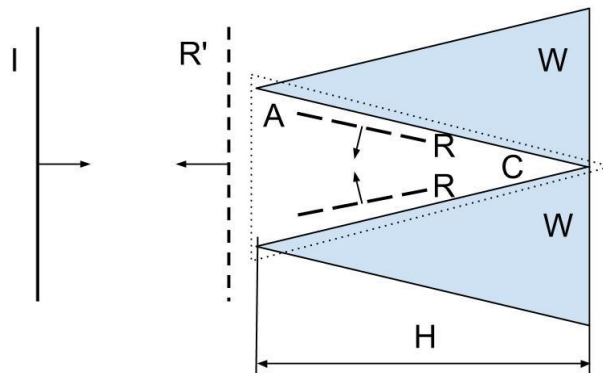


Figure A.3. Wedge absorbers in anechoic chamber

Vector Network Analyzer

The Anritsu MS2038C vector network analyzer is used for measurements of S-parameters as shown in Figure A.4. For accurate measurements it is mandatory to calibrate the VNA. The transmission coefficient (S_{21}) is measured using two ports of VNA. One port acts as a source while the other is terminated with a match load. The measurement of reflection coefficient (S_{11}) requires single port.

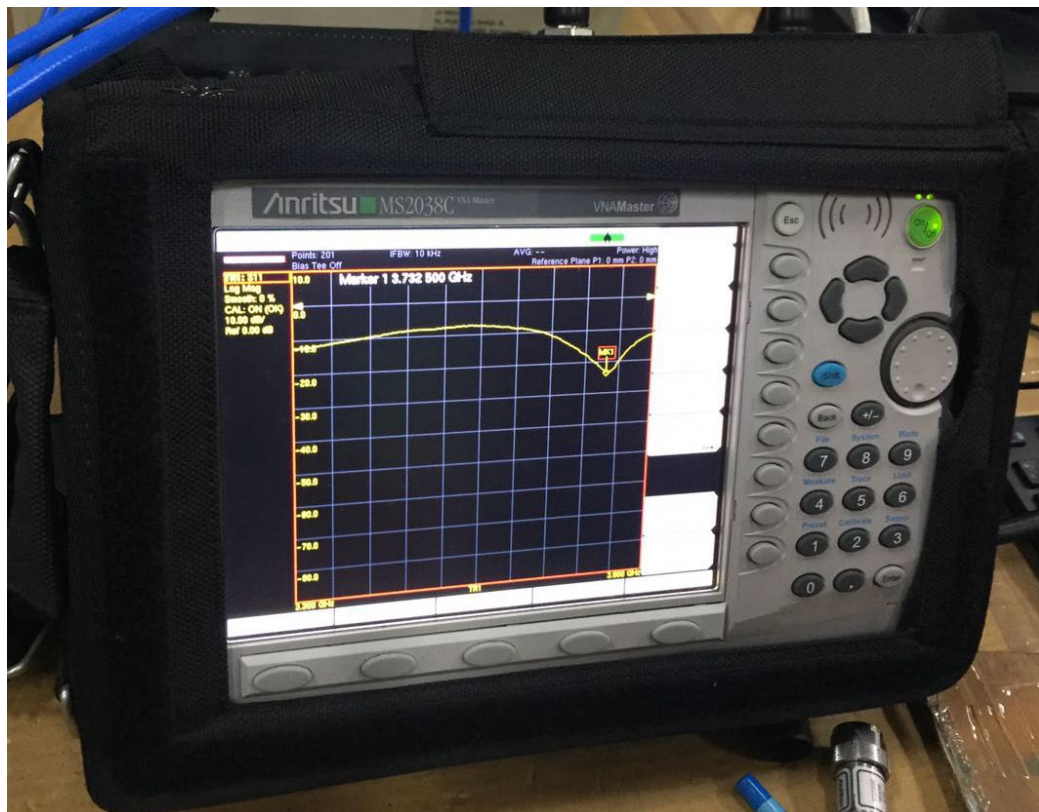


Figure A.4. Vector Network Analyzer

LIST OF PUBLICATIONS

Journals:

- [1] K. Katoch, N. Jaglan and S. D. Gupta, "Design of a triple band notched compact FSS at UWB frequency range" *Progress In Electromagnetics Research M*, vol. 87, pp. 147-157, Dec 2019, doi: [10.2528/PIERM19091103](https://doi.org/10.2528/PIERM19091103) (ESCI/Scopus)
- [2] K. Katoch, N. Jaglan, S. D. Gupta and Mohammad S. Sharawi, "Design of a triple band notched polarization independent compact FSS at UWB frequency range", *International Journal of RF and Microwave Computer Aided Engineering*, e22631, vol. 31, no. 6, pp. 1-14, June 2021, doi: <https://doi.org/10.1002/mmce.22631> (SCI)
- [3] K. Katoch, N. Jaglan and S. D. Gupta, "Analysis and design of a simple and compact bandstop Frequency Selective Surface at mobile WiMAX and Satellite Communication X-band", *Journal of Electromagnetic Waves and Applications*, vol. 35, no. 10, pp. 1321-1336, May 2021, doi: <https://doi.org/10.1080/09205071.2021.1888319> (SCI)
- [4] K. Katoch, N. Jaglan and S. D. Gupta, "Design and Analysis of Single Sided Modified Square Loop UWB Frequency Selective Surface", *IEEE Transactions on Electromagnetic Compatibility*, vol. 63, no. 5, pp. 1423 - 1432, October 2021. DOI: [10.1109/TEMC.2021.3063143](https://doi.org/10.1109/TEMC.2021.3063143) (SCI)

Research paper Communicated:

- [5] K. Katoch, N. Jaglan and S. D. Gupta, "Design of a 2.5D FSS for Sub-6GHz 5G Wireless Communication", *IEEE Antennas and Wireless Propagation Letters*, 2021 (SCI)

Book Chapter:

- [6] K. Katoch, N. Jaglan, S. D. Gupta and B. K. Kanaujia, "Design of Frequency Selective Surface (FSS) for Printed Antennas" *Printed Antennas: Theory and Design*, November 2020, doi: [10.1201/9780367420451-12](https://doi.org/10.1201/9780367420451-12)

International Conference:

- [7] K. Katoch, N. Jaglan and S. D. Gupta, “A Review on Frequency Selective Surfaces and its Applications”, International conference on signal processing and communication, Noida, India, pp. 1-7, March 2019, **doi:** [10.1109/ICSC45622.2019.8938161](https://doi.org/10.1109/ICSC45622.2019.8938161)
- [8] K. Katoch, N. Jaglan and S. D. Gupta, “Band notched polarization insensitive simple FSS for electromagnetic shielding”, International conference on signal processing and communication, Wagnaghat, Solan, India, May 2021 (*Accepted and presented*)